

**TECHNICAL
TRANSACTIONS**

**CIVIL
ENGINEERING**

**ISSUE
1-B (11)**

**YEAR
2015 (112)**

**CZASOPISMO
TECHNICZNE**

BUDOWNICTWO

**ZESZYT
1-B (11)**

**ROK
2015 (112)**



**WYDAWNICTWO
POLITECHNIKI
KRAKOWSKIEJ**

TECHNICAL TRANSACTIONS

CZASOPISMO TECHNICZNE

CIVIL ENGINEERING

BUDOWNICTWO

ISSUE 1-B (11)
YEAR 2015 (112)

ZESZYT 1-B (11)
ROK 2015 (112)

Chairman of the Cracow University
of Technology Press Editorial Board

Jan Kazior

Przewodniczący Kolegium
Redakcyjnego Wydawnictwa
Politechniki Krakowskiej

Chairman of the Editorial Board

Józef Gawlik

Przewodniczący Kolegium
Redakcyjnego Wydawnictwa
Naukowych

Scientific Council

Jan Błachut
Tadeusz Burczyński
Leszek Demkowicz
Joseph El Hayek
Zbigniew Florjańczyk
Józef Gawlik
Marian Giżejowski
Sławomir Gzell
Allan N. Hayhurst
Maria Kušnierova
Krzysztof Magnucki
Herbert Mang
Arthur E. McGarity
Antonio Monestiroli
Günter Wozny
Roman Zarzycki

Rada Naukowa

Civil Engineering Series Editor

Marek Piekarczyk

Redaktor Serii Budownictwo

Section Editor
Editorial Compilation
Native Speaker
Typesetting
Cover Design
Cover Photo

Dorota Sapek
Aleksandra Urzędowska
Tim Churcher
Anna Pawlik
Michał Graffstein
Jan Zych

Sekretarz Sekcji
Opracowanie redakcyjne
Weryfikacja językowa
Skład i łamanie
Projekt okładki
Zdjęcie na okładce

Basic version of each Technical Transactions magazine is its online version
Pierwotną wersją każdego zeszytu Czasopisma Technicznego jest jego wersja online
www.ejournals.eu/Czasopismo-Techniczne www.technicaltransactions.com www.czasopismotechniczne.pl

Civil Engineering Series

1-B/2015

Editor-in-Chief:

Marek Piekarczyk, Cracow University of Technology, Poland

Editorial Board:

Marek Cała, AGH University of Science and Technology, Poland
Roberto Capozucca, Marche Polytechnic University, Italy
Andrzej Cholewicki, Building Research Institute, Poland
Wit Derkowski, Cracow University of Technology, Poland
Jean-François Destrebecq, French Institute for Advanced Mechanics, France
Grzegorz Dzierżanowski, Warsaw University of Technology, Poland
Andrzej Flaga, Cracow University of Technology, Poland
Dariusz Gawin, Lodz University of Technology, Poland
Jacek Gołaszewski, Silesian University of Technology, Poland
Kocsán Lajos György, University of Miskolc, Hungary
Klaudiusz Holeczek, Dresden University of Technology, Germany
Bożena Hoła, Wrocław University of Technology, Poland
Hartwig Künzel, Fraunhofer Institute for Building Physics, Germany
Maria E. Kamińska, Lodz University of Technology, Poland
Oleg Kapliński, Poznan University of Technology, Poland
Tadeusz Kasprowicz, Military University of Technology, Poland
Renata Kotynia, Lodz University of Technology, Poland
Robert Kowalski, Warsaw University of Technology, Poland
Mária Kozlovská, Technical University of Košice, Slovakia
Andrzej Łapko, Białystok University of Technology, Poland
Marco Menegotto, Sapienza University of Rome, Italy
Peter Mesároš, Technical University of Košice, Slovakia
Piotr Noakowski, TU Dortmund University, Germany
Andrzej Nowak, University of Michigan, United States
Zygmunt Orłowski, AGH University of Science and Technology, Poland
Hartmut Pasternak, Brandenburg University of Technology Cottbus–Senftenberg, Germany
Edyta Plebankiewicz, Cracow University of Technology, Poland
Maria Polak, University of Waterloo, Canada
Elżbieta Radziszewska-Zielina, Cracow University of Technology, Poland
Charles Rodrigues, Universidade Nova de Lisboa, Portugal
Tomasz Siwowski, Rzeszow University of Technology, Poland
Anna Sobotka, AGH University of Science and Technology, Poland
Marcela Spišáková, Technical University of Košice, Slovakia
Zuzana Struková, Technical University of Košice, Slovakia
Maria Szerszeń, University of Nebraska – Lincoln, United States
Jolanta Tamošaitienė, Vilnius Gediminas Technical University, Lithuania
Alena Tažiková, Technical University of Košice, Slovakia
Balázs Tóth, University of Miskolc, Hungary
Martins Vilnītis, Riga Technical University, Latvia
Szczepan Woliński, Rzeszow University of Technology, Poland

JACEK BOROŃ*, KAZIMIERZ MARSZAŁEK*

DISTRIBUTION OF THE TEMPERATURE FACTOR IN TERMS OF BUILDING ENVELOPE PROTECTION AGAINST MOULD GROWTH

ROZKŁAD WARTOŚCI CZYNNIKA TEMPERATUROWEGO W ASPEKCIE OCHRONY PRZEGRÓD BUDOWLANYCH PRZED ROZWOJEM PLEŚNI

Abstract

This paper describes the criterion for the protection of building envelopes against the growth of mould. As a criterion for assessing the risk to envelopes, the f_{Rsi} temperature factor is adopted. The paper provides the resultant temperature factor $f_{Rsi,max}$ for the critical month in 61 areas in Poland for which typical year-long meteorological data is available on the website of the Ministry of Infrastructure and Development. While calculating the temperature factor, various room humidity classes were taken into account. The results of calculations of the temperature factor $f_{Rsi,max}$ have been illustrated with isolines drawn for the whole area of Poland.

Keywords: building envelopes, isolines, mould, temperature factor

Streszczenie

W artykule opisano kryterium ochrony przegród budowlanych przed rozwojem grzybów pleśniowych. Jako kryterium oceny zagrożenia przegród przyjęto czynnik temperaturowy f_{Rsi} . Podano wyniki obliczeń wartości czynnika temperaturowego $f_{Rsi,max}$ dla miesiąca krytycznego w 61 miejscach w Polsce, dla których dane dotyczące typowych lat meteorologicznych są dostępne na stronie internetowej Ministerstwa Infrastruktury. W obliczeniach czynnika temperaturowego uwzględniono różne klasy wilgotności pomieszczeń. Wyniki obliczeń wartości czynnika temperaturowego $f_{Rsi,max}$ zilustrowano izoliniami sporządzonymi dla całego obszaru Polski.

Słowa kluczowe: przegrody budowlane, izoliny, pleśń, czynnik temperaturowy

DOI: 10.4467/2353737XCT.15.074.3874

* Ph.D. Eng. Jacek Boroń, Ph.D. Eng. Kazimierz Marszałek, Faculty of Civil Engineering, Wrocław University of Technology.

1. Introduction

The presence of mould on wall surfaces is a problem affecting buildings in many European countries [3]. In Western Europe, the presence of mould on walls was not recognised as a problem until the mid-nineteen-eighties. It was then that countries like Belgium, the Netherlands, Italy, Germany and the United Kingdom created a working group investigating, among other things, the phenomena of surface condensation and the associated formation (and growth) of mould on the surfaces of building envelopes [5]. It was noted that the problem of the presence of mould on the surfaces of the envelopes appears not only when the surfaces are damp due to condensation of water vapour – as we know, this occurs when the relative humidity at the surface of the envelope reaches 100% (i.e. when the partial pressure of water vapour in room air p_i is equal to the pressure of saturated vapour p_{sat}).

Specifically, it was noted that moulds also appear and develop on building envelope surfaces having contact with air, the relative humidity of which being less than 100%. Actually, the risk of mould development is already present when the relative humidity is around 80% – this occurs in situations of contact with moisture sensitive materials when the moisture persists for at least several days. Therefore, recognising 80% relative humidity of air as the critical humidity [2], the following condition for the possibility of mould growth was formulated:

$$p_i \geq 0.8 \cdot p_{sat}(\theta_{si}) \quad (1)$$

where:

- p_i – partial pressure of water vapour in the air of the room,
- $p_{sat}(\theta_{si})$ – saturated vapour pressure.

As follows from the above formula, surface condensation and mould growth heavily depends upon the partial pressure of water vapour in the room p_i , and on the saturated vapour pressure on the surface of the envelope $p_{sat}(\theta_{si})$.

According to the regulations which were in force in Poland until the end of 2008, it was only required to prove that the surface temperature of the envelopes was 1 K higher than the dew point of the air in the room in the so-called design conditions to allow a conclusion that there would be no condensation and mould growth on the surface of the envelopes. Detailed regulations in this respect were formulated in the regulation on technical conditions to be met by buildings [6]. As we now know, this condition has been proven to be insufficient to protect homes against the occurrence of mould.

Checking whether the condition specified in formula (1) has been fulfilled entails the necessity to calculate the minimum allowable surface temperature $\theta_{si,min}$, i.e. the lowest temperature of the inner surface of the outer envelope, below which mould growth begins. By knowing the value of the minimum allowable surface temperature $\theta_{si,min}$, the temperature of the air in the room θ_i and the temperature outside the building θ_e , it is possible to calculate the minimum value of the dimensionless temperature of the inner surface $f_{Rsi,min}$ for each month of the year. This value is also known as the minimum temperature factor or the minimum temperature coefficient. The critical month, as is mentioned in [8], is the one in which the required value of $f_{Rsi,min}$ is the highest. The value of the temperature factor for this month is known as $f_{Rsi,max}$. Thus, in order to prevent the appearance of mould, building envelopes

should be designed so that the value of $f_{Rsi,max}$ will always be lower than the temperature factor f_{Rsi} – which describes the thermal performance of the building envelope:

$$f_{Rsi} > f_{Rsi,max}, \quad (2)$$

where f_{Rsi} can be written as:

$$f_{Rsi} = \frac{\theta_{si} - \theta_e}{\theta_i - \theta_e}, \quad (3)$$

which in practice, for flat envelopes, i.e. for a one-dimensional heat flow system, allows the calculation of the temperature factor f_{Rsi} from the formula:

$$f_{Rsi} = 1 - \frac{U}{R_{si}^{-1}}, \quad (4)$$

where:

- U – the heat transfer coefficient, determined according to [11],
- R_{si} – the resistance of heat transfer (the value assumed for the calculations is 0.25 m²K/W).

However, in the case where the heat transfer takes place in a two- or three-dimensional heat flow system, f_{Rsi} can be determined by use of the method provided, for example, in standard [9].

In Poland, the temperature factor f_{Rsi} began to be used as a criterion for assessing the risk of the appearance and growth of mould on the inner surfaces of building envelopes at the beginning of 2009, when the Minister of Infrastructure changed the regulation on technical conditions to be met by buildings and their location [7]. At this point, the question of why these changes were introduced so late arises, considering that the method of calculating the temperature factor $f_{Rsi,min}$ had been known for many years and had been available, among others, in standard [8]. The reason for this must have been the lack of universal access to data from a typical meteorological year for a large number of areas in Poland. Files with typical meteorological year-long data for 61 places in Poland were prepared by the Ministry of Infrastructure and Development and published on its website [11] in July 2008 (mainly for the requirement of energy performance certification of buildings). This enabled the practical application of the temperature factor as a criterion for assessing the risk of mould growth on the interior surfaces of building envelopes. More information on typical meteorological year data for Poland can be found in [4].

The aim of this work is to provide, in tabular and graphic form, the temperature factor $f_{Rsi,max}$ for the critical month in 61 locations in Poland for which typical meteorological year data has been published on the website of the Ministry of Infrastructure and Development [11]. The results of the calculations of $f_{Rsi,max}$ are provided for various room humidity classes. In order to evaluate the distribution of the temperature factor $f_{Rsi,max}$ for the entire Polish territory, and not just for the 61 selected locations, the paper provides the results of calculations of the temperature factor in the form of isolines. The authors believe that the proposed way of calculating the temperature factor $f_{Rsi,max}$ will allow a fast determination of this factor for designing needs.

2. Room air humidity

To define room air humidity conditions, we may use either the partial pressure of water vapour or moisture by volume. Partial pressure of water vapour (in the room) depends on:

- partial pressure of water vapour in the outside air p_e or condensation of water vapour in the outside air c_e ,
- multiple air exchange rate in the room n ,
- volume (cubic capacity) of the room V ,
- water vapour production in the room (internal moisture production) G .

As long as there is no surface condensation and no hygroscopic absorption and storage of moisture by envelope materials, we can write the moisture balance of the room in the following way [1]:

$$\Phi_{in} + G = \Phi_{out}, \quad (5)$$

where:

- Φ_{in} – the moisture flowing into the room from outside the building,
- G – internal moisture production,
- Φ_{out} – the moisture leaving the room.

Assuming that there is no difference between the air temperature outside the building and in the room, the amount of moisture flowing into the room from outside the building is:

$$\Phi_{in} = n \cdot V \cdot c_e, \quad (6)$$

where:

- n – the multiple air exchange rate in the room,
- V – the cubic capacity of the room, and c_e is water vapour concentration outside the room.

In contrast, the amount of moisture leaving the room can be written as:

$$\Phi_{out} = n \cdot V \cdot c_i \quad (7)$$

where:

c_i – water vapour concentration in the air of the room.

Taking into account the moisture balance written as formula (5), we can obtain the difference of concentrations of water vapour between the air inside and outside the room:

$$c_i - c_e = \frac{G}{n \cdot V}. \quad (8)$$

By adjusting formula (8) due to changes in air volume caused by the difference in air temperature inside and outside of the room and using Boyle Gay-Lussac's law [5] we obtain:

$$c_i - c_e \frac{T_e}{T_i} = \frac{G}{n \cdot V}, \quad (9)$$

where T_e and T_i are the absolute temperatures in K.

Water vapour concentration can be expressed by its partial pressure as:

$$p = c \cdot R \cdot T, \quad (10)$$

where:

R – the gas constant for vapour, amounting to 462 J/kg·K.

The difference of the partial pressure of water vapour in the air in the room and outside the building can then be written as the following formula:

$$P_i - P_e = \frac{462 \cdot (\theta_i + 273) \cdot G}{n \cdot V}. \quad (11)$$

As seen from the above formula, the difference of the partial pressure of water vapour in the air inside the room and outside of Δp , also known as the excess internal pressure of water vapour, depends on the air temperature in the room as well as the type, size and usage of the room. In the absence of Polish studies conducted in buildings of various purposes and usage, in order to calculate the temperature factor f_{Rsi} , the values of the excess internal pressure Δp provided in [8] have been adopted as for buildings located and designed in Western Europe. In this case, the values of the excess internal pressure depend on the so-called room humidity class. For the calculation of the temperature factor f_{Rsi} , three (i.e. the second, third and fourth) of the five humidity classes are taken into account. In the calculations of f_{Rsi} , the upper limits for each of the classes were adopted. Table 1 shows examples of rooms assigned to given humidity classes.

Table 1

Room humidity classes according to [8]

Room humidity classes	Examples of rooms and buildings	Δp^* , [Pa]
1	storage facilities, dry production plants	≤ 270
2	offices, shops	$> 270 \leq 540$
3	low occupancy flats	$> 540 \leq 810$
4	high occupancy flats, sports halls, kitchens, canteens, rooms in buildings heated with gas heaters without flues	$> 810 \leq 1080$
5	rooms in special buildings, e.g. laundries, breweries, swimming pools	> 1080

^{*)} the given values relate to excess internal pressure Δp at air temperature $\theta_e \leq 0^\circ\text{C}$

3. The results of calculations of the temperature factor for the critical month

With the help of the files published on the Ministry's website containing typical meteorological year data [11], average monthly air temperatures θ_e and average monthly relative humidity values φ_e for 61 selected Polish meteorological stations were calculated. By adopting the calculated average monthly temperature and air humidity values outside the building, defining the air temperature inside the room $\theta_i = 20^\circ\text{C}$ and adopting the excess internal water vapour pressure values Δp for three room humidity classes and the maximum allowable relative humidity at the surface $\varphi_{si} = 0.8$, the minimum allowable pressure of saturated vapour $p_{sat}(\theta_{si})$ for each of the 12 months of the year and each of the mentioned 61 meteorological stations was calculated.

On the basis of the calculated minimum allowable pressures at saturation, for each month, the minimum allowable surface temperature $\theta_{si,min}$ was determined, i.e. the lowest allowable temperature of the inner surface of the envelope, below which mould growth begins. Knowing the value of the minimum allowable surface temperature θ_{si} , the minimum value of the temperature factor $f_{Rsi,min}$ for each month was calculated, the critical months and the corresponding temperature factors $f_{Rsi,max}$ assigned to 61 meteorological stations were then determined.

The results of the calculations of the temperature factor $f_{Rsi,max}$ with critical months indicated are shown in Table 2. From the analysis of the above results, it becomes clear that the highest values of the temperature factor $f_{Rsi,max}$ occur in Chojnice and Suwałki. In Chojnice, $f_{Rsi,max}$ for humidity class 2 equals 0.618, and in Suwałki it equals 0.616. For humidity class 3, the highest value of the factor $f_{Rsi,max}$ also occurs in Chojnice and in Suwałki (and equals 0.793), while for humidity class 4, it equals 0.942 in Suwałki and 0.939 in Chojnice. The critical month in Chojnice is December, whereas in Suwałki, it is November. The lowest value of the temperature factor occurs in Zakopane, where for humidity class 2, $f_{Rsi,max} = 0.566$, humidity class 3 $f_{Rsi,max} = 0.741$ and for humidity class 4, $f_{Rsi,max} = 0.891$.

Table 2

Temperature factor $f_{Rsi,max}$ values (the critical $f_{Rsi,max}$ values) for 3 humidity classes

No.	Town/City	Humidity Class 2		Humidity Class 3		Humidity Class 4	
		$f_{Rsi,max}$	critical month	$f_{Rsi,max}$	critical month	$f_{Rsi,max}$	critical month
1	Białystok	0.598	December	0.772	December	0.918	November
2	Bielsko Biala	0.575	December	0.760	December	0.913	December
3	Bydgoszcz	0.604	February	0.784	February	0.933	February
4	Chojnice	0.618	December	0.793	December	0.939	December
5	Częstochowa	0.602	December	0.775	December	0.919	December
6	Elbląg	0.606	December	0.785	December	0.935	December
7	Gdańsk	0.572	December	0.752	December	0.904	December
8	Gorzów Wlkp.	0.600	December	0.780	January	0.930	January
9	Hel	0.607	January	0.786	January	0.935	January
10	Jelenia Góra	0.587	December	0.769	December	0.920	December
11	Kalisz	0.606	December	0.782	December	0.927	December
12	Kasprowy Wierch	0.583	May	0.762	May	0.913	May
13	Katowice	0.581	December	0.756	December	0.900	December
14	Kętrzyn	0.615	December	0.790	December	0.935	December
15	Kielce	0.610	December	0.789	December	0.938	December
16	Kłodzko	0.593	December	0.769	January	0.918	January

continued Tab. 2

17	Koło	0.605	December	0.781	December	0.926	January
18	Kołobrzeg	0.583	January	0.765	January	0.917	January
19	Koszalin	0.595	January	0.772	January	0.920	January
20	Kraków	0.591	December	0.770	December	0.917	December
21	Krosno	0.591	December	0.768	December	0.916	November
22	Łeba	0.604	December	0.784	December	0.934	December
23	Lębork	0.583	February	0.765	February	0.916	February
24	Legnica	0.597	December	0.778	December	0.928	December
25	Lesko	0.577	December	0.759	December	0.910	February
26	Leszno	0.597	December	0.776	January	0.924	January
27	Łódź	0.605	December	0.782	December	0.932	December
28	Lublin	0.595	November	0.773	November	0.923	November
29	Mikołajki	0.606	December	0.781	December	0.925	December
30	Mława	0.602	December	0.775	December	0.918	December
31	Nowy Sącz	0.569	December	0.754	January	0.907	January
32	Olsztyn	0.612	December	0.788	December	0.934	December
33	Opole	0.603	December	0.782	December	0.932	December
34	Ostrołęka	0.601	December	0.776	December	0.922	December
35	Piła	0.613	December	0.788	December	0.933	December
36	Płock	0.608	December	0.785	December	0.933	December
37	Poznań	0.609	December	0.788	December	0.936	December
38	Przemysł	0.584	December	0.762	December	0.908	December
39	Racibórz	0.586	January	0.769	January	0.920	January
40	Resko	0.592	January	0.768	January	0.917	December
41	Rzeszów	0.587	December	0.764	December	0.916	February
42	Sandomierz	0.611	December	0.789	December	0.936	December
43	Siedlce	0.598	December	0.771	December	0.915	December
44	Stubice	0.597	January	0.776	January	0.926	January
45	Śnieżka	0.608	April	0.783	April	0.928	April
46	Sulejów	0.605	December	0.782	December	0.928	December
47	Suwałki	0.616	November	0.793	November	0.942	November
48	Świnoujście	0.601	January	0.780	January	0.930	January
49	Szczecin	0.597	January	0.775	January	0.925	January

50	Szczecinek	0.606	January	0.785	January	0.934	January
51	Tarnów	0.589	December	0.770	December	0.920	December
52	Terespol	0.598	December	0.772	December	0.916	December
53	Toruń	0.598	January	0.775	January	0.922	January
54	Ustka	0.590	January	0.771	January	0.921	January
55	Warszawa	0.602	December	0.780	December	0.929	December
56	Wieluń	0.599	December	0.773	December	0.917	December
57	Włodawa	0.606	December	0.780	December	0.924	December
58	Wrocław	0.595	December	0.771	December	0.919	February
59	Zakopane	0.566	January	0.741	January	0.891	November
60	Zamość	0.603	November	0.783	November	0.932	November
61	Zielona Góra	0.605	January	0.784	January	0.933	December

4. Summary

This paper presents calculations of the temperature factor for the locations of 61 meteorological stations in Poland and determines the values of $f_{Rsi,max}$ for the critical months at these locations. Based on the results provided in Table 2, it can be hypothesised that the factor having the greatest impact on the value of the temperature factor $f_{Rsi,max}$ is the room humidity class. The room humidity class is dependent on internal moisture production as well as room ventilation (multiple air exchange rate) and thus, on the type and usage of the room. Moreover, a belief has to be expressed at this point that it is necessary to conduct research of flats and rooms in non-residential buildings in Poland in order to enable their correct classification (i.e. their assignment to an appropriate humidity class). The calculated differences between the average values of $f_{Rsi,max}$ for the whole Polish territory determined for humidity classes 2 and 3 equal 0.178 and for classes 3 and 4 differences equal 0.148.

The average value of the maximum temperature factor $f_{Rsi,max}$ for Poland (for 61 selected meteorological stations) for humidity class 2 is 0.597, for humidity class 3, it is 0.775, and for humidity class 4, it equals 0.923.

The distribution of the values of the temperature factor $f_{Rsi,max}$ on Polish territory for each humidity class has been shown in the Figures 1–9 below in the form of graphs and isolines. On the basis of the visual material it can be concluded that the values of $f_{Rsi,max}$ vary within the following ranges:

0.566 – 0.618	for humidity class 2,
0.741 – 0.793	for humidity class 3,
0.891 – 0.923	for humidity class 4.

The presented results show that if the external walls meet the requirements regarding the heat transfer coefficient U (as provided in Regulation [8], for the condition where

$U \leq U_{(\max)} = 0.3 \text{ W/m}^2\text{K}$) then both residential and non-residential rooms assigned to humidity class 3, everywhere in Poland, fulfil the condition that the value of the temperature factor $f_{Rsi} > f_{Rsi,\max}$ – this is illustrated in Figs. 1, 2 and 3. In these cases, it is not necessary to perform calculations to ascertain whether the condition $f_{Rsi} > f_{Rsi,\max}$ is met. This is also the case for all external walls whose heat transfer coefficient is less than $U = 0.75 \text{ W/m}^2\text{K}$. The presented results show that if the external walls meet the requirements regarding the heat transfer coefficient U (as provided in regulation [7], for the condition where $U \leq U_{(\max)} = 0.3 \text{ W/m}^2\text{K}$) then both residential and non-residential rooms assigned to humidity class 3, everywhere in Poland, fulfil the condition that the value of the temperature factor $f_{Rsi} > f_{Rsi,\max}$ – this is illustrated in Figs. 1, 2 and 3. In these cases, it is not necessary to perform calculations to ascertain whether the condition $f_{Rsi} > f_{Rsi,\max}$ is met – this is also the case for all external walls whose heat transfer coefficient is less than $U = 0.75 \text{ W/m}^2\text{K}$.

Of course, the above conclusion does not apply to external walls with thermal bridges; in their case, it is necessary to calculate the temperature factor f_{Rsi} for such a wall for the place where the thermal bridge is located and to compare the result with the values of $f_{Rsi,\max}$ provided in this paper.

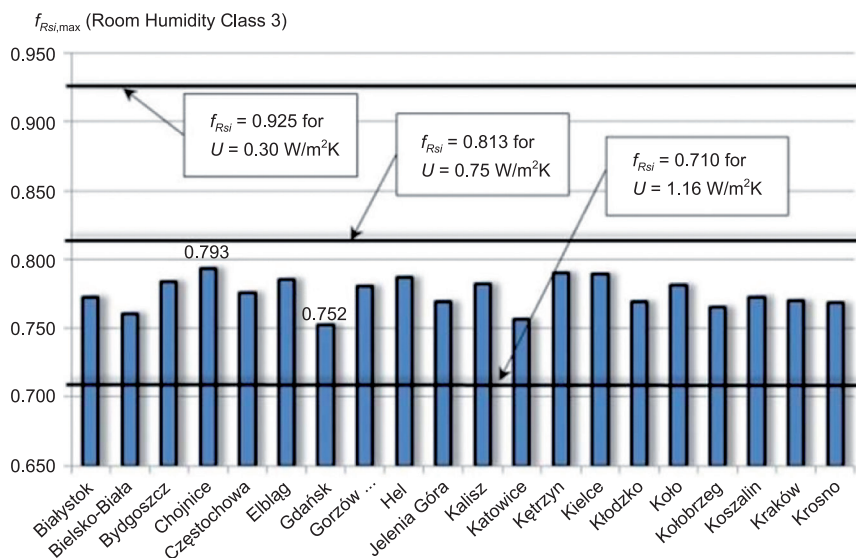


Fig. 1. Comparison of the temperature factor f_{Rsi} , determined for three types of building envelopes characterised by the heat transfer coefficient U with the maximum temperature factors $f_{Rsi,\max}$, determined for 20 meteorological stations and for room humidity class 3

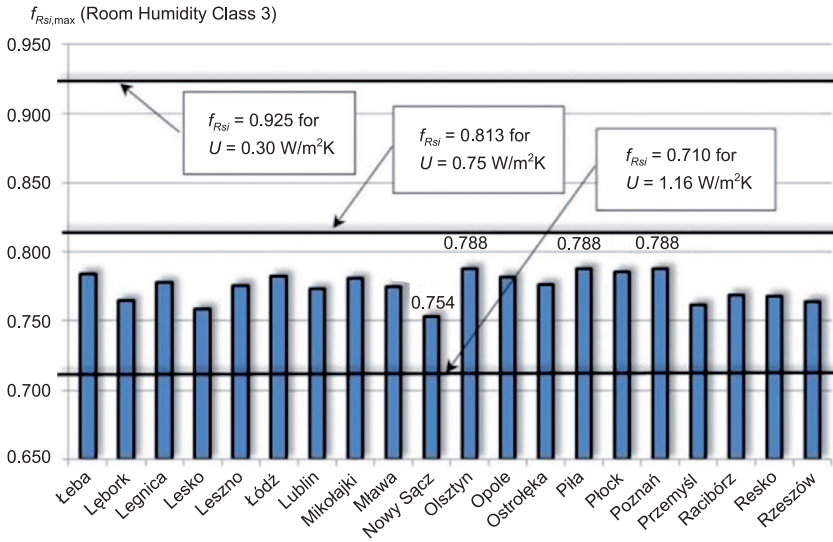


Fig. 2. Comparison of the temperature factor f_{Rsi} , determined for three types of building envelopes characterised by the heat transfer coefficient U with the maximum temperature factors $f_{Rsi,max}$, determined for 20 meteorological stations and for room humidity class 3

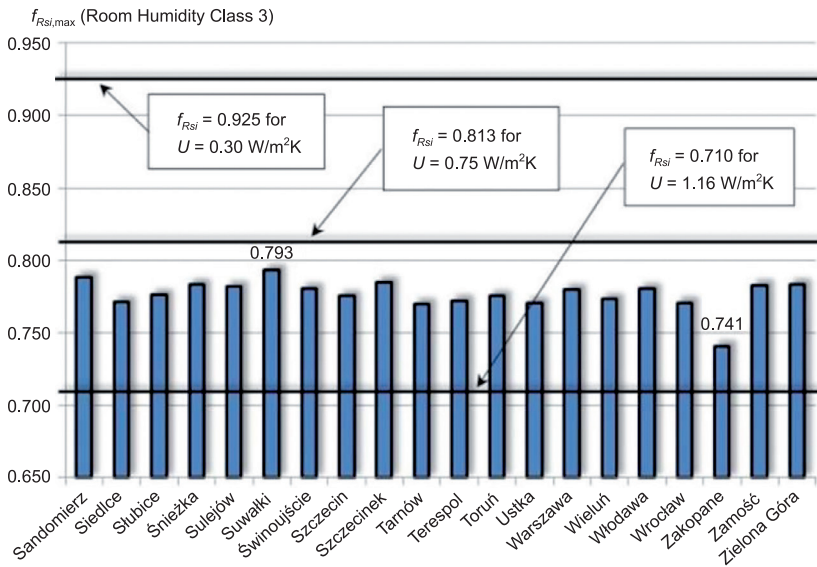


Fig. 3. Comparison of the temperature factor f_{Rsi} , determined for three types of building envelopes characterised by the heat transfer coefficient U with the maximum temperature factors $f_{Rsi,max}$, determined for 20 meteorological stations and for room humidity class 3

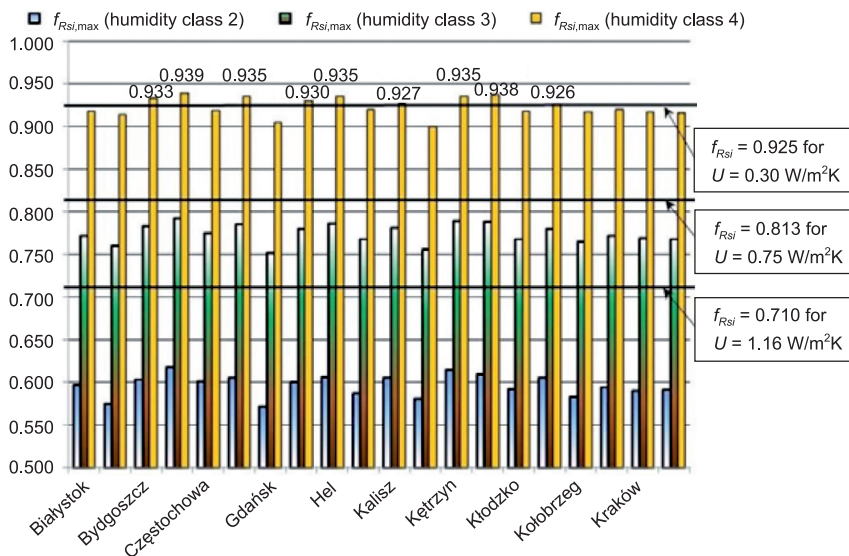


Fig. 4. Comparison of the temperature factor f_{Rsi} determined for three types of building envelopes characterised by the heat transfer coefficient U with the maximum temperature factors $f_{Rsi,max}$ determined for 20 meteorological stations, depending on room humidity class

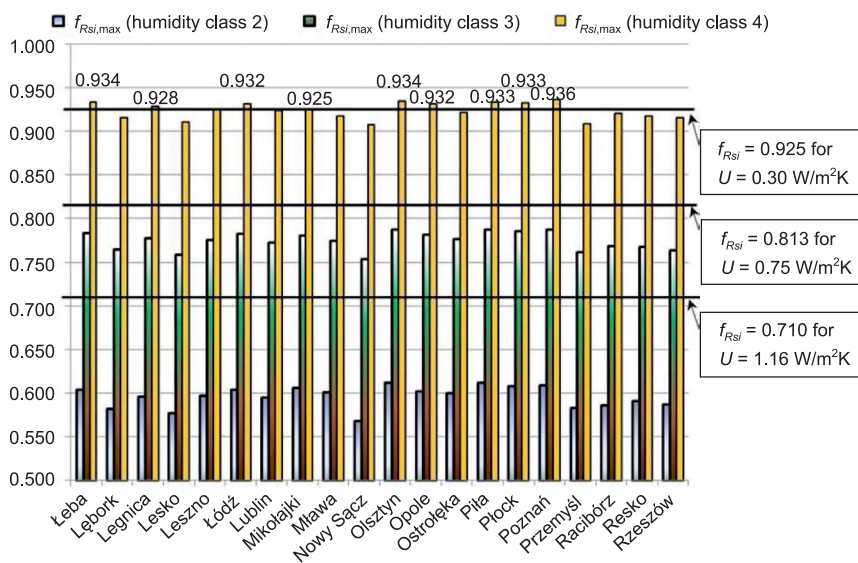


Fig. 5. Comparison of the temperature factor f_{Rsi} determined for three types of building envelopes characterised by the heat transfer coefficient U with the maximum temperature factors $f_{Rsi,max}$ determined for 20 meteorological stations, depending on room humidity class

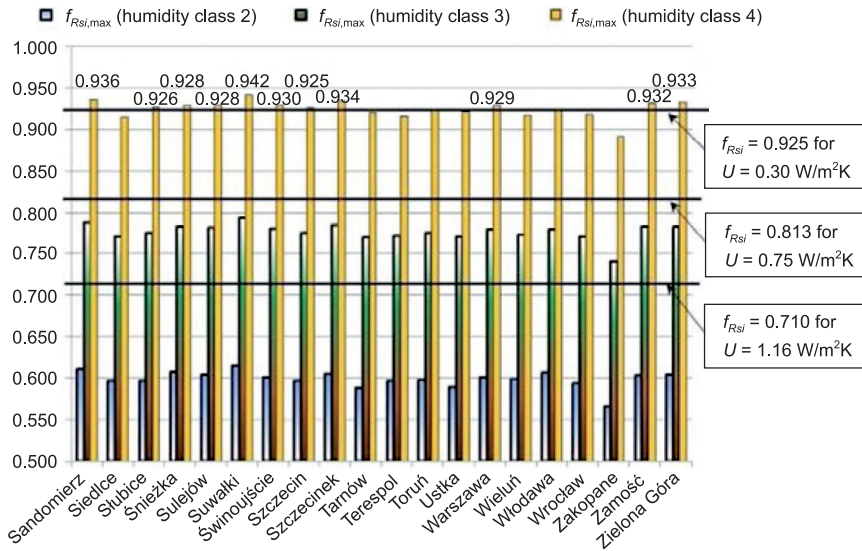


Fig. 6. Comparison of the temperature factor f_{Rsi} determined for three types of building envelopes characterised by the heat transfer coefficient U with the maximum temperature factors $f_{Rsi,max}$ determined for 20 meteorological stations, depending on room humidity class

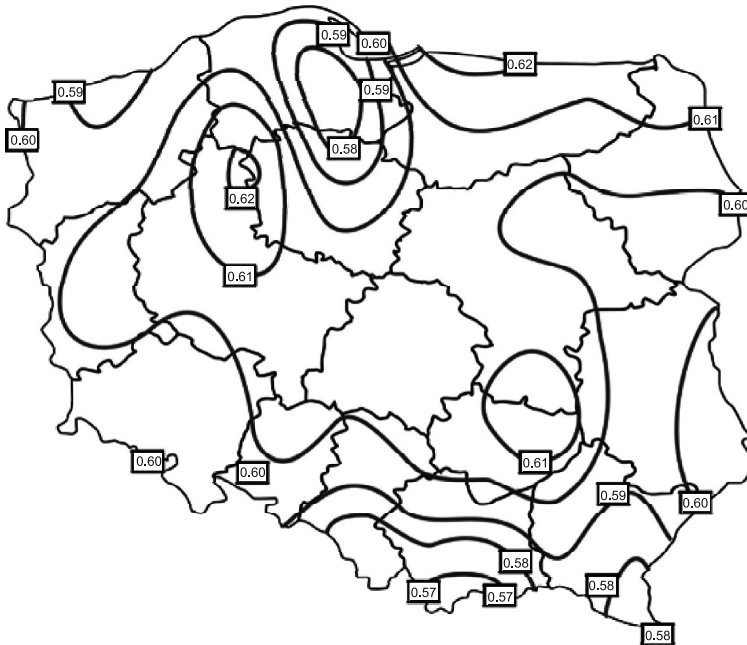


Fig. 7. Isolines of the temperature factor $f_{Rsi,max}$ for humidity class 2

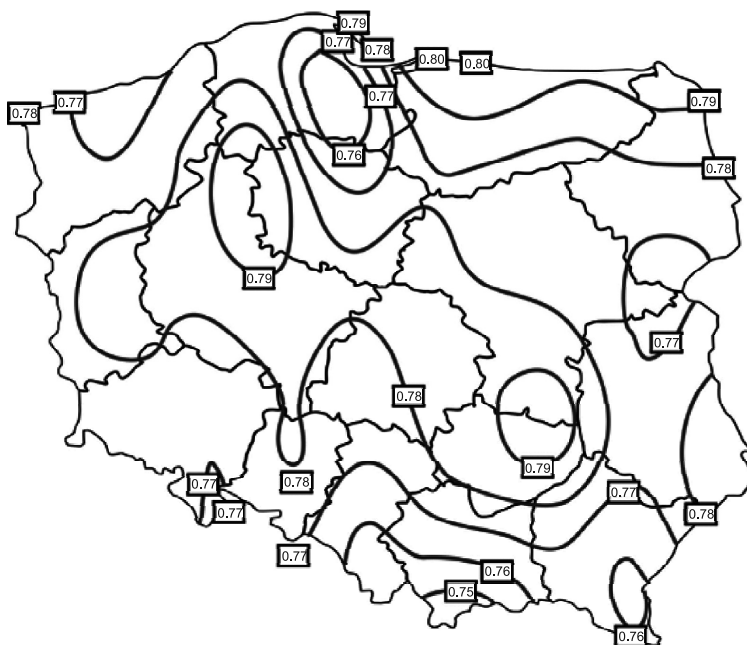


Fig. 8. Isolines of the temperature factor $f_{Rsi,max}$ for humidity class 3

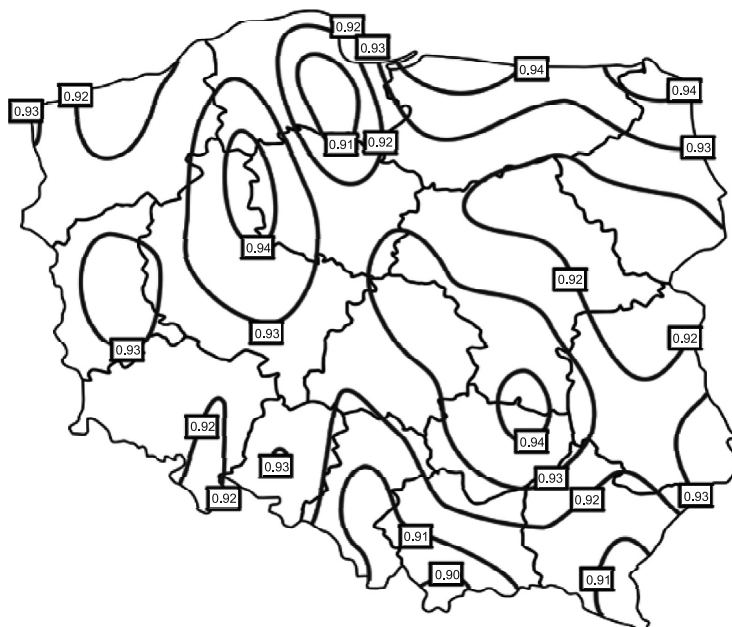


Fig. 9. Isolines of the temperature factor $f_{Rsi,max}$ for humidity class 4

References

- [1] Fischer H.M., Jenish R., Klopfer H., Freymuth H., Richter E., Petzold K., *Lehrbuch der Bauphysik*, B.G. Teubner, Stuttgart 1997.
- [2] Klemm P. (ed.), *Building Construction*, Vol. 2, Arkady, Warszawa 2005 (in Polish).
- [3] Sanders C., *Thermal Bridges at Junctions and Openings*, UK conference on thermal bridging, Part L & Thermal Bridging – Getting In Right?, BRE Garston UK, 24th May 2002.
- [4] Narowski P., *Climatic data for building energy calculations in Energy and buildings*, 2008, 9 (18), 18-24, 9 (in Polish).
- [5] Schellen H., *Thermal insulation and moisture problems*, Eindhoven University of Technology. Text of the presentation at the Spring School of Building and Environmental Physics, Karpacz 1991.
- [6] Regulation of the Minister of Infrastructure dated 12 April 2002 (as amended) on the technical conditions to be met by buildings and their location (Journal of Laws No. 690, pos. 75).
- [7] Regulation of the Minister of Infrastructure dated 6 November 2008 (as amended) on the technical conditions to be met by buildings and their location (Journal of Laws No. 201, pos. 1238).
- [8] PN-EN ISO 13788:2003 – Hygrothermal Performance of Building Components and Building Elements. Internal Surface Temperature to Avoid Critical Surface Humidity and Interstitial Condensation - Calculation Methods.
- [9] PN-EN ISO 10211:2008 – Thermal Bridges In Building Construction – Heat Flows and Surface Temperatures - Detailed Calculations.
- [10] PN-EN ISO 6946:2008 – Building Components and Building Elements – Thermal Resistance and Thermal Transmittance – Calculation Method.
- [11] http://www.mir.gov.pl/budownictwo/rynek_budowlany_i_teknika/efektywnosc_energetyczna_budynkow/typowe_lata_meteorologiczne/strony/start.aspx

MARIA FIERTAK*, TERESA STRYSZEWSKA*, STANISŁAW KAŃKA*

THE SUSTAINABLE CONSTRUCTION INDUSTRY VS. THE FINAL PHASE LIFE CYCLE ASSESSMENTS OF THE INTERNAL LAYER OF INDUSTRIAL CHIMNEYS

ZRÓWNOWAŻONE BUDOWNICTWO A KOŃCOWA FAZA CYKLU ŻYCIA WNEŹRZA KOMINÓW PRZEMYSŁOWYCH

Abstract

The properties of ceramic construction materials used in industrial facilities are constantly changing during the second Life Cycle Assessment (LCA) phase which relates to the accumulation of harmful substances. These materials are scrapped during subsequent maintenance, upgrade or demolition of the facility and their harmful properties may impact entire ecosystems. This means that the final phase of the LCA in such facilities involves waste products that are difficult to reuse or neutralise due to the polluting effect of the harmful substances they contain. This problem with the final phase of an LCA is highlighted by the example of an industrial chimney in Poland with a height of 160 m. During modernisation, after 30 years of service, the chimney was updated by processes that include the exchange of the thermal insulation of mineral wool and the ceramic liner (made of ordinary bricks bound with cement mortar), which were replaced with foam glass and a liner with acid-resistant bricks layed with silicate putty, respectively.

Keywords: industrial chimney, demolition, construction waste, LCA

Streszczenie

Na etapie remontu, modernizacji czy też rozbiórki obiektu budowlanego wiele materiałów, z których są wykonane, staje się odpadami niosącymi realne zagrożenia dla środowiska. Jest to związane z procesem akumulacji w drugiej fazie LCA substancji zagrażających środowisku. W artykule wykazano, że w ostatniej fazie cyklu życia obiektu budowlanego powstają odpady trudne zarówno do ponownego wykorzystania, jak i utylizacji, ze względu na stopień zanieczyszczenia substancjami szkodliwymi dla człowieka i ekosystemu.

Słowa kluczowe: kominy przemysłowe, wyburzenie, odpady budowlane, LCA

DOI: 10.4467/2353737XCT.15.075.3875

* Prof. Maria Fiertak, Ph.D. Eng. Teresa Stryszewska, Ph.D. Eng. Stanisław Kańka, Institute of Building Materials and Structures, Faculty of Civil Engineering, Cracow University of Technology.

1. Introduction

Currently, when designing a building or structure, attention needs to be paid to the environmental impact that the construction would have on the site in question; although the primary focus is durability, it is equally as important for an account of the influence construction has on the environment to be included [5, p. 18-21; 17, p. 105-110; 14]. This effect starts early at the stage of selecting and obtaining raw materials, it continues through to the preparation of land, which introduces significant changes to the local ecosystem, and is finally concluded at the time of demolition and the effective utilisation and disposal of waste [1, p. 23-38; 16]. Generally, the disposal of scrap material after demolition has not been taken into consideration in recent years. Primarily, projects have focused on aspects of the bearing capacity and usefulness of the structure, but with time, more attention is also being paid to durability with regards to the environment in which it will be used [7, p. 38-39].

Taking into account the life cycle of the raw materials used in the building process, construction waste can be divided into two categories [21]:

- waste which is created during the production process of the construction work, the production of products or the construction works,
- waste which arises from the demolition of the object.

The discussion below deals with the problems of environmental pollution associated with the second category – that of waste generated during demolition – and will be presented with the selected example of industrial chimneys. This example has been chosen as it represents a type of industrial chimney currently utilised throughout Poland.

Industrial chimneys commonly use a ceramic liner to protect the concrete of the chimney shaft against the effects of aggressive flue gases aiding them in securing a relatively long life [11, 22]. However, as practice shows, a ceramic liner – especially that which is made from ordinary bricks – gradually degrades as a result of the impact of discharged flue gases [8, p. 91-98; 3, p. 55-58; 2, p. 219-220].

These flue gases include: carbon dioxide, sulfur oxides, nitrogen oxides and fluorine oxides. When these components come into contact with water vapor, oxidation occurs and they transform into sulphates, nitrates and chlorides, respectively. During the transportation of flue gases through the interior of the chimney, a proportion of these compounds penetrates into the porous structure of the ceramic bricks and accumulates within them. Structures implementing binded are also subject to this destructive effect as they often allow for the easy migration of harmful substances into the chimney shaft. After decades of use, it is typical for a significant accumulation of these harmful substances to have occurred. Furthermore, in addition to the fly ash collected by electrostatic precipitators, there is a thick layer of ash that is not captured and builds up on the liner of the chimney. This fly ash is eventually embedded into the liner and this creates the need to replace the lining.

Thus, beyond the economic aspect associated with the cost of replacing the lining and the organisational issues resulting from the need to maintain the continued use of the chimney, there is the additional problem connected with the utilisation or disposal of the demolished ceramic liner.

It should be noted that both brick and ceramic binding materials are at risk of containing compounds that are a direct threat to the environment. During many years of use, and as

a result of the impact of discharging flue gases, many substances embed into the porous structure of ceramic bricks, mortar and isolation [9, 12, 15]. In fact, none of these compounds have a neutral effect on the environment – this hinders attempts at finding safe alternatives for waste management. These problems also arise during the demolition of industrial concrete chimney shafts [6]. Figure 1 shows the interior of a chimney, construction waste resulting from the demolition of the structure or its element (removal of the inner layers) and a photo of the demolished chimney.

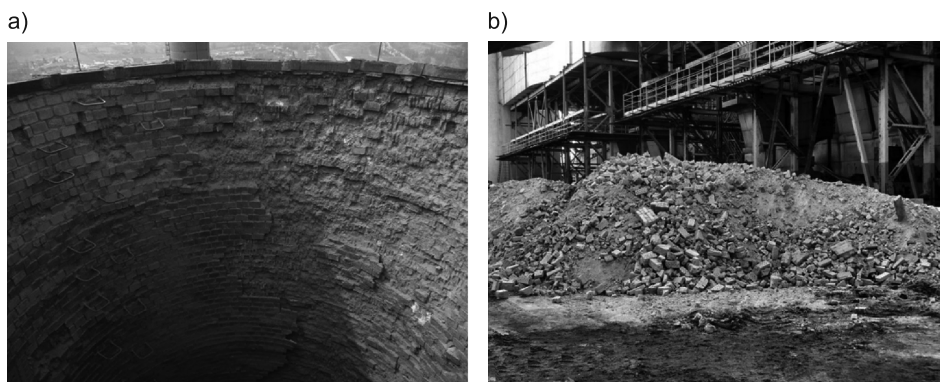


Fig. 1. Construction waste: a) the interior of the chimney, b) the ceramic liner removed from the chimney

After the demolition of the liner, the space unveils (opens) itself, which hitherto was practically closed between the hearth and a chimney liner, which was originally occupied by the thermal insulation. In many cases, when the space of a chimney that has had a long life is examined, the insulation is found to be heavily damaged and filled with precipitates which are the products of the corrosion of the insulation, concrete and ceramic brick [19, p. 378-386]. The occurrence of this type of waste material after the modernisation of the lining or demolition of a chimney liner carries the risk of having a negative impact on the environment. In particular, these compounds contribute to acidification and the salinisation of soil and groundwater, inserting hazardous substances into the ecosystem of plants, animals and humans [13; 18, p. 2032-2040; 23, p. 737-749].

Research findings of examined industrial chimneys indicate that both the ceramic bricks and the binding mortar become contaminated [10]. Evidence for this is understood by changing pH levels and increased levels of sulphate and chloride ions in both of the tested materials. Furthermore, the level of contamination of ceramic bricks, binding material and thermal insulation is significantly different. An analysis of the results carried out by examining 15 chimneys helped to systematise the available information [9]. Due to the different degrees of contamination, the received results are shown in the form of histograms. The frequency distributions of the quantitative contamination of the material were prepared and are presented in Figs. 2–4. Intervals of occurrence were chosen in this way to illustrate the gradual build-up of the content of chlorides and sulphates in the lining materials of the chimney.

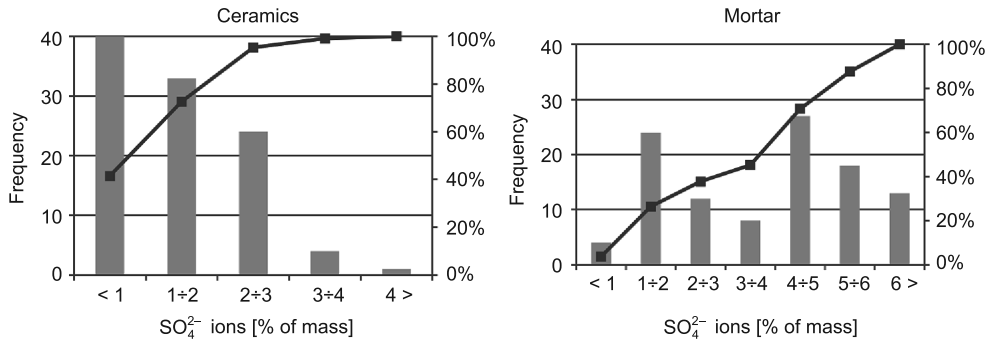


Fig. 2. The frequency distribution of occurrence, defined by intervals, the content of sulphate ions in the ceramics and mortar. Number of samples $n = 106$

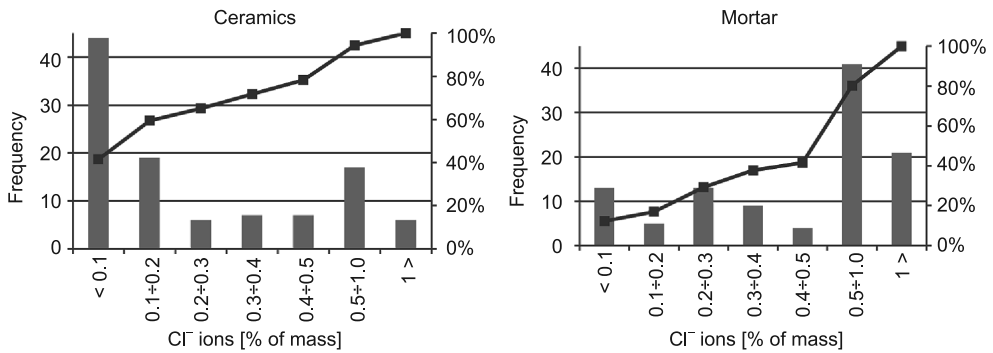


Fig. 3. The frequency distribution of occurrence, defined by intervals, the content of chloride ions in the ceramics and mortar. Number of samples $n = 106$

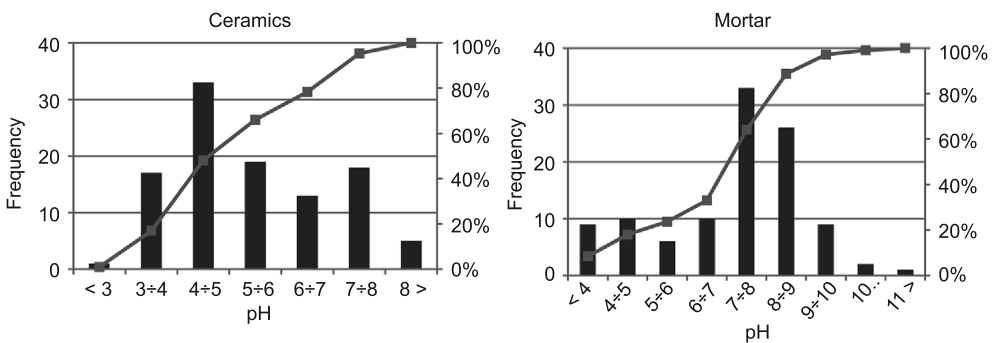


Fig. 4. The frequency distribution of occurrence, defined by intervals of the pH in aqueous extracts of ceramics and mortar. Number of samples $n = 106$

The data explains that the problem which the accumulation of harmful substances in materials has at the time of partial or complete demolition of an industrial building is the danger that the contaminated waste poses for the environment.

Based on the histograms of frequency of occurrence in the defined ranges of the content of sulphate ions, it was found that in 95% of tested ceramic samples, the content of SO_4^{2-} does not exceed 3%. However, in the mortar, in 62% of tested samples the content of sulphate ions exceeds 3% by weight of the binder. The analysis of histograms concerning the frequency of occurrence of the content of chloride ions shows that among the tested samples of bricks, 63% of them contain occurrence of Cl^- at a level of 0.2% by weight, whereas in the case of mortar, 62% of samples include Cl^- more than 0.3% by weight of binder.

Distribution of values of the pH of ceramics in the analysed chimneys indicates that it has been contaminated by acidic corrosion products (78% had a $\text{pH} < 7$). It can be concluded that the porous structure of these materials accumulates a significant amount of aggressive ingredients discharged from flue gases. Similarly, the distribution of the pH of the cement mortar, where cement was mainly used as a binder, indicates that the mortar was significantly contaminated. The dominant pH value is within the range of 7 to 9, which indicates that the accumulation occurs in the binder and, in a sense, neutralisation (inactivation) of the aggressive components of the flue gases discharged through the chimney.

2. Materials

The results of research presented in this article concern a chimney of 160m, in which the scope of modernisation, after 30 years of utilisation, includes the exchange of the exploited thermal insulation of mineral wool and ceramic lining ceramic brick binding with ordinary cement mortar.

This paper deals with free-standing industrial chimneys. Such chimneys are constructed with concrete cores converging towards the top which are protected inside by thermal insulation and a ceramic liner. Figure 5 shows a schematic cross-section of an industrial

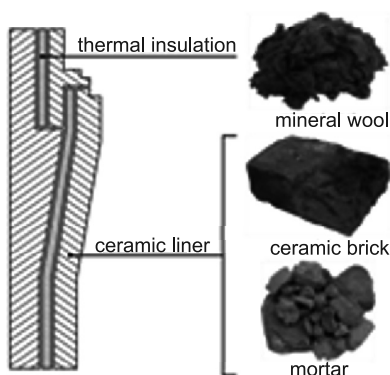


Fig. 5. Schematic cross-section of chimney and pictures of materials

chimney and its materials. Table 1 presents the weight of the ceramic lining removed from the chimney including the mass fraction of ceramic bricks and the binding material and the mass of the thermal insulation which was originally applied.

Table 1

Presentation of the mass of materials inside the chimney

Level [m]	Surface of the linear ceramic [m ²]	Weight mortar [t]	Weight ceramic [t]	Weight thermal insulation [t]
147–157	176	10.0	30.1	3.7
137–147	185	10.6	31.6	3.9
127–137	194	11.0	33.1	4.0
117–127	202	11.5	34.5	4.2
107–117	210	12.0	35.9	4.4
97–107	217	12.4	37.2	4.5
87–97	226	12.9	38.6	4.7
77–87	234	13.3	40.0	4.8
67–77	247	14.1	42.1	5.1
57–67	266	15.1	45.4	5.5
47–57	283	16.1	48.4	5.8
37–47	300	17.1	51.3	6.2
27–37	317	18.1	54.3	6.5
17–27	332	18.9	56.8	6.8
7–17	355	20.2	60.7	7.3
sum	3744	213.3	639.9	77.1

As a result of the demolition of the degraded inner layers of the chimney, 930 tons of construction waste were created, including 640 tons of contaminated ceramic bricks, 213 tons of mortar and 77 tons of damaged mineral wool. Long-term use caused an accumulation of harmful substances to occur in the brick and the binding material. The materials were taken from different heights of the chimney at random so that the results obtained characterised the quantitative state of contamination of the removed inner layers.

3. Methods and apparatus for testing

The aim of this study was to determine the nature of the formed corrosion products and accumulated substances in the removed ceramic lining. Another important element of the research was to carry out a quantitative assessment of substances which are harmful to the environment. A major issue, from the point of view of the environmental impact of the scrap, was to determine the amount of substances that can be easily leached from the structure of tested materials. For this purpose, a ceramic brick and cement mortar were percolated to leach out all the substances from tested materials. The next test was to study

the structure of porosity of ceramic bricks and mortar. In order to determine the size of the pores, which is where principal pollutants accumulate, the study was conducted in two stages. The first stage involves the determination of the pore structure of the samples of a contaminated material, while the second stage involves determining the porosity of the samples after leaching (through the percolation process).

3.1. The test apparatus

X-ray studies were conducted in Diffraktometer Philips PW 1050/70 apparatus with X'Pert High Score. For this purpose, the samples were dried and crushed to a grain size less than 0.063 mm. The results were obtained in the form of diffraction patterns together with a description of crystalline phases.

Observations of the microstructure and EDS analysis were conducted with a Zeiss scanning Nova 100 microscope. Tests were carried out on fractures of samples. Photos were taken in the chosen places and an EDS point analysis was performed.

The percolation process was carried out using Soxhlet apparatus. The aim was the leaching out of substances that have accumulated over many years of exploitation of the porous structure of ceramic bricks, cement mortar and thermal insulation. In this way, three aqueous extracts were obtained which have been used in chemical analysis, the sample materials being tested in a mercury porosimeter.

The chemical analysis of the received water extracts (in the percolation process) was carried out with a spectrophotometer V-630. The aim was to determine the content of sulphate and chloride ions and the pH.

The study of the pore structure was carried out in a Quantachrome Poremaster Nova 1000e mercury porosimeter. The study involved samples containing accumulated materials and samples of the same materials after the percolation process (leaching out).

4. Results and analysis

4.1. Results of *X*-ray crystallography

The aim of the *X*-ray crystallography tests was to verify the presence of crystalline phases present in the tested materials, including substances which are corrosive. Table 2 shows the test results of the substances in question and reveals that the contaminants in the brick, binding material and thermal insulation are, for the most part, harmful to the environment [19, p. 378-386; 20, p. 282-284].

Based on the results of *X*-ray crystallography on the waste materials, traces of sulphate compounds, such as gypsum, kaledonit, ferrous sulphate, magnesium sulphate, potassium sulphate, and ettringite and alunogen were identified. Compounds of chlorine and calcium carbonate were also identified. Some compounds are sparingly slightly soluble (gypsum, anhydrite), which will slowly leach out of the material. However, there are also readily soluble compounds which, in contact with moisture or water, will dissolve quickly and easily penetrate into the ecosystem. These include magnesium sulphate or potassium sulphate, for example. These salts are a major threat to the environment and reduce the possibility of utilising the waste.

Environmentally hazardous substances identified in the inner layers of industrial chimneys

Materials	Chemical compound	Chemical formula
Ceramic brick	anhydrite gypsum kaledonit ferrous sulphate magnesium sulphate	CaSO_4 $\text{CaSO}_4 \cdot 2\text{H}_2\text{O}$ $\text{KAl}(\text{SO}_4)_2 \cdot 3\text{H}_2\text{O}$ FeSO_4 MgSO_4
Cement mortar	anhydrite gypsum calcium chloride potassium sulphate ettringite alunogen ferrous sulphate magnesium sulphate	CaSO_4 $\text{CaSO}_4(\text{H}_2\text{O})_2$ CaCl_2 K_2SO_4 $3\text{CaO} \cdot \text{Al}_2\text{O}_3 \cdot 3\text{CaSO}_4 \cdot 32\text{H}_2\text{O}$ $\text{Al}_2(\text{SO}_4)_3$ FeSO_4 MgSO_4
Thermal insulation	anhydrite alunogen ferrous sulphate magnesium sulphate hydrate gypsum carbonates, bicarbonates	CaSO_4 $[\text{Al}(\text{H}_2\text{O})_{6,12}(\text{SO}_4)_3(\text{H}_2\text{O})_5]$ FeSO_4 , $\text{FeSO}_4(\text{H}_2\text{O})_4$ $\text{MgSO}_4(\text{H}_2\text{O})$ $\text{CaSO}_4(\text{H}_2\text{O})_2$ CaCO_3 , $\text{Ca}(\text{HCO}_3)_2$

4.2. Results of Microstructural Research

The purpose of microstructural observations and EDS analysis was to identify non-crystalline (amorphous) corrosion products present in the studied materials. By using the EDS probe, a qualitative assessment of the contamination of exploited materials was possible. In representative (characteristic) places scanning photos were taken and EDS

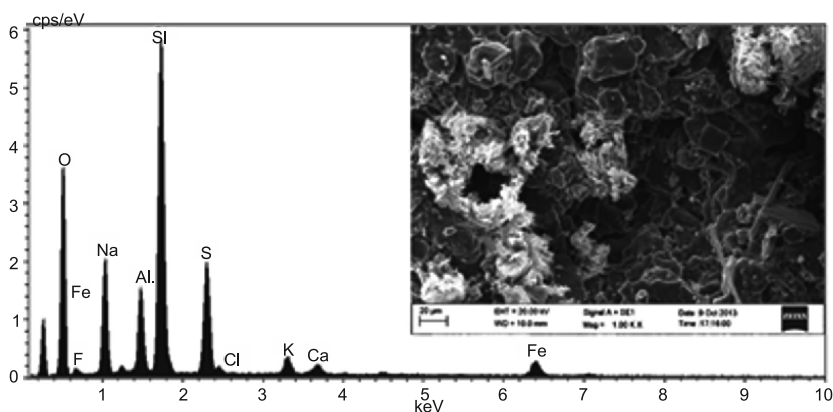


Fig. 6. Microstructure of ceramic brick and EDS analysis of the surface

analysis was performed. Sample images of the microstructure of damaged ceramic bricks, cement mortar and mineral wool observed in the SEM and EDS analysis are shown in Figs. 6–8.

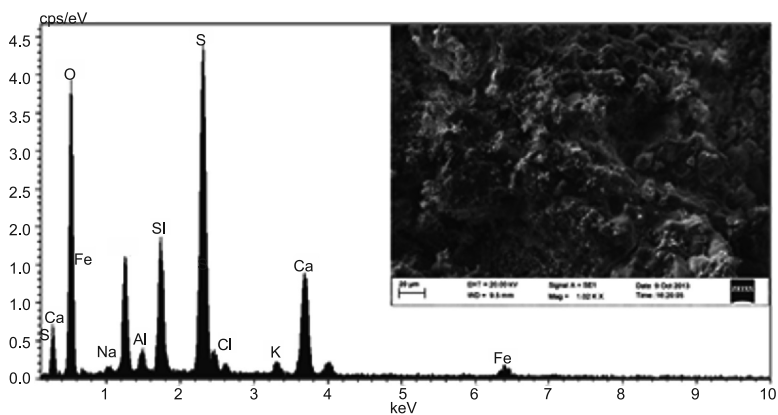


Fig. 7. Microstructure of cement mortar and EDS analysis of the surface

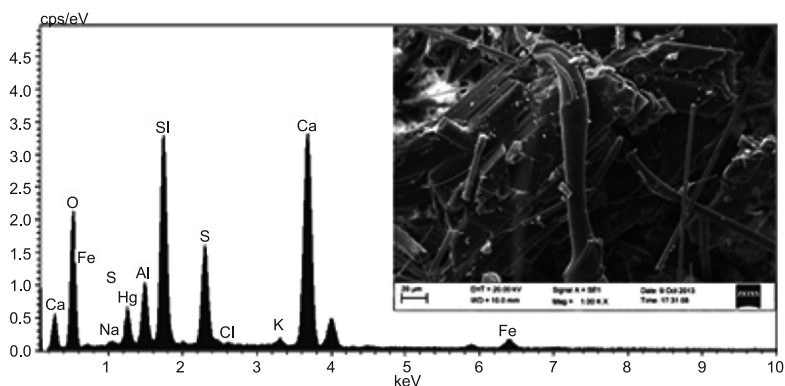


Fig. 8. Microstructure of thermal insulation and EDS analysis of the surface

Microstructural studies confirmed the presence of crystalline phases shown in *X*-ray crystallography studies. In addition, they revealed that the sulphate and chloride ions are incorporated in the form of ions in the structure of the aluminosilicate phases of ceramic bricks and in the CSH phase structure in the cement mortar. In the place of thermal insulation, numerous corrosive products containing sulphate and chloride ions in their compositions, were identified [19].

4.3. Results of quantitative and qualitative analysis

4.3.1. Content of weight of harmful substances

In the process of percolation from test materials, most of the substances which accumulated in the pores of materials were removed. On the basis of mass change before and after the process of percolation, the percentage loss of mass of the tested materials was calculated. The loss of weight obtained in this way stands for a quantitative (mass) content of substances which are a real threat to the environment, as they are leached out from the material when they come into contact with water. These are not permanently associated with any of the tested materials. The results are shown in Table 3.

Table 3

The percentage of soluble substances and the mass accumulated in the ceramic brick, cement mortar and mineral wool

Material	Ceramic brick	Cement mortar	Mineral wool
Contamination			
Amount of waste material	640 tons	213 tons	77 tons
Amount of harmful compounds that are susceptible to leaching	13.4 tons	19.6 tons	4.8 tons
Content of harmful chemical compounds susceptible to leaching	2.1% of mass	9.2% of mass	6.2% of mass

Studies have shown that most of the chemical compounds which are harmful to the environment are located in the cement mortar. Their content equals 19.6 tons. In turn, the content of these substances in ceramic brick is at a level of 13.4 tons. Additionally, in the mineral wool, which contains the smallest amount of this material, there are considerable amounts of harmful substances. This results from the fact that the space between the ceramic lining and the shaft of the chimney makes an ideal location for the accumulation of the components of discharged flue gases. When these compounds come into contact with moisture, it causes a condensation of acidic components from the flue gases to occur. As a result, it induces a strong destruction of the material in places where the so-called corrosive precipitates are formed – its main ingredients are substances considered harmful to the environment. In extreme causes, the spaces between the ceramic liners and the concrete shafts are completely filled with corrosive products.

4.3.2. Quantitative assessment of the content of sulphate and chloride ions

Solutions (extracts) obtained as a result of the percolation of brick, mortar and insulation were subjected to chemical analysis. The degree of contamination by harmful substances differentiated and depended on the material being tested. Respectively, for the ceramic bricks, mortar, and thermal insulation, are at the levels:

- 0.7%, 4.7% and 1% by weight of the material in the case of sulphate ions,
- 0.4%, 1.1% and 1% by weight of the material in the case of chloride ions.

The degree of contamination of the particular ions expressed as a percentage is relatively small, but in relation to the total weight of the liner and the insulation, gives a tremendous

amount of sulphates and chlorides, which are observed into the demolished liner and the removed insulation. The results are presented in Table 4.

Table 4

The percentage and the mass of SO_4^{2-} and Cl^- ions in materials removed from the chimney

Harmful substances \ Materials	Ceramic brick	Cement mortar	Mineral wool
Mass of waste materials	640 tons	213 tons	77 tons
Content of ions SO_4^{2-}	0.7% of mass 4.5 tons	4.7% of mass 10.8 tons	1.0% of mass 0.8 tons
Content of ions Cl^-	0.4% of mass 2.6 tons	1.1% of mass 2.5 tons	1.0% of mass 0.8 tons

The ceramic bricks contain 4.5 tons of sulphate ions and 2.6 tons of chloride ions. In total, the bricks contain nearly 7.1 tons of the substances which carry a strong threat to the environment. However, in the mortar there is 10.8 tons of SO_4^{2-} and 2.5 tons of Cl^- , and this adds up to a total of more than 13 tons. The smallest pollution comes from the thermal insulation and is 0.8 tons for both substances. Thus, in the demolished liner and damaged insulation, the total sulphate content is 16.1 tons, while the chlorides measured 5.9 tons. These numbers appear due to the fact that 67% of the sulphates were built up in the mortar, 28% in the brick and 5% in the insulation. However, the chloride ions are in a comparable amount in both the mortar and brick and equal to 42% and 44%, respectively. In turn, the thermal insulation contains 14% of all chlorides. Figure 9 shows the percentage of the content of toxic substances depending on the type of a material.

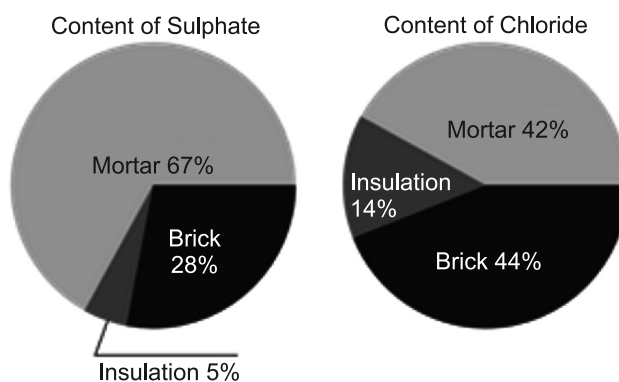


Fig. 9. Percentage of harmful chemical compounds in materials removed from the chimney

Taking into account the percentage of each ion, it was found that the most contaminated material that was removed from the chimney during the repair works is mortar – this contains 67% of sulphate and 42% of all of chloride ions. Although the binding material is

almost three times less (by weight) than the brick, it is the greatest source of the pollution of hazardous substances to the environment.

4.4. Research results of the pore structure

One of the main factors determining the corrosive resistance of ceramics is its porosity. The relatively high porosity of the material (such as an ordinary ceramic brick which is more than 30%) makes it accessible to external media (including corrosion), which facilitates the penetration and removal of corrosive products. In addition to the volume fraction of pores, their size and shape are also very important [4, 18]. Additionally, the fact that in traditional ceramics the spaces between grains are filled with corrosive products means that the situation is only aggravated. As a result of the accumulation of harmful substances in the materials of the ceramic liner, evidence suggests that the structure of porosity changes. The purpose of this research was to determine the category of the pores forming a place of accumulation of harmful substances – results are presented below. For this purpose, the mercury porosimetry method was used to determine the porosity structure of contaminated mortar and ceramic brick. Then, using a percolation method, the accumulated substances were removed from test materials and the designation of structure of porosity was re-made. The obtained results are presented in the form of a population curves determined for each test material before and after the leaching process – these are displayed in Fig. 10.

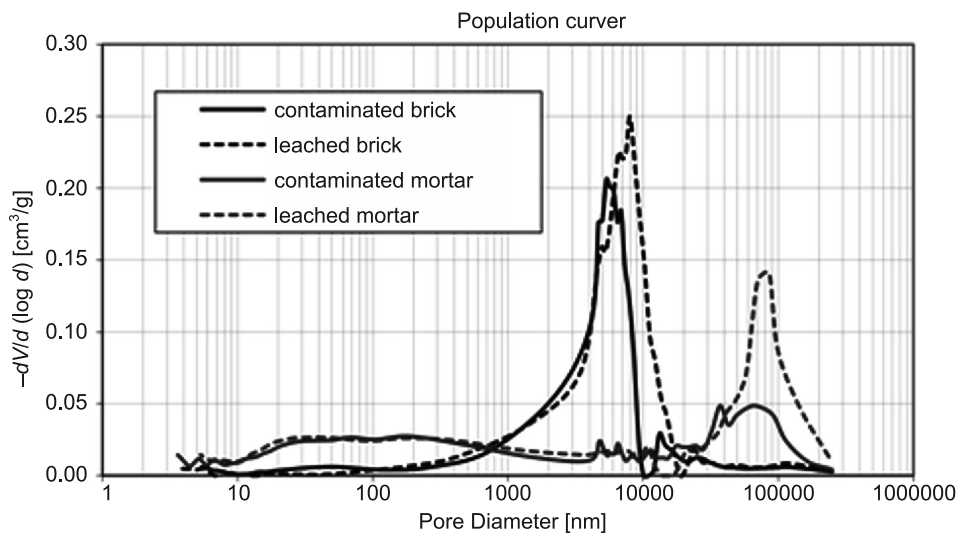


Fig. 10. Population curves of ceramic brick and mortar set before and after the process of percolation

All pores in the tested materials are categorised according to their diameters. This method of presentation of pore structure allows for the specification of the size of the pores which are dominant places for the accumulation of harmful substances in the brick and mortar. Division of the pores into categories according to their diameter are shown in Tables 5 and 6.

Table 5

Categories of pores in the ceramic brick

Ceramic brick	Leached	Contaminated
Total pore volume	0.1391 cm ³ /g 100%	0.1104 cm ³ /g 100%
Below 100 nm	0.0023 cm ³ /g 1.7%	0.0069 cm ³ /g 6.3%
100–9000 nm	0.1135 cm ³ /g 81.6%	0.0924 cm ³ /g 83.7%
9 000–20 000 nm	0.0158 cm ³ /g 11.6%	0.0049 cm ³ /g 4.5%
Above 20 000 nm	0.0075 cm ³ /g 5.4%	0.0062 cm ³ /g 5.5%

Table 6

Categories of pores in the cement mortar

Cement mortar	Leached	Contaminated
Total pore volume	0.1310 cm ³ /g 100%	0.0971 cm ³ /g 100%
Below 100 nm	0.0279 cm ³ /g 21.3%	0.0258 cm ³ /g 26.5%
100–50 000 nm	0.0578 cm ³ /g 44.1%	0.0558 cm ³ /g 57.5%
50 000–100 000 nm	0.0388 cm ³ /g 29.6%	0.0139 cm ³ /g 14.5%
Above 100 000 nm	0.0065 cm ³ /g 5%	0.0015 cm ³ /g 1.5%

As a result of the accumulation of various substances in the pores of ceramic bricks, porosity of the material has decreased by more than 20%. These changes relate primarily to the pores with diameters ranging from 100 to 100.000 nm. The accumulation of the substance leads to decrease of the pores. Thus, in the structure of ceramic brick, there is a greater quantity of smaller pores in comparison to the pore structure observed in the leached brick.

In the cement mortar, the process of accumulation of pollutant substances is also clearly visible. The porosity of the material at the time of the demolition was over 25% lower in comparison to the porosity of the material after leaching. From among all the categories of pores, the changes pertain primarily to pores having a diameter of 100 to 100 000 nm – this means that the process of accumulation of harmful substances occurs mainly in these pores.

5. Conclusions

As mentioned in the introduction, in the EU report there was a statement that of all the waste generated in the member states, 32% is as a result of activities of the construction and dismantling of buildings. They mainly consist of inert materials such as brick, ceramic tiles, asphalt, concrete, and to a lesser extent, wood, plastics and metals. Although they are characterised by relatively low levels of impact to the environment per unit of weight, construction waste is crucial in terms of waste management.

The results of research on industrial constructions presented in this paper refer to the last phase of the LCA of a building according to EN-15804. They show that the bricks, plastic, cement and mineral wool can be characterised by a high degree of pollution. It significantly hinders the process of utilization and effectively limits the directions of their reuse and disposal.

It should also be noted that demolition, which in this case is that of an industrial chimney, is inevitably associated with the production of large amounts of waste that are not neutral to humans and the environment. Because of this, it is particularly important to the development of an EU-wide market for the recycling of waste in pursuit of a closed loop economy, in which the new European standards for quality grades of recycled materials.

References

- [1] Ajdukiewicz A., *Beton a środowisko – zasady projektowania konstrukcji betonowych z uwagi na trwałość i wpływ na środowisko*, Conference Awarie Budowlane 2011, Międzyzdroje, 2011, 23-38.
- [2] Barycz S., Oruba R., *Demolition of technical worn out high reinforced concrete chimneys*, Inżynieria Środowiska, 9/2004, 219-220.
- [3] Barycz S., Oruba R., *Przykład modernizacji znacznie zużytego żelbetowego komina przemysłowego*, Przegląd Budowlany, 5/2010, 55-58.
- [4] Baszkiewicz J., Kamiński M., *Korozja Materiałów*, Warsaw University of Technology, Warszawa 2006.
- [5] Czarniecki L., Laproń M., Piasecki M., Wall S., *Budownictwo zrównoważone budownictwem przeszłości*, Inżynieria i Budownictwo, 1/2012, 18-21.
- [6] Eberle A., Barnsteine M., *Demolition and Dismantling of Chimneys*, CICIND Report, 24.02.2008.
- [7] Fangart J., *Jak zagadnienia środowiskowe zmieniają wymagania podstawowe dotyczące obiektów budowlanych? Podsumowanie*, Materiały Budowlane, 10/2012, 38-39.
- [8] Fiertak M., Kańka S., *Methods and interpretation of material testing in power sector chimneys*, Proceedings of the 5th International Conference Concrete and concrete structures, Zilina, 15–16 October 2009, 91-98.
- [9] Kańka S., *Materiałowe i eksploatacyjne uwarunkowania trwałości żelbetowych kominów przemysłowych*, Dissertation, Cracow University of Technology, Kraków 2013.
- [10] Lechman M., *Diagnostics of Masonry Chimneys used as Antenna Carrier*, CICIND Report, 24.02.2008.
- [11] Lohr R., Solar J., *Brick Liners and Chimneys ... again?*, CICIND Report, 24.02.2008.
- [12] McCauley R.A., *Corrosion of Ceramic and Composite Materials*, 2nd ed, Marcel Dekker, New York 1994.
- [13] Model Code 2010. International Federation for Structural Concrete, Lausanne 2010, Vol. 1, Bulletin 55 and 56, March, April 2010.

- [14] Noakowski P. et. al., *Wind Farms-Environmental Issues, Design, Perspectives*, CICIND Report, 25.01.2010.
- [15] Oruba R., *Oddziaływanie środowiska przemysłowego i eksploatacji górniczej na bezpieczeństwo żelbetowych kominów przemysłowych*, Monograf No. 211., AGH, Kraków 2010.
- [16] PN-EN 15804 Sustainability of construction works – Environmental product declarations – Core rules for the product category of construction products.
- [17] Rakhshan K., Friess W.A., Tajerzadeh S., *Evaluating the sustainability impact of improved building insulation: A case study in the Dubai residential built environment*, Building and Environment, 67/2013, 105-110.
- [18] Roussat N., Méhu J., Abdelghafour M., Brula P., *Leaching behaviour of hazardous demolition waste*, Waste Management, 28/2008, 2032-2040.
- [19] Stryzewska T., Kańska S., *Osady zalegające przestrzeń pomiędzy trzonem a wykładziną źródłem zagrożenia konstrukcji żelbetowych kominów przemysłowych*, Materiały Ceramiczne, 3/2013, 378-386.
- [20] Stryzewska T., *Mechanizm korozji cegły ceramicznej w kominach energetycznych*, Ochrona przed korozją, 6/2011, 282-284.
- [21] Środowisko Europy – stan i perspektywy 2010, Raport KE Zrównoważone Budownictwo w UE, 2012.
- [22] The CICIND Chimney Book. CICIND, Zurich 2005.
- [23] Watt D., Colston B., *Investing the effects of humidity and salt crystallisation on medieval masonry*, Building and Environment, 35/2000, 737-749.

ALEKSANDRA GRYC*, JAN RADOŃ*, GRZEGORZ NAWALANY*

MEASUREMENTS AND CALCULATIONS
OF TEMPERATURE IN THE GROUND
AND IN ASSEMBLIES ADJACENT
TO AN INTERMITTENTLY HEATED BASEMENT

POMIARY I OBLICZENIA TEMPERATURY
W GRUNCIE I PRZEGRODACH
W PIWNICY OGRZEWANEJ OKRESOWO

Abstract

Cellars of the main building of the University of Agriculture in Krakow are used as storage areas, laboratories and as classrooms. This article presents the results of many years of temperature measurements in one cellar room; internal and external air temperature as well as temperatures of the walls, the floor and adjacent ground were recorded. In the winter season, the examined room was intermittently heated. Using measured boundary conditions, transient, three-dimensional heat flow in the basement foundation interface was calculated. WUFI@Plus software was used for calculation. By means of statistical analysis, the calculated temperature distribution in assemblies and the ground was then compared with the measurement results. The analysis allowed for the determination of the accuracy of theoretical calculations of thermal conditions in the environment of the periodically heated cellar room.

Keywords: ground, heat flow, measurements and calculations, intermittent heating

Streszczenie

Piwnice w budynku głównym Uniwersytetu Rolniczego w Krakowie są używane jako magazyny, laboratoria oraz sale lekcyjne. Artykuł prezentuje wyniki wieloletnich pomiarów w pomieszczeniu piwnicznym; temperatury powietrza wewnętrznego i zewnętrznego, ścian, podłogi oraz w gruncie. W ziemi piwnica była ogrzewana z przerwami. Obliczenia trójwymiarowego, niestacjonarnego przepływu ciepła wykonano, wykorzystując pomierzone warunki brzegowe. Do obliczeń zastosowano program WUFI@Plus. Wyniki pomiarów i obliczeń temperatury w przegrodach i gruncie porównano statystycznie. Wyniki pozwoliły określić dokładność obliczeń warunków termicznych wokół piwnicy okresowo ogrzewanej.

Słowa kluczowe: piwnica, grunt, przepływ ciepła, pomiary i obliczenia, ogrzewanie okresowe

DOI: 10.4467/2353737XCT.15.076.3876

* Ph.D. Aleksandra Gryc, Ph.D. Jan Radoń, Ph.D. Grzegorz Nawalany, Dept. of Rural Building, Faculty of Environmental Engineering and Land Surveying, University of Agriculture in Cracow.

1. Introduction

In addition to active heating systems, the ground and the external climate are factors affecting heat and moisture phenomena in buildings. Most of the external partitions are in contact with the outside air; however, some of the rooms have partitions adjacent to the ground – these can be not only floors, but also, external walls if the building is recessed in the ground. If the room has more than 70% of the walls adjacent to the ground, it is defined as a basement.

If the ground and water conditions allowed, cellars were usually included in buildings. Initially, these were for the purpose of storing fuel and keeping food products, mainly due to their favourable hygrothermal parameters. Cellars in modernised buildings are now often adapted for use as storage rooms, offices, service rooms, commercial rooms or even for residential purposes. New buildings are often designed as partially recessed in the ground.

The ground is an additional kind of barrier between the internal and external environment of the building and to some extent, reduces heat loss. The large heat capacity of the ground environment stabilises the temporary heat balance of the room by taking heat in times of internal air temperature increase and by releasing it back during periods of lower temperature. These phenomena, to some extent, lead to a reduction of the room's demand for heating and cooling energy. An additional effect is a positive impact on the microclimate. In summer, the temperature of ground surrounding the building is lower and in winter, it is higher than the external air temperature.

Today, in order to reduce energy consumption, intermittent heating and/or variable heating power is commonly used. The switching on and off of heating systems causes fluctuations in the internal air temperature of the room – this results in a significant, temporary heat exchange between partitions and the ground. The heat flow in partitions and the ground is transient and due to the geometry, three-dimensional; therefore, in most cases, it cannot be analysed in stationary terms.

The aim of the experimental measurements and calculations was the recognition of temperature in the environment of cellar rooms being periodically heated over the period of the whole year. Ground surface near to the building ascends 1.5m embankment like and becomes flat at a distance of about 5m.

Experimental measurements were constantly performed in the years from 2007 to 2015. Results from the period from 2007–2009 were used to evaluate the thermal comfort of the room, as well as to analyse the thermal and humidity conditions in the basement [2, 3]. This paper presents the results of comparative calculations made by means of the WUFI®plus software. Calculations include the period from 2010–2014. The article provides detailed measurement and calculation results for the years 2010 and 2011 and the results of the statistical, comparative analysis for this period. The aim of the study was the determination of the possibilities of using the model and the WUFI®Plus software to calculate the thermal conditions in the room and the ground. The program was previously validated in terms of standards [1] for thermal bridges and by the analysis of the passive house foundation interface [4]. However, the case of the floor below grade and inclination of the near ground surface, has not yet been analysed.

2. Methodology of experimental measurements and calculations

The object of the research is a basement room of the main building of the Agricultural University, built in the nineteen-sixties, used today as laboratory and teaching space. The basement walls are made of solid brick with plaster on both sides with a total thickness of 0,55 m. The floor is made of PVC tiles lying on a concrete slab with a thickness of 10 cm. Thermal insulation of basement walls or floor has not been applied. A horizontal section of the basement and investigated room is shown in Fig. 1.

On the partition surfaces of the tested room and in the surrounding ground, 20 PT 100 resistive sensors of TOP 106 type [5] (accuracy ± 0.15 K) were located. Additionally, the same sensors were installed to measure the inside and outside air temperature. The results were recorded at 15 minute intervals in the memory of a MPS-1 recorder [6], linked to two 8-channel loggers. The basement geometry and the arrangement of measurement points are shown in Fig. 2.

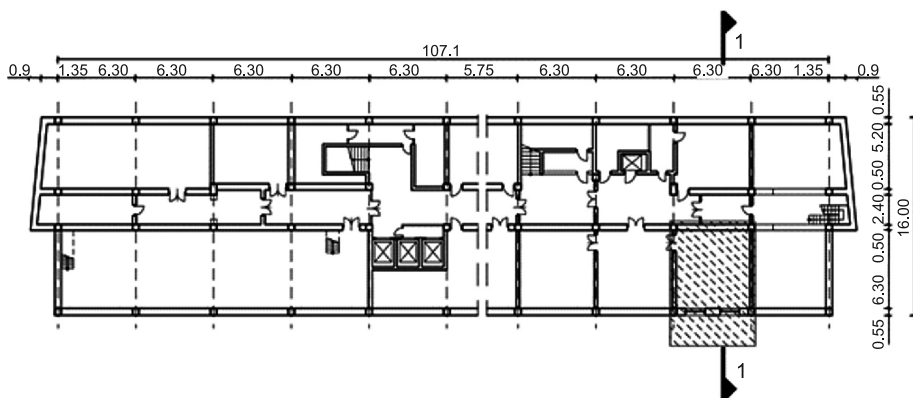


Fig. 1. Investigated cellar room

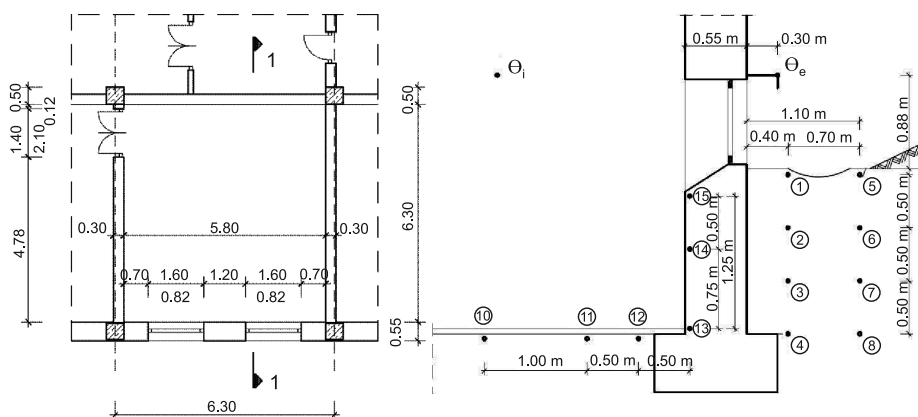


Fig. 2. Basement geometry and location of measurement points

The WUFI@Plus software [7] was used for the calculations – this allowed performing the thermal and energy analysis of the building in transient conditions. The program allowed the calculation of the transient heat balance (heated area) with full thermal coupling with the ground. Visualisation of the examined room, heat conducting space and boundary conditions is shown in Fig. 3, this was made with WUFI@Plus software.

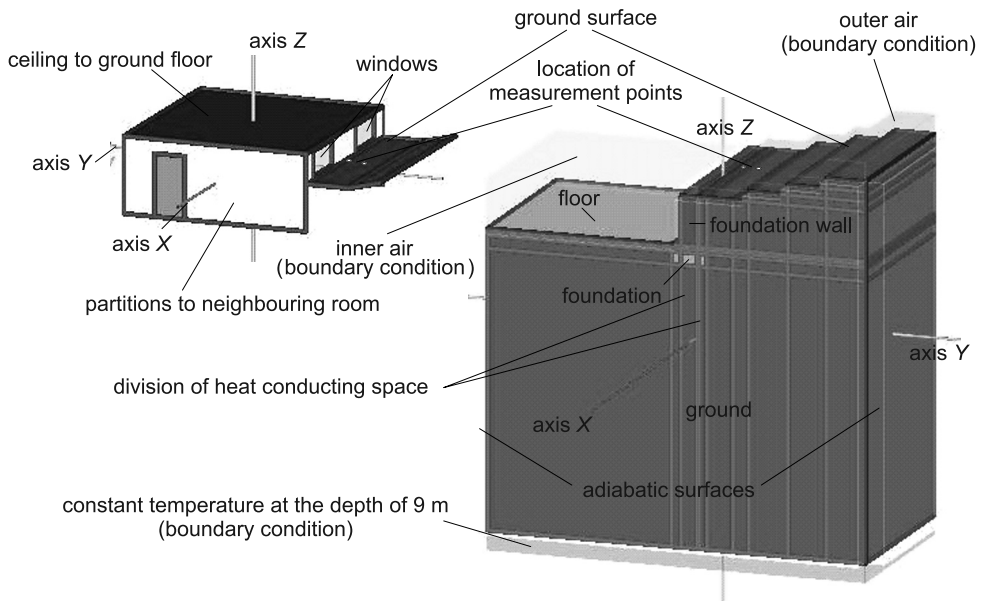


Fig. 3. Calculation room and ground model

It was assumed that within the particular assembly (wall, floor, ground), the thermal properties of the material continuum are homogeneous and isotropic. Ground surface inclination was modelled geometrically with steps. The basic data of the room is summarised in Table 1. Construction of partitions and adopted material parameters are shown in Table 2. The window parameters in the tested room are summarised in Table 3.

The calculation of heat flow in the partitions and the ground was made for the entire measurement period. Air temperature measured inside and outside the room was used as a boundary condition. Heat exchange coefficients were assumed according to PN-EN ISO 6946 standard. Other factors, such as wind and solar radiation, were omitted – these parameters were not measured. However, it should be noted, that the ground surface outside the tested room is shaded from sunlight and to some extent, sheltered from the wind.

The results of calculations of the temperature in the walls and the ground were compared with the results of measurements and analysed statistically. The following measures were used: the arithmetic mean, minimum, maximum, quartiles and also standard deviation as a measure of differentiation.

In order to determine the correlation, a Pearson test was used when the variables were normally distributed, and a Spearman test, when the variables were not normally distributed.

For all conducted tests, a level of significance of $\alpha = 0.05$ was adopted. Normality of distribution of the variables was checked by means of a Kolmogorov-Smirnov test. For statistical calculations, the STATISTICA program, version 10, was used.

Table 1

Room parameters used in the calculation

Specification	Unit	Value
Net volume	[m ³]	89.52
Floor area	[m ²]	36.54
Wall surface adjacent to the ground	[m ²]	11.59
Exterior wall area (to outer air)	[m ²]	3.43
Window area	[m ²]	2.62
Internal walls:		
– wall adjacent to the library		15.44
– wall adjacent to the corridor	[m ²]	14.21
– wall adjacent to the teaching room		12.50
Inner door	[m ²]	2.94
Internal heat source (1 adult working 8 ⁰⁰ –16 ⁰⁰)	[W]	80/41*
Maximum power of the radiators in the room	[kW]	2.6
Computational internal temperature	[°C]	20

* Convection part/radiation part

Table 2

Arrangement of layers (from inside to outside) and material parameters

Specification material/layer	Thermal conductivity λ [W·m ⁻¹ ·K ⁻¹]	Heat capacity c [J·kg ⁻¹ ·K ⁻¹]	Bulk density ρ [kg·m ⁻³]	Thickness [m]
Outer wall				
Cement-lime plaster	0.85	840	1850	0.02
Solid brick	0.8	870	1770	0.51
Cement-lime plaster	0.85	840	1850	0.02
Moisture insulation on glue	0.18	1460	1000	0.003
Floor				
PCV floor covering	0.2	1460	1300	0.004
Concrete	1.8	850	2200	0.1
Other				
Ground	1.6	1430*	1950	–

* Includes 15% of the ground moisture in the natural state

Window parameters in the test room

Parameter	Unit	Value
The heat transfer coefficient U	$\text{W}\cdot\text{m}^{-2}\cdot\text{K}^{-1}$	2.6
Framework coefficient f'_R	–	0.7
Average coefficient of solar radiation transmission T_R	–	0.65

3. Measurement and calculation results

As already mentioned (Introduction), calculations were performed for the years 2010 and 2011. Fig. 4 shows the example results of the calculation of the temperature pattern at two measuring points against the measurement results.

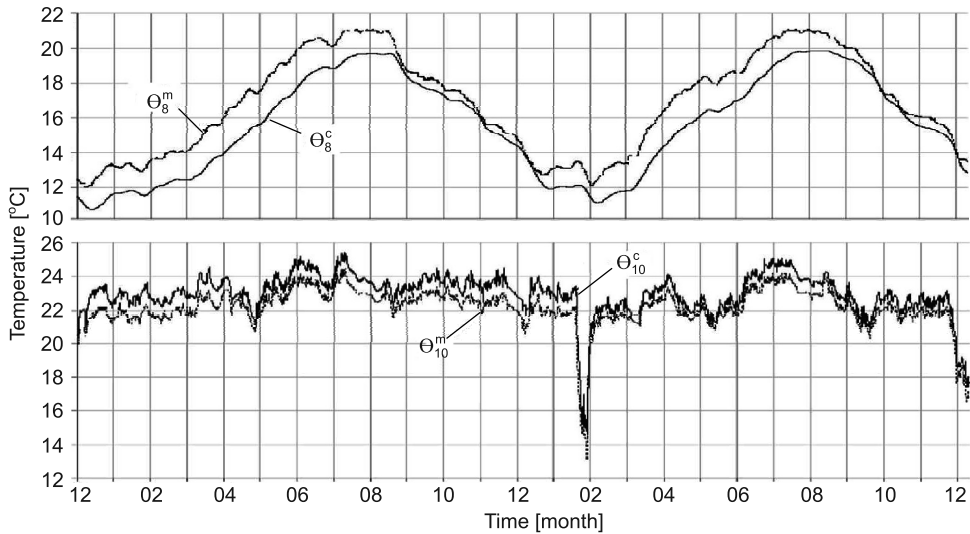


Fig. 4. The course of the temperature measured and calculated at measuring points 10 and 8 in 2010 and 2011. Upper indicators m and c indicate the temperature as measured and calculated, respectively

Point number 10 is in the middle of the floor of the room (Fig. 2). It can be seen that in this case, the influence of the boundary condition is stronger. Whereas, point number 8 is significantly further away from both the room and from the ground surface (outside air). Agreement of calculation and measurement results is usually stronger for points which are located 'closer' to boundary conditions. This is also confirmed in the case of other measurement points.

It can be seen (Fig. 4) that in February 2011, there was a fall in temperature for approximately 2 weeks – this was caused by switching off the heating in the room during

the winter holidays. If no heating is available, the temperature in the room is shaped passively as a result of the instantaneous heat balance (heat exchange with partitions and ventilation). Figure 5 shows the course of the internal air temperature and the temperature at measuring points 8 and 10 against the outside air temperature with particular emphasis put on the cut-off period.

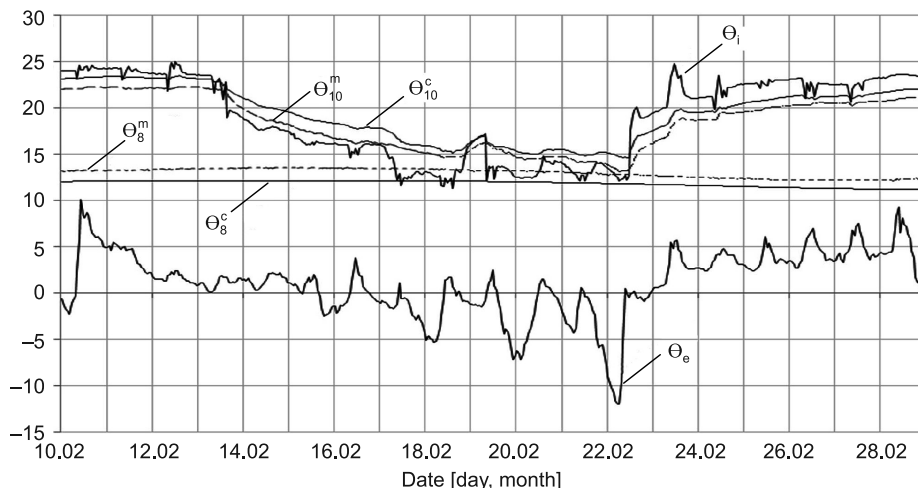


Fig. 5. The pattern of the temperature measured and calculated at measuring points 10 and 8 in February 2011. Θ_i – inside air temperature, Θ^m – temperature measured in the ground and the floor, Θ^c – temperature calculated in the ground and the floor, Θ_e – outside air temperature

A large thermal inertia causes a slow decrease of the air and ground temperature. At the beginning, heat flowed from the partitions and the ground to the internal air; within two weeks, the air temperature decreased from above 20°C to about 12°C. The floor temperature (measuring point 10) decreased along with the air temperature, but it remained higher by approx. 2°C. The dynamics of the temperature decrease diminished with time. After turning on the heating, there was a rapid increase in air temperature. This time, the floor temperature was lower than the air temperature by approx. 2.5°C. After turning on the heating, the floor and the ground take heat from the indoor air. At measuring point number 8 (1.65 m away from the room) no effect of switching off the heating was observed. Analysis of the temperature in the remaining sections allows us to state that the spatial scope of the thermal effect caused by the two weeks switching off is about 1 m.

The coincidence of calculations and measurements results was determined by statistical analysis of value pairs (see section 2). The results in terms of the average value, minimum, maximum, lower and upper quartile are illustrated in the so-called box diagram (Fig. 6). The correlation is shown in Table 4.

Figure 6 reveals that the results for the measurements and calculations are very similar both in terms of value and amplitude. Maximum differences do not exceed 5°C. Deviations in terms of the lower and upper quartiles are less than 2°C. The correlation is highly

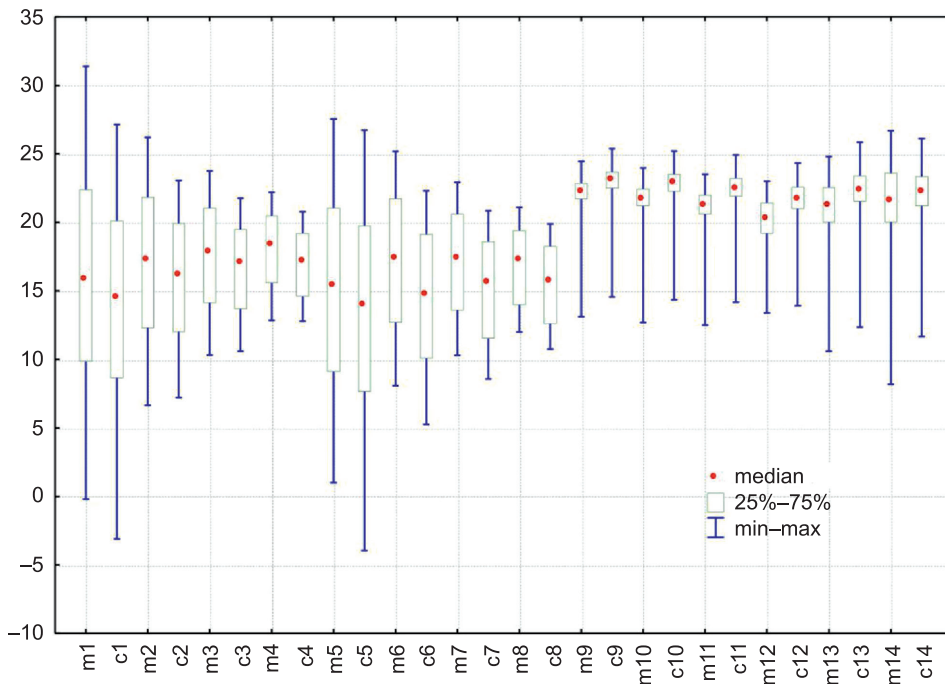


Fig. 6. Statistics of the results of calculated (c) and measured (m) temperature at particular measurement points

Table 4

Correlation between measured and calculated patterns

Measurement point	Correlation coefficient
1	0.9906
2	0.9853
3	0.9826
4	0.9690
5	0.9953
6	0.9951
7	0.9870
8	0.9753
10	0.9753
11	0.9691
12	0.9612
13	0.9235
14	0.9529
15	0.9491

significant at all measurement points. This means that the calculated courses of temperature are closely related to the measurement. At measuring points 3, 4, 7 and 8, the differences between calculation and experimental results are slightly greater than those at other measurement points. These points are further away from the boundary conditions, which are internal and external air temperature. The calculation results at these points are more dependent on physical properties of the ground such as conductivity and heat capacity.

The accuracy of calculations, in terms of coincidence can be improved by the so-called model calibration, which includes adaptation of material parameters and boundary conditions. However, the purpose of this article is to show the accuracy which can be obtained by assuming simplified boundary conditions (omission of radiation and the effect of wind on the exchange of air) and homogeneous, consistency over time, and estimated thermal properties of partitions and the ground.

4. Conclusions

This paper presents results of long term measurements and calculations of temperature and heat flow in the assemblies and ground in the vicinity of an intermittently heated cellar. Measurements were made under real operating and climate conditions. During the whole measurement period, a great thermal stabilising effect caused by the ground was observed.

During 2 weeks heating cut off, inner air temperature dropped from 20 to 12°C, whereas set point temperature was reached within 1–2 days after heating was switched on. The floor temperature remained higher (by approx. 2°C) during cut off and lower (by approx. 2.5°C) than the air temperature. It could be estimated that approximately 1m ground thickness exchanged heat with inner air during this period.

Results of comparative calculations with measured air temperatures as boundary conditions showed strong agreement with measurements. Maximum, absolute differences did not exceed 5°C. The correlation was highly significant at all measurement points. Calculation accuracy was slightly better in points located geometrically nearer to the boundary conditions. However, calculation results, obtained with estimated material properties of assemblies and the ground, correctly reflect the thermal performance of a cellar room and heat exchange with the surrounding soil.

References

- [1] Antretter F., Pazold M., Radon J., Künzel H., *Kopplung von dynamischer Wärmebrückenberechnung mit hygrothermischer Gebäudesimulation*, Bauphysik, 35, 2013, Heft 3, 181-192.
- [2] Gryc A., Radoń J., *Ocena komfortu cieplnego pomieszczenia biurowego w piwnicy w świetle badań eksperymentalnych*, Ciepłownictwo, Ogrzewnictwo, Wentylacja, 42/5, 2011, 217-219.
- [3] Gryc A., Wąs K., Radoń J., *Experimental research on thermal conditions in intermittently heated basement*, Infrastructure and Ecology of Rural Areas, 12/2011, Commission of Technical Rural Infrastructure, Polish Academy of Sciences, 2011, 135-145.
- [4] Radoń J., Wąs K., Flaga-Maryńczyk A., Antretter F., *Thermal performance of slab on grade with floor heating in a passive house*, Technical Transactions, 3-B/2014, 405-413.

- [5] KFAP, *Resistance sensor of type TOP 106*, Krakowska Fabryka Aparatów Pomiarowych S.A., Information Flyer, 2003.
- [6] ProgStar, MPS-1. Register memory. Zakład Elektroniki, Automatyki i Informatyki. User's guide, 2007.
- [7] WUFI®, <http://www.wufi.de>

MAŁGORZATA JANUS-MICHALSKA*, DOROTA JASIŃSKA*

A COMFORT COMPARISON OF A FOAM SEAT AGAINST A SEAT WITH AN AUXETIC SPRING SKELETON

PORÓWNANIE KOMFORTU SIEDZISKA FOTEŁA PIANKOWEGO I SIEDZISKA O SZKIELETCIE AUKSETYCZNYM

Abstract

This paper presents a comfort analysis of two different office chair types. The first is made of foam and the second is comprised of auxetic springs with foam upholstery. Several steps of quasi-static loads are chosen for comfort analysis in order to assess the dependence of measures of comfort on the mechanical properties of the applied structural solutions. Numerical analysis is performed by means of ABAQUS software – this allows the comparison and selection of optimal structures with respect to comfort requirements.

Keywords: seat structure, FEM modelling, comfort analysis

Streszczenie

W artykule przedstawiono analizę komfortu dwóch siedzisk foteli biurowych o różnych konstrukcjach. Pierwsze siedzisko jest typowym piankowym, drugie jest konstrukcją złożoną ze szkieletu o połączonym układzie sprężyn poliamidowych pokrytych pianką wyściełającą. Analizę komfortu i jego zmienności przeprowadzono dla kilku stadiów obciążenia kwazistatycznego, co pozwoliło na określenie jakościowych zależności między własnościami mechanicznymi zastosowanych strukturalnych rozwiązań a miarami komfortu. Zamodelowano struktury siedziska fotela biurowego za pomocą MES w środowisku ABAQUS. Analiza wyników pozwala oszacować przydatność zastosowanych rozwiązań konstrukcyjnych pod względem spełnienia warunków projektowych komfortu użytkownika.

Słowa kluczowe: siedzisko fotela, analiza komfortu, modelowanie MES

DOI: 10.4467/2353737XCT.15.077.3877

* Ph.D. Eng. Małgorzata Janus-Michalska, Ph.D. Eng. Dorota Jasińska, Institute of Structural Mechanics, Faculty of Civil Engineering, Cracow University of Technology.

1. Introduction

A variety of materials with differing mechanical properties are used nowadays for designing composite structures in order to achieve special requirements. Existing solutions are replaced with new ideas which can be easily verified through numerical prototypes, which can be created whilst avoiding the cost of experiments on real structures. Innovative solutions are based on designers' engineering intuition.

One of the new smart materials which can introduce untypical mechanical properties is negative Poisson's ratio material (NPR material). The term 'auxetics' relates to negative Poisson's ratio materials due to the fact that they expand in a perpendicular direction when subjected to a tensile load. Auxetic materials are of particular interest due to their counterintuitive behaviour and improved properties such as enhanced strength, fracture toughness, energy absorption and indentation resistance [1, 2]. Auxetic materials can be used for a wide range of applications: auxetic fibers, threads, technical textiles, fasteners, shock absorbers, sound absorbers, curved body parts for the aerospace industry, wing panels, protection materials for the construction of crash helmet, protective clothing, car bumpers and also furniture. Different types of auxetic materials include auxetic bio-materials, auxetic foams, auxetic honeycombs, auxetic microporous polymers, auxetic structures and auxetic composites. On a macro scale, we can use NPR structures to obtain effects similar to micro-mechanical effects. Auxetics change contact pressure distribution and can be useful for reducing peak contact pressure. The behaviour of NPR materials has been examined in the context of the contact problem before the idea of its application in the design of office seats [5]. Literature on the application of auxetic skeleton structures in office chairs has been written by Smardzewski, Jasińska, Janus-Michalska [6–9]. Negative Poisson ratio materials have been also investigated with regard to quasi-static and dynamic indentation compliances [2, 3], and also to indentation resilience [2]. It has been shown that indentation and impact compliances are significantly affected when Poisson's ratio of the material assumes negative values [2]. Indentation resilience of auxetic materials are strongly strain dependent according to a study presented by Alderson et al [2]. It was found that the auxetic material was more difficult to indent than the other materials at low loads.

Seating comfort is an important factor used to distinguish competitive products in the furniture industry. The literature attempting to correlate seat comfort with interface mechanical measures is not extensive. Some indications of optimal seat modelling for achieving seating comfort are described by Verver et al [15]. The relationship of comfort with interface pressure is described by Looze [10]. Experimental investigation of the interaction between driver and seat and numerical analyses of pressure distribution have been carried out by Montmayeur et al. and Xiaoming et al [16]. Attempts at identifying relationships between seat pressure and comfort were described by Oudenhuijzen [11]. For furniture seats, as opposed to car seats, similar analyses were carried out by Smardzewski J., Prekrat S. [12], Smardzewski et al. Jasińska et al. [13].

This paper presents a numerical study of pressure distribution with respect to comfort for two different seat structures. The first is a typical structure made of foam and the second is comprised of auxetic springs with foam upholstery. These examples have been previously studied in the context of the application of auxetic elastic media to the contact problem [9].

The current study is devoted to comfort analysis. Comfort requirement is not only important for the maximal load for which the structure is designed, but also for intermediate stages. The study concerns quasi-static loading or loads not reaching the maximal value. The designed seats should be comfortable for users with a wide range of weight and duration of sitting. Several steps of quasi-static loads are chosen for comfort analysis in order to assess the dependence of measures of comfort on the mechanical properties of the applied structural solutions. Clear differences are identified between the foam seat and the seat with an auxetic skeleton with respect to comfort.

2. Mechanical measure of comfort

Stress distribution induced by load is complex due to the occurrence of non-uniform pressure, pinch shear and horizontal shear stress. Shear stresses of both kinds cause discomfort. To measure discomfort caused by nonuniformity of contact pressure, the seat pressure distribution coefficient SPD is defined as follows [13]:

$$SPD = \frac{\sum_{i=1}^n (p_i - p_m)^2}{4n p_m^2} \cdot 100\%. \quad (1)$$

where:

- p_i – contact stress in point i ,
- p_m – mean contact stress for n points,
- n – number of points of registered or calculated contact pressure.

The latest mechanical measure of sitting discomfort based on the analysis of contact stress and verified experimentally was proposed in work by Smardzewski et al [13]. It is defined as scalar D given according to the following formula:

$$D = \frac{p_m}{A} \cdot SPD \quad (2)$$

where:

- A – contact area

In the ideal situation, the uniform distribution of contact stress SPD coefficient equals zero and the seat is at its most comfortable on the condition that the mean contact pressure is not higher than the critical value. A near uniform pressure distribution also reduces shear. To reduce discomfort, it is recommended to make contact surfaces with a low friction coefficient. The contact area should be as maximal as possible.

3. Two types of seat structures

A foam seat and a seat with an auxetic skeleton are considered in this study. The first seat (seat A) is of a typical design and is made of components described in Fig. 1. A cross-section of the seat is presented in the figure.

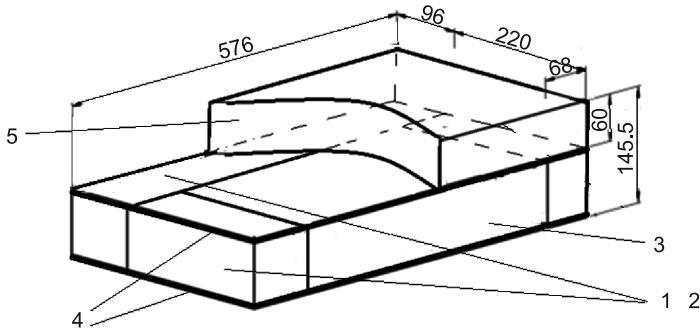


Fig. 1. Cross-section of the foam seat (seat A). Seat components: 1, 2 – frames, 3 – foam filling, 4 – upper and bottom layers of felt, 5 – seat upholstery (dimensions [mm])

The main load bearing section of the second seat is a set of springs arranged as a skeleton spatial framed structure. For the purpose of contact stress distribution, the skeleton is chosen as it is a structure with an auxetic. The shape of the auxetic spring is shown in Fig. 2.

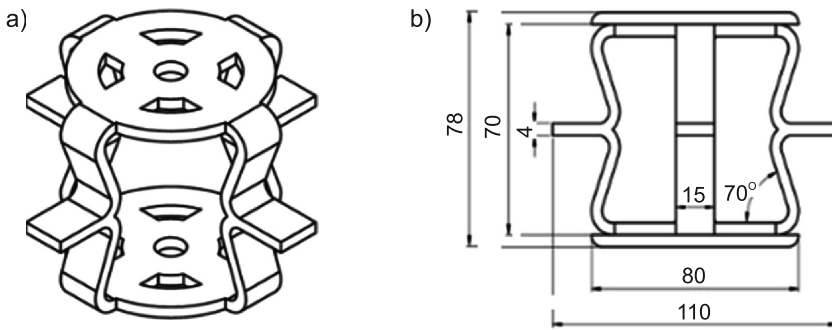


Fig. 2. Auxetic spring: a) spring shape, b) spring (dimensions [mm])

The components of the seat with the skeleton (seat B) are shown in Fig. 3.

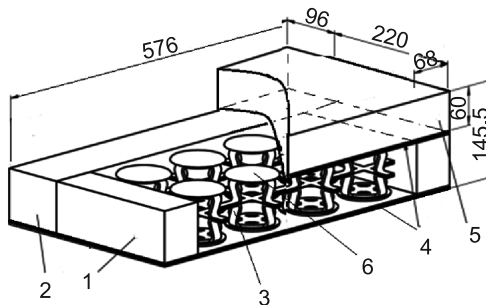


Fig. 3. Seat structure (seat B): 1, 2 – seat frame; 3 – spring, 4 – felt, 5 – foam upholstery, 6 – cover of spring (dimensions [mm])

4. Mechanical properties of seats' structural components

The chosen materials for both seats have properties as described in Table 1.

Table 1

Mechanical properties of the materials of the seats' structural elements

Structural element	Material	Elastic properties
Foam filling (seat A)	Foam T3037	Nonlinear characteristic Fig. 4
Spring (seat B)	Silicon Shore's 75	Mooney-Rivlin hyper-elastic model $E = 9.32$ MPa, $K_0 = 77.7$ MPa, $C_{10} = 1.05$, $C_{01} = 0.30$
spring cover (seat B)	Rubber Shore's 95	Mooney Rivlin hyper-elastic model $E = 21.80$ MPa, $K_0 = 18.16$ MPa, $C_{10} = 16.91$, $C_{01} = 55.35$
Seat frame	Foam T3546	Nonlinear characteristic Fig. 4
Seat upholstery	Foam T3037	Nonlinear characteristic Fig. 4
Aligning layer	Felt	Linear elastic $E = 2.58$ kPa, $\nu = 0.3$

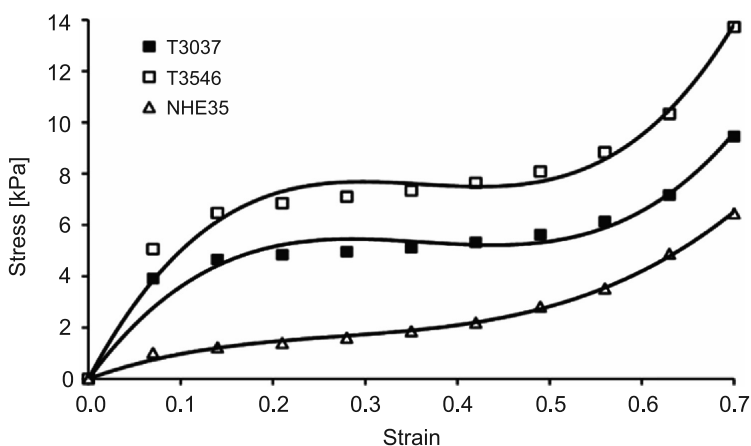


Fig. 4. Seat foam and seat upholstery foam characteristics obtained from experiment

Foam stiffness has been established in compression test according to standard PN-EN ISO 3386-1:2000/A1:2010E [17].

Spring elements are modelled as hyper-elastic materials with strain energy given by formula (3):

$$U = C_{10}(I_1 - 3) + C_{01}(I_2 - 3) + \frac{K_0}{2}(J_{el} - 1)^2 \quad (3)$$

where:

- C_{10} , C_{01} , K_0 – material parameters for silicon [9, 13],
- I_1 , I_2 , J_{el} – deviatoric strain first and second invariant and elastic volume ratio.

The human body is modelled by timber oak indenter used in experiments [13]. The elastic material data are: $E = 12 \text{ GPa}$, $\nu = 0.3$.

5. Numerical simulation and finite element model

Numerical simulation of the indentation test is carried out by means of ABAQUS FEA [19]. A static incremental load was applied to the rigid indenter up to a load of 790 N representing the weight of a human body. A nonlinear analysis involving material and geometric nonlinearity with the contact problem is performed. As a result of the analysis, seat characteristics and maps of contact stress distribution in subsequent stages are obtained. This allows for the calculation of discomfort coefficient. For this purpose, author FORTRAN codes were developed.

The described spatial models are imported into the ABAQUS FE analysis software package. Due to symmetry, it was only necessary to analyse half of the structure. The following discretisation was applied:

Seat type *A*:

56000 8-node linear brick elements with reduced integration, modelling aligning foam and frame foam, 2400 3-node triangular facet rigid elements for model of indenter.

Seat type *B*:

spring skeleton – 94000 10-node quadratic tetrahedron elements, frame and aligning foam – 82200 8-node linear brick elements, felt – 5100 4-node quadrilateral membrane elements, indenter– 2400 3-node triangular facet rigid elements,

Boundary conditions:

elements stuck together: frame parts, frame and felt, spring and disc, parts of seat frame.

Contact conditions:

contact of the indenter with the seat is frictionless.

6. Results

The stiffness characteristics of the two analysed structures are shown in Fig. 6. The structures are chosen in such a way that load – displacement curves are very similar. It allows comparing the discomfort of seats with similar indentation resistance.

For both seats, comfort analysis is carried out in the chosen four stages with loads of the following values: 200 N, 400 N, 600 N, 790 N.

The author's program in Fortran code is applied to calculate the following comfort parameters: mean contact stress, contact area, seat pressure distribution coefficient and discomfort coefficient.

Maps of normal stresses in subsequent stages of quasi-static load for the foam seat and for the auxetic seat are shown in Fig. 6. and 7. Comfort parameters are given below the maps of stresses.

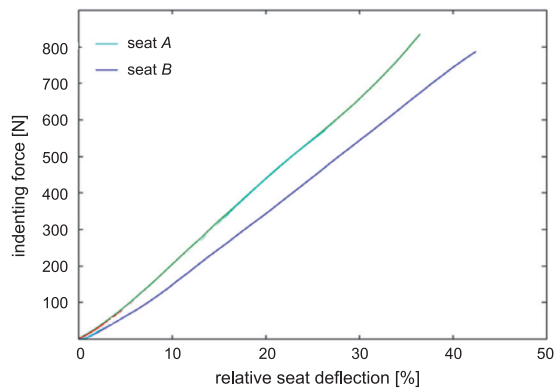


Fig. 5. Seat stiffness characteristics

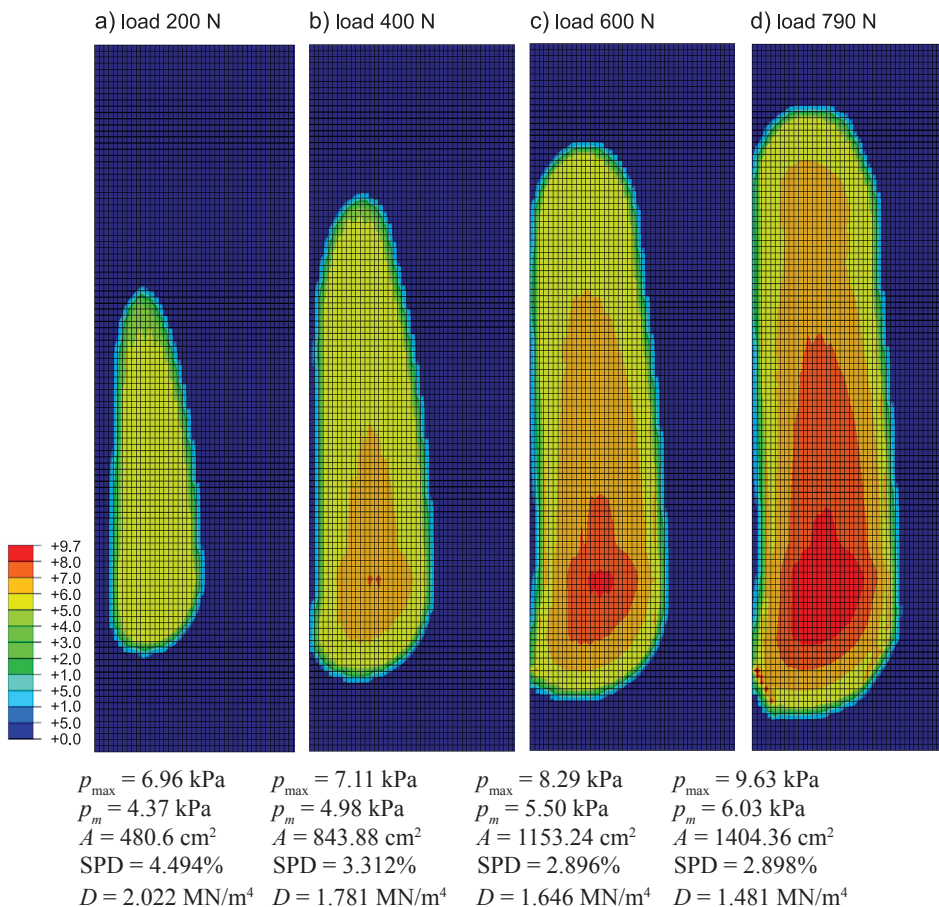


Fig. 6. Contact pressure maps for foam seat [kPa] and comfort parameters

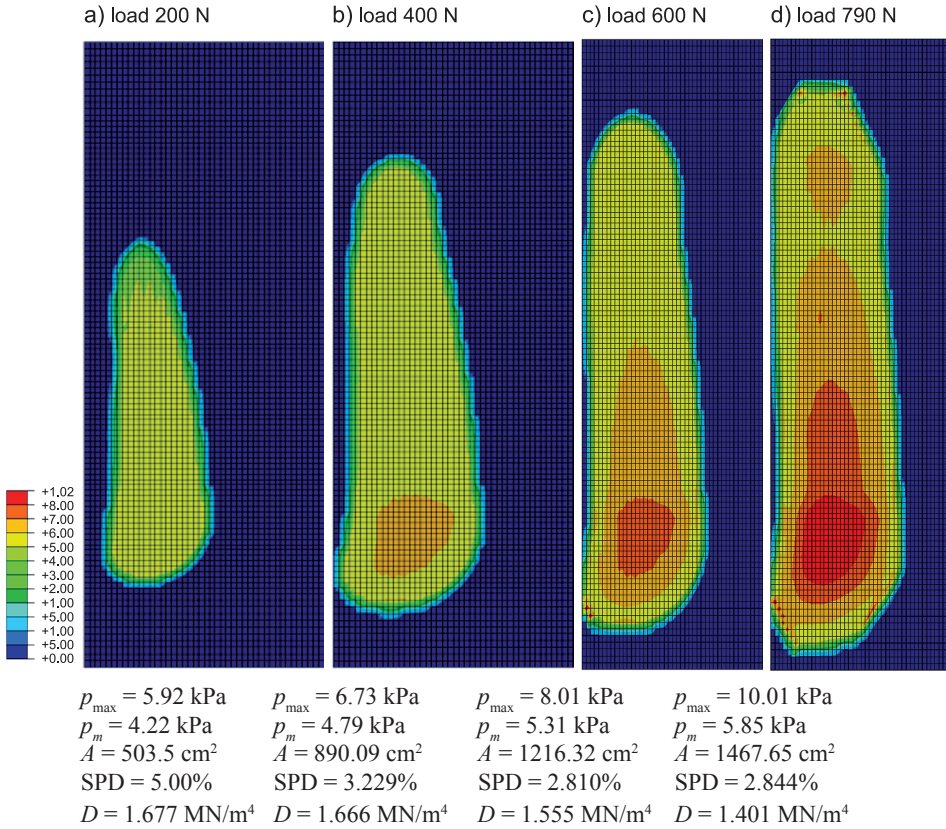


Fig. 7. Contact pressure maps for auxetic seat [kPa] and comfort parameters

A detailed analysis of all maps of normal stresses and comfort parameters leads to the general observation that the auxetic seat provides similar levels of comfort across the full range of loads. For all stages, the difference between p_{\max} and p_m is smaller than for the foam seat – this means that the distribution of contact stress is more uniform. Moreover contact area for auxetic seat is greater. Both of these two factors increase the comfort of the auxetic seat and as a result, make it more comfortable than the foam seat. Auxeticity has an influence on indentation resistance, so we expect comfort dependence on the negative of Poisson's ratio of applied auxetic materials or structures.

The foam seat becomes more comfortable with greater loads. Since majority of usual materials have a similar positive Poisson's ratio, smaller comfort properties are expected in the first stages of loading.

7. Conclusions

Quasi-static contact problems involving the interaction of the human body with the seat structure is of significant practical interest because of the need to consider comfort in the design of seats.

On the basis of the conducted calculations and the determination of the discomfort coefficient, the following conclusions can be made:

- auxetic structures can be more comfortable across the full range of load, especially in the first stages of loading,
- a software based prototype proposed to simulate pressure distribution on the seat is a tool which allows tracing the comfort properties of the final product,
- the model can be improved by changing structural elements,
- the auxetic skeleton presents a novel solution which can be applied in the construction of comfortable seats.

References

- [1] Alderson A., Alderson K.L., *Auxetic materials*, Proc IME G.J. Aero. Eng., 221, 2007, 565-575.
- [2] Alderson, K., Fitzgerald K., Evans E., *The strain dependent indentation resilience of auxetics*, Journal of Materials Science, Vol. 35, 2000, 4039-4047.
- [3] Argatov I., Guinovart-Diaz R., Sabina F., *On local indentation and impact compliance of isotropic auxetic materials from the continuum mechanics viewpoint*, International Journal of Engineering Science, Vol. 54, 2012, 42-57.
- [4] Corlett E., *Background to sitting at work: Research-based requirements for the design of work seats*, Ergonomics, Vol. 49, 2006, 1538-1546.
- [5] Janus-Michalska M., Jasińska D., *Zagadnienie kontaktu sprężystego ośrodka anizotropowego na przykładzie materiału komórkowego o ujemnym współczynniku Poissona*, Czasopismo Techniczne, 4-B/2010, 25-36.
- [6] Janus-Michalska M., Jasińska D., Smardzewski J., *Studium obliczeniowe nad auksetyczną strukturą siedziska na obciążenia statyczne i dynamiczne od siadania*, Czasopismo Techniczne, 2-B/2011.
- [7] Janus-Michalska M., Jasińska D., Smardzewski J., *MES we wspomaganiu projektowania własności sprężystych oraz doboru kształtu szkieletu ergonomicznego siedziska fotela*, [in:] *Poliptymalizacja i komputerowe wspomaganie projektowania*, tom XI, ed. Tomasz Kiczowski, Wojciech Tarnowski, Politechnika Koszalińska, Koszalin 2013, 151-160.
- [8] Jasińska D., Janus-Michalska M., *Wpływ auksetycznej struktury szkieletu siedziska na nośność i warunki użytkowania*, [in:] *Optymalizacja i mechanika konstrukcji*, Instytut Mechaniki Budowli PK, Monografia No. 47, Seria Inżynieria Lądowa, Kraków 2014.
- [9] Jasińska D., Janus-Michalska M., Smardzewski J., *Comparison of contact stress distribution for foam seat and seat of auxetic spring skeleton*, IJAME International Journal of Applied Mechanics and Engineering, Vol. 18, No. 1, University Press, Zielona Góra 2013, 55-72.
- [10] Looze M., Kuijt-Evers L., *Dien Sitting comfort and discomfort and the relationships with the objective measures*, Ergonomics, Vol. 46, No. 10, 2003, 985-997.
- [11] Montmayeur, N., Marca, C., Choi, H.-Y., Sah, S., *Experimental and Numerical Analyses of Seating Pressure Distribution Patterns*, SAE Paper 05DHM-16, 2005.
- [12] Oudenhuijzen, A., Tan, K., Morsch, F., *The Relationship Between Seat Pressure and Comfort*, SAE Paper 2003-01-2213.

- [13] Smardzewski J, Jasińska D., Janus-Michalska M., *Structure and properties of composite seat with auxetic springs*, Composite Structures, Vol. 113, 2014, 354-361.
- [14] Smardzewski J., Prekrat S., *Research of contact stresses between seat cushion and human body*, Drvna Industrija, Vol. 61, 2010, 91-101.
- [15] Verver, M., Lange, D., Hoof, J., Wismans J., *Aspects of seat modelling for seating comfort analysis*, Applied Ergonomics, 36, 2005, 33-42.
- [16] Xiaoming, D., Jindong, R., Chunlei, S., Lemeng, Li., *Simulation of the Interaction between Driver and Seat*, Chinese Journal of Mechanical Engineering, Vol. 26, No. 6, 2013.
- [17] PN-EN ISO 3386-1:2000/A1:2010E Polymeric materials, cellular flexible. Determination of stress-strain characteristics in compression. Low density materials.
- [18] Hibbitt, Karlsson, Sorensen. ABAQUS Theory Manual, 6th ed., Abacom Software GmbH, 2000.
- [19] Hibbitt, Karlsson, Sorensen. ABAQUS User's Manual, 6th ed., Abacom GmbH, 2000.

PATRYCJA KARCIŃSKA*, JAROSŁAW MALARA*

EVALUATION OF THE EFFICIENCY OF CONSTRUCTION WORKERS ON DIFFERENT DAYS OF THE WEEK IN TERMS OF FUZZY SETS

OCENA WYDAJNOŚCI PRACOWNIKÓW BUDOWLANYCH W POSZCZEGÓLNYCH DNIACH TYGODNIA ROBOCZEGO W KATEGORIACH ZBIORÓW ROZMYTYCH

Abstract

This paper presents the methodology for comparing previously designated efficiencies of teams of workers using the fuzzy set theory. Efficiency was tested using timekeeping on different days of the week in the execution of specific construction tasks by the same team. The article also presents previously tested factors in this aspect and evaluates the impact of a particular day of the week on resource efficiency.

Keywords: work efficiency, impact of the weekday on work efficiency, fuzzy logic

Streszczenie

W artykule przedstawiono metodologię porównywania wcześniej wyznaczonych wydajności brygad roboczych z wykorzystaniem teorii zbiorów rozmytych. Wydajności badano metodą chronometrażu w poszczególnych dniach tygodnia roboczego przy realizacji określonych robót budowlanych przez te same brygady. Przedstawiono również dotychczas badane w tym aspekcie czynniki i przeprowadzono ocenę wpływu konkretnego dnia tygodnia pracy na wydajność zasobów.

Słowa kluczowe: wydajność pracy, wpływ dnia tygodnia na wydajność pracy, logika rozmyta

DOI: 10.4467/2353737XCT.15.078.3878

* M.Sc. Eng. Patrycja Karcińska, M.Sc. Eng. Jarosław Malara, Institute of Building and Transport Management, Faculty of Civil Engineering, Cracow University of Technology.

1. Introduction

The need for the selection of teams of workers to carry out various tasks within the scope of an entire construction project in the phase of preparation of the investment is a common and very important consideration when planning investment in a project. The reason is that the necessary workload on the execution of tasks and the number of allocated resources are often decisive for the efficient completion of the works. Assumptions relating to worker teams made by the planner during project preparation will have a significant impact on the planned completion deadline of the entire project and the ability to meet the deadline in the construction phase. In the process of executing the works, in addition to the number and qualifications of workers involved, worker efficiency is also a significant factor.

Recognising the causes affecting the efficiency of workers would increase the awareness of engineers determining the selection of worker teams in the phase of investment preparation. This would be an essential prerequisite for the development of a rational model of project management and would minimise the risk of exceeding deadlines from the point of view of resource efficiency.

The purpose of this article is to examine the influence of a particular working day (i.e. Monday, Tuesday, Wednesday, Thursday, Friday and Saturday) on the efficiency of worker teams. To achieve this goal, the rules of fuzzy logic were used, in particular, the concept of the membership function. In the latter part of the article, on the basis of the review of selected Polish and foreign literature, other factors that have thus far been taken into account in terms of examining work efficiency are presented – the day of the week was not included among them.

2. The basis of the theory of fuzzy sets

The basic concept of the theory used in this article is the concept of a fuzzy set. The definition of a fuzzy set can be most simply stated as follows: a fuzzy set is such set A whose elements x are characterised by the lack of a sharp boundary between whether x belongs or does not belong to A . The degree of membership of element x to the fuzzy set A is described by the function $\mu_A(x)$ which is called the membership function. Function $\mu_A(x)$ assumes values in the interval $[0, 1]$, wherein:

- $\mu_A(x) = 0$ means no membership whatsoever of x to A ;
- $\mu_A(x) = 1$ means full membership of x to A .

A fuzzy set A in certain space $X = \{x\}$, which is written as $A \subseteq X$, is called a set of pairs [5]:

$$A = \{(\mu_A(x), x), \forall x \in X \quad (1)$$

In the literature, one can find different definitions of a fuzzy number. One of the most accurate definitions was given by Goetschel and Voxmann in [2]. A fuzzy number A is a special kind of fuzzy set defined on the set of real numbers ($X = R$), which further satisfies the following conditions:

- **it is normal**, and a set is normal if there is an argument for which the function has a value of 1;
- **it is convex**, and set A is convex if

$$\forall x, y \in X \quad \forall \lambda \in [0; 1] \quad \mu_A(\lambda \cdot x + (1-\lambda) \cdot y) \geq \min(\mu_A(x), \mu_A(y)); \quad (2)$$

- carries of function $\mu_A(x)$ is an interval;
- $\mu_A(x)$ is a function of continuous intervals.

The characteristic diagrams of the membership function $\mu_A(x)$ are generated assuming a trapezoidal or triangular fuzzy numbers distribution. A fuzzy number with a trapezoidal diagram is illustrated in Fig. 1.

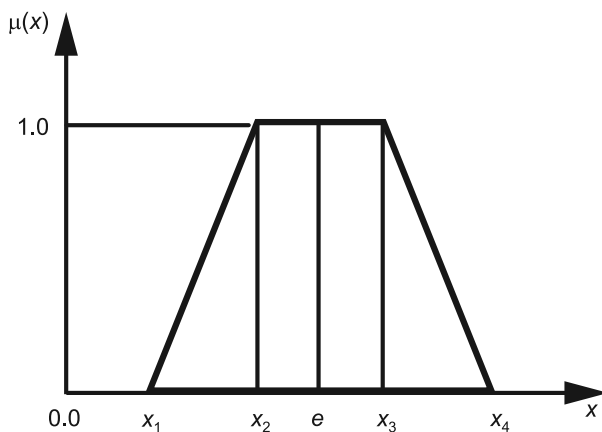


Fig. 1. Trapezoidal membership function

A description of a trapezoidal membership function is also presented in the literature using a table of values (Formula 3).

$$\mu_A(x) = \begin{cases} 0, & x < x_1 \\ (x - x_1) / (x_2 - x_1), & x_1 < x < x_2 \\ 1, & x_2 < x < x_3 \\ (x_4 - x) / (x_4 - x_3), & x_3 < x < x_4 \\ 0 & x > x_4 \end{cases} \quad (3)$$

A fuzzy number with a triangular diagram is illustrated in Fig. 2.

Description of a triangular membership function is also presented in the literature using a table of values (Formula 4).

$$\mu_A(x) = \begin{cases} 0, & x < x_1 \\ (x - x_1) / (x_2 - x_1), & x_1 < x < x_2 \\ (x_3 - x) / (x_3 - x_2), & x_2 < x < x_3 \\ 0, & x > x_3 \end{cases} \quad (4)$$

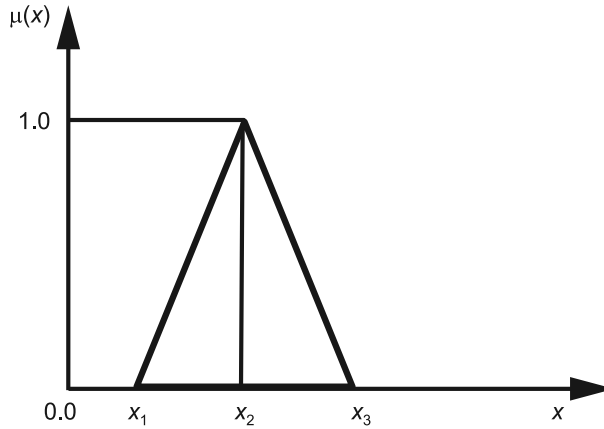


Fig. 2. Triangular membership function

A fuzzy number can be interpreted as a four $\{x_1, x_2, x_3, x_4\}$. x_2 and x_3 are the interval in which the membership function reaches the value of 1. x_1 and x_4 are respectively the left and right width of the distribution of a membership function. A fuzzy number with a trapezoidal diagram can be clearly identified by setting an ordered four of numbers and is written as:

$$X = (x_1, x_2, x_3, x_4) \quad (5)$$

A fuzzy number with a triangular diagram can be clearly identified by setting an ordered four of numbers and is written as:

$$X = (x_1, x_2, x_2, x_3) \quad (6)$$

A fuzzy number can also be expressed in another way – this would be as a fuzzy number with a multi-point membership function or a linear membership function but always with a set of values from 0 to 1.

3. Factors affecting worker efficiency

In modern literature, we can find many models, e.g. WLB (work-life-balance) developed in Australia [8] and the study of factors affecting the efficiency of construction workers. Among other factors important in this regard are, rest outside the workplace [1] and atmospheric conditions; more important factors are the temperature and humidity of the working environment [6], psychophysical condition of workers [3] and the appropriate management and organisation of the workplace [4, 7]. There are no results of current research on the effects of the day of the week on the efficiency of construction workers in either Polish literature, or indeed, world literature. This factor can also significantly affect the efficiency of the work, which according to the assumption made by the authors, changes with the change of the working day.

In this context, the authors of the article carried out tests in Warsaw, Poland, using timekeeping. The observed workers were installing lining in ten staircases using prefabricated terrazzo tiling. Actions for which the efficiency of the workers was assessed, included:

- assembly of steps (c_1),
- levelling of landings and corridors (c_2),
- laying of landings and corridors (c_3),
- installation of perimeter stair plinths (c_4),
- installation of perimeter landing plinths (c_5).

For all of these tasks, efficiency was specified using the formula:

$$w = \frac{p}{n} \quad (7)$$

where:

- w – efficiency,
- p – amount of work performed expressed in the unit of measure,
- n – workload expressed in work hours.

Many of the factors affecting the efficiency of the workers is hard to quantify and are imprecise. Fuzzy logic is well suited to solve these type of problems.

4. Analysis of the problem in fuzzy terms

In determining the efficiency of teams of workers, we use qualitative criteria in addition to quantitative criteria. Most of these criteria are quantifiable – their value is determined verbally. The interpretation of these criteria performed according to qualitative evidence leads to the categorisation of worker efficiency in a unmeasurable manner, i.e. as ‘good’, ‘satisfactory’, ‘average’, ‘mediocre’, or ‘bad’. The properties of fuzzy sets, which were chosen to be applied, make it possible to describe and compare the efficiency of workers during the performance of various tasks. In the research presented in this article, five specific finishing tasks were taken into account – these are listed in Chapter 3.

The diversity of the works and their different units of amount measurement prevents direct comparison of these works to each other. A common unit of measurement used for the installation of steps (each step is one element) is linear meters of the element (length of the elements constructed), the levelling of the surface and the laying of landings and corridors were described in square metres, while the installation of stair plinths was calculated in the number of sets (one set consist of two plinths – vertical and horizontal for each stair). Using the elements of fuzzy logic, a problem with different units found a solution. Workers efficiency in the implementation of various works with different units of measure, but expressed in a qualitative manner, can be compared.

Another aspect that led to the choice of fuzzy logic was the different ranges of values for each set of results for different tasks, for example:

- installation of steps 0.41–1.58 m/h,
- assembly of plinths 4.88–6.62 sets/h.

Although quantitative criteria are different, they can be determined in an identical manner to each other, using linguistic terms, and included in the same ranges. In order to compare worker efficiency on different days, it was necessary to determine the degree of membership of particular values to the fuzzy set of construction worker efficiency W , consisting of pairs according to equation (8):

$$W = \{(\mu W(w), w)\}, \forall w \in W \quad (8)$$

5. Worker efficiency depending on the days of the week in fuzzy conditions

In order to be able to compare each of the five tasks ($c_1 \dots c_5$), the minimum value (x_1) and the maximum value (x_4) of efficiency achieved by the workers were determined for each of them.

$$\bigwedge_{w_c \in W_c} \bigwedge_{c \in (1..5)} x_1(c) = \min(w_c) \quad (9)$$

$$\bigwedge_{w_c \in W_c} \bigwedge_{c \in (1..5)} x_4(c) = \max(w_c) \quad (10)$$

where:

- c – task
- w_c – efficiency of a single measure of tasks c ,
- W_c – set of efficiencies of all measures of tasks c ,
- $x_1(c)$ – the value of the minimum efficiency for tasks c ,
- $x_4(c)$ – the value of the maximum efficiency for tasks c .

After determining the maximum and minimum efficiency determined during the test, a function was defined, evaluating the membership of the result obtained to the set of high efficiencies or low efficiencies. The range of results (efficiency achieved by the workers) is divided into three parts, of which all efficiencies found in the first 25% of the range were considered as inefficient and given a value of 0. The top 25% of the range of the results was identified as high efficiency and the value of the function was specified as 1. The middle range of the results was determined using a linear relationship with the values belonging to the interval (0, 1). To determine the characteristic points of the monotonic change of the function, two designations (x_2 and x_3) were introduced.

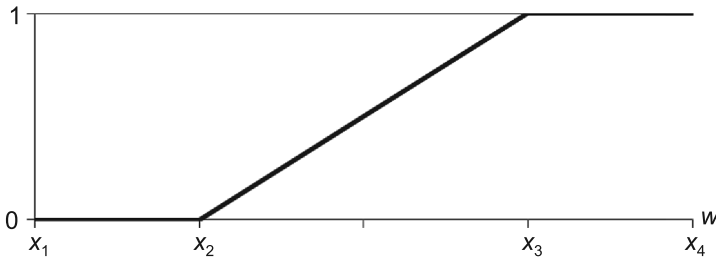


Fig. 3. Graph of the membership function for the set of high efficiencies $\mu W(w)$

$$x_2 = x_1 + 0.25(x_4 - x_1) \quad (11)$$

$$x_3 = x_1 + 0.75(x_4 - x_1) \quad (12)$$

$$\mu W(w) = \begin{cases} 0, & w \leq x_2 \\ \frac{w - x_2}{x_3 - x_2}, & x_2 < w < x_3 \\ 1, & w \geq x_3 \end{cases} \quad (13)$$

After the calculations, all the characteristic values for each of the works were obtained.

Table 1

Characteristic values of x_1, x_2, x_3, x_4 determined for each task based on the relationship, respectively (9)–(12)

	Installation of steps	Levelling of landings	Laying of landings	Installation of stair plinths	Installation of landing plinths
Unit of efficiency	[m/h]	[m ² /h]	[m ² /h]	[set/h]	[m/h]
Determination of tasks	c_1	c_2	c_3	c_4	c_5
Value of x_1	0.41	1.13	0.79	4.88	3.39
Value of x_2	0.7	1.44	0.95	5.32	3.84
Value of x_3	1.29	2.05	1.26	6.19	4.74
Value of x_4	1.58	2.36	1.42	6.62	5.19

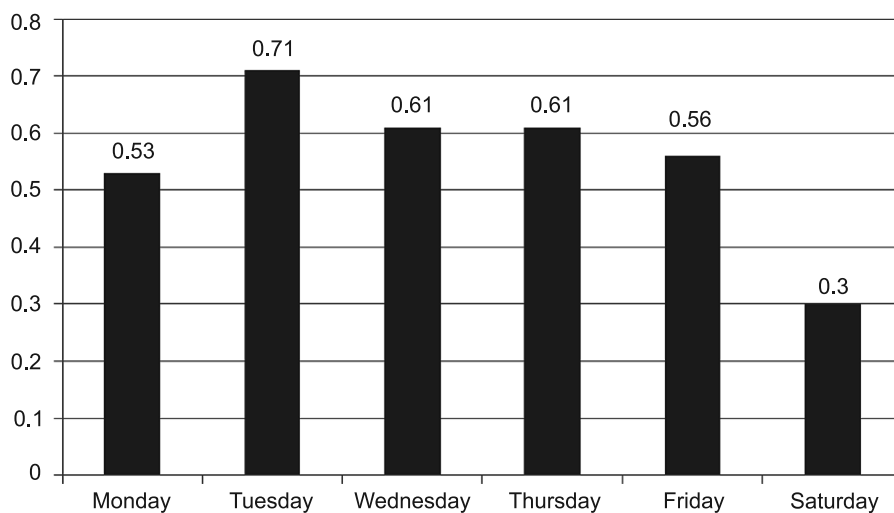


Fig. 4. Average value of the membership function for the results for the set of high efficiencies on different days of the week

After determining all the characteristic values, each measurement result for each task was assigned the value of the function $\mu W(w)$ based on equation (13). The collected results of calculations were ranked by days of the week. For example, on Monday, for all the tasks ($c_1 \dots c_5$), the following results for the membership function for the set of high efficiencies were obtained: 0.01; 0; 0.3; 0.67; 0.51; 0.8; 0.22; 0; 0.75; 0.64; 0.78; 0.26; 1; 0.28; 0.7; 1; 0.84; 0.8; 0.99; 0.18; 1; 0. Then, the arithmetic mean of the combined results was calculated (0.53). Similar calculations were made for each day of the week, and the resulting averages are presented in the chart.

6. Conclusions

The paper presents a scientifically valid methodology for assessing the impact of the day of the week on the efficiency of teams of workers in their performance on five specific construction works. The method is based on the theory of fuzzy sets and uses the concept of a membership function. Despite the use of fuzzy logic, operations performed on previously collected timekeeping data are simple; thus, they do not raise difficulties in their practical application. This gives a greater potential for its use in construction, where the efficiency of workers has a very large and direct impact on the duration of the works.

The results show that there is a relationship between labour efficiency and the day of the week. The smallest efficiency was achieved on Saturday (0.3), while the greatest was on Tuesday (0.71). The rest of the results are comparable: the results for Monday and Friday are very similar, and for Wednesday and Thursday exactly the same (0.61). This information may be useful in planning and the detailed scheduling of works. It shows that there is a relationship between labour efficiency and the day of the week, and the resulting ratio expresses its size.

In further work on this topic, I plan to expand the study to other factors and to create a model supporting the planning of works in practice. Analyses will continue to be conducted in terms of labour efficiency of teams of workers.

References

- [1] Ahn S., Lee S., Steel R.P., *Effects of Workers' Social Learning: Focusing on Absence Behavior*, Journal of Construction Engineering and Management, Vol. 139, 2013, 1015-1025.
- [2] Goetschel R., Voxmann W., *Topological properties of fuzzy numbers*, Fuzzy Sets Systems, 9, 1983, 31-43.
- [3] Hermanowski T., *Absencja chorobowa pracowników a funkcjonowanie przedsiębiorstw i rynku – wyniki analizy z użyciem symulacyjnego modelu wieloagentowego*, [in:] *Szacowanie kosztów społecznych choroby i wpływu stanu zdrowia na aktywność zawodową i wydajność pracy*, ed. T. Hermanowski, Wolters Kluwer Polska SA, Warszawa 2013, 48-70.
- [4] Jaworski K.M., *Fizjologiczne, psychologiczne i socjologiczne podstawy organizacji budowy*, [in:] *Podstawy organizacji budowy*, ed. K.M. Jaworski, PWN, Warszawa 2004, 13-14.
- [5] Konior J., *Przedsięwzięcia i procesy budowlane w kategoriach zbiorów rozmytych*, [in:] *Metody i modele badań w Inżynierii Przedsięwzięć Budowlanych*, ed. O. Kapliński, PAN, Warszawa 2007, 249-284.

- [6] Lee H.S., Shin J.W., Park M., Ryu H.G., *Probabilistic Duration Estimation Model for High-Rise Structural Work*, Journal of Construction Engineering and Management, Vol. 135, 2009, 1289-1298.
- [7] Maj T., *Organizacja podstawowych robót budowlanych*, [in:] Idem, *Organizacja budowy*, Wydawnictwa Szkolne i Pedagogiczne Spółka Akcyjna, Warszawa 2007, 115-180.
- [8] Townsend K., Lingard H., Bradley L., Brown K., *Complicated Working Time Arrangements: Construction Industry Case Study*, Journal of Construction Engineering and Management, Vol. 138, 2012, 443-448.

TOMASZ MICHAŁOWSKI*

SELECTED ISSUES OF AERODYNAMICS OF STEEL CHIMNEYS

WYBRANE ZAGADNIENIA AERODYNAMIKI KOMINÓW STALOWYCH

Abstract

This paper presents general principles of managing the reliability of steel chimneys according to Eurocodes EN 1990 and EN 1993-3-2. It discusses the basis for static calculations and dimensioning and compares Eurocode guidelines to the requirements of old Polish Standards. The use of standard procedures is illustrated by an example of static calculations and dimensioning of a steel chimney shell.

Keywords: static calculations of steel chimney

Streszczenie

W artykule przedstawiono ogólne zasady zarządzania niezawodnością kominów stalowych wg Eurokodów EN 1990 i EN 1993-3-2. Omówiono podstawy ich obliczeń statycznych i wymiarowania, a także porównano wytyczne Eurokodu z wymaganiami stawianymi przez stare polskie normy. Sposób wykorzystania procedur normowych zilustrowano przykładem liczbowym obliczeń statycznych i wymiarowania powłoki komina stalowego.

Słowa kluczowe: obliczenia statyczne kominów stalowych

DOI: 10.4467/2353737XCT.15.079.3879

* Ph.D. Eng. Tomasz Michałowski, Chair of Metal Structures, Institute of Building Material and Structures, Faculty of Civil Engineering, Cracow University of Technology.

1. Introduction

This article presents an analysis of the reliability of a steel chimney according to the principles of Eurocode EN 1993-3-2 [1]. The standard applies to vertical steel chimneys of a circular or conical cross-section. Possible solutions include cantilevered (in lattice or self-bearing towers) and guyed chimneys. The article introduces general principles of managing the reliability of steel chimneys according to old standards and Eurocodes, it compares loads under old standards and Eurocodes as well as presenting the basis for their calculation and dimensioning in a deteriorated condition. Moreover, it describes a comparative analysis of static calculations of chimneys according to old Polish Standards and Eurocodes

2. Elements of the reliability analysis

The European Standards (Eurocodes) introduced a few years ago contain requirements that are different from old Polish Standards in terms of static and strength calculations of steel chimneys. The main change is the implementation of reliability management by defining the reliability class of a chimney. This depends on the consequences to society, environment and economy of the destruction of a chimney. Depending on the reliability class, the standard requires various values of partial coefficient γ_F to static and dynamic loads. Their differentiation has a great impact on the calculation procedure carried out according to the Eurocode guidelines.

Eurocodes require a comparison of the design values: the bearing capacity R_d and the load effect E_d . According to the recommendations included in EN 1990 [2] regarding the basics of structure design, the ultimate limit state condition can be expressed as a scalar one-parameter bearing capacity R and the related impact effect E as follows:

$$E_d = E(F_{d1}, \dots, a_{d1}, \dots, \theta_{d1}, \dots) \leq R(X_{d1}, \dots, a_{d1}, \dots, \theta_{d1}, \dots) \quad (1)$$

where:

- index $_d$ refers to the design values,
- F_{di} – impact on the structure,
- X_{di} – mechanical properties of the structure's material,
- a_{di} – geometric properties of the structure,
- θ_{di} – uncertainty parameters of the calculation model.

According to the Eurocodes, the method for testing reliability does not usually necessitate that the design values x_d be substituted into the ultimate limit state equation. Instead, the equation is substituted with so-called representative values X_{rep} and F_{rep} , which can be:

- characteristic values, i.e. quantiles of loads – F_k , material strength – ηX_k and geometric properties – a_d (where η is the conversion factor);
- nominal values (central values of geometric properties a_{nom}).

The design values F_d and X_d are determined by multiplying or dividing the representative values by relevant partial coefficients:

$$F_d = F_{rep} \gamma_F \rightarrow E_d = E(F_{rep} \gamma_F) \quad (2)$$

$$X_d = \eta X_{\text{rep}} / \gamma_M \rightarrow R_d = R(\eta X_{\text{rep}} / \gamma_M) \quad (3)$$

Partial coefficients γ_F in formula (3) and γ_M in formula (4) account for random variation of impacts, material strength and modelling error of the random variables, and can be presented as the following products:

$$\gamma_F = \gamma_f \gamma_{Sd} \quad \gamma_M = \gamma_m \gamma_{Rd} \quad (4)$$

The numeric values of load factors γ_F specified in Eurocode EN 1990 are presented as three sets, depending on the analysed ultimate limit state. Technically, the specifications are secure for all objects and buildings. However, partial coefficients γ_F for impacts on chimneys are additionally specified in EN 1993-3-2 as an alternative for the recommendations included in Eurocode EN 1990. The differentiation of chimneys in terms of their reliability class is presented in Table 1.

Table 1

Reliability differentiation for chimneys [1]

Reliability class	Definition
3	Chimneys erected in strategic locations, such as nuclear power plants or in densely populated urban locations. Major chimneys in manned industrial sites where the economic and social consequences of their failure would be very high.
2	All normal chimneys at industrial sites or other locations that cannot be defined as Class 1 or Class 3.
1	Chimneys built in open countryside whose failure would not cause injury. Chimneys less than 16m high in unmanned sites.

Partial factors for material property γ_M are specified in [1, 3, 4] as follows:

- $\gamma_{M0} = 1.00$ – resistance of structural elements or members related to the yield strength f_y , where no global or local buckling occurs;
- $\gamma_{M1} = 1.10$ – resistance of structural elements or members related to the yield strength f_y , where global or local buckling is considered;
- $\gamma_{M2} = 1.25$ – resistance of structural elements or members related to the ultimate tensile strength f_u , resistance of bolts and welds;
- $\gamma_{M3} = 1.25$ – slip resistance of preloaded bolts at ultimate limit state;
- $\gamma_{M3,ser} = 1.10$ – slip resistance of preloaded bolts at serviceability limit state;
- $\gamma_{M6} = 1.10$ – fatigue resistance of shell;
- $\gamma_{Ff} = 1.00$ – partial factor for the fatigue loading;
- γ_{Mf} – partial factor for the fatigue strength, depending on the selected fatigue assessment method.

Coefficient values depending on the reliability class are juxtaposed in Table 2.

Table 2

Partial factors for actions γ_F [1]

Type of Effect	Reliability class	Permanent Actions	Variable Actions
Unfavourable	1	1.2	1.6
	2	1.1	1.4
	3	1.0	1.2
Favourable	All classes	1.0	0.0
Accidental situations		1.0	1.0

3. Comparison of old and new standards

Steel chimneys are designed according to the provisions specified in standard [1]. Its requirements contain references to standards [3–5]. Those calculations are different from the guidelines of old Polish Standards [6, 7] in terms of load values and the analysed conditions. Table 3 presents a juxtaposition of various loads and environmental impact according to the old and new standards.

Table 3

Load outlines

Load	PN B 03201	EN 1993-3-2
Dead load	Considered	Considered
Technological loads	Considered	Considered
Load during execution	Considered	Considered
Dust and ashes	Omitted	Considered
Imperfections	Only if second-order effects are necessary	Always accounted for
Snow loads	May be omitted	May be omitted
Atmospheric icing	May be omitted	Accounted for
Wind action; pressure	Accounted for	Accounted for
Wind action; vortex	A simplified and detailed procedure (alternative)	A simplified and detailed procedure (alternative)
Wind action; galloping	Accounted for	Accounted for
Wind action; interference	Accounted for	Accounted for
Gas internal pressure	Omitted	Accounted for
Gas temperature	Only for guyed chimneys if the core temperature exceeds 50°C	Accounted for

Gas temperature; impact on mechanical properties of steel	If over 70°C, reduction of fatigue strength	Reference to standard [8]
Gas temperature; checking the possibility of the formation of condensate (corrosion)	Accounted for	Reference to standard [8]
Outside temperature	Only for guyed chimneys if the core temperature exceeds 50°C	Always accounted for
Temperature impact on steel creep	Omitted	If the core temperature exceeds 400°C
Inner fire	Omitted	Accounted for
Chemical; corrosion	Include the impact of thickness change (corrosion allowance)	Include the impact of thickness change (corrosion allowance)
Chemical; change of mechanical properties of steel	Decreased design strength of steel	Reference to standard [8]
Seismic and paraseismic impact	Accounted for	Reference to standard [8] and [9]
Mining terrain deformation	Accounted for	Reference to standard [8] and [9]
Ground settlement	Accounted for	Reference to standard [2], [8] and [9]

The comparison of loads that need to be accounted for in the design of chimneys shows that the Eurocode requires a deeper consideration of loads that have an impact on the chimney. Impacts that could be omitted in some cases (such as imperfections or icing) are now obligatory to analyse. There are also conditions that were previously unaccounted for (fire inside the chimney, material creep or a clearly stated obligation to consider the impact of dust and ashes).

The article includes a detailed analysis of the guidelines regarding the values of technological load and wind pressure.

Standard [1] establishes slightly different requirements regarding technological load as compared to [6]. A comparison of recommended values according to both standards is presented in Table 4.

The old Polish Standards were not consistent in terms of wind load. Although there was a standard defining wind load [10], in case of many tower type buildings there were separate regulations (for example [6, 10, 11–14]) that significantly changed the wind load profile. A comparison of these standards is presented in [15].

According to the provisions of standard [10], wind load is defined in the following way:

$$p = \gamma_f q_k C_e C \beta \quad (5)$$

where:

- γ_f – partial wind load coefficient;
- q_k – characteristic value of the wind velocity pressure, depending on the structure location in the country;
- C_e – wind exposure factor describing vertical wind profile depending on the terrain category;
- C – aerodynamic drag coefficient depending on the structural shape;
- β – gust response factor depending on the structure dynamic properties.

Table 4

Comparison of technological load values

Load	PN B 03201	EN 1993-3-2
Imposed loads on platforms: (vertical)	2.0 kN/m ² alternatively 3.0 kN	2.0 kN/m ²
On railings: (horizontal)	0.3 kN/m	0.5 kN/m
On ladders (vertical)	1.0 kN	No guidelines

The relationship between wind speed and altitude (coefficient C_e) can be presented as a polygonal curve. Chimneys should be regarded as structures prone to the dynamic impact of wind, thus it is necessary to precisely calculate the value of coefficient β . The minimum value is 1.8.

Standard [6] introduces changes to the wind load formula. According to the provisions of the standard, wind load is calculated in the following way:

$$p = \gamma_f q_k c_{te} c_e c_s n \beta \quad (6)$$

where:

- γ_f – partial wind load coefficient;
- q_k – characteristic value of the wind velocity pressure depending on the structure location in the country (value consistent with standard [10]);
- C_{te} – coefficient accounting for the scheduled chimney lifetime;
- C_e – wind exposure factor (equivalent of C_e in standard [10], yet calculated differently);
- C_s – aerodynamic drag coefficient (equivalent of C in standard [10], yet with a different value);
- β – gust response factor depending on the structure dynamic properties (calculated according to the recommendations of standard [10], yet with slight changes to parts of the formulae);
- n – number of flues in one structure not covered by a external shell.

According to the guidelines of Eurocode [16] defining the wind load, in the case of chimneys, it should be calculated in the following way:

$$P = \gamma_f q_b c_e c_f c_s c_d \quad (7)$$

where:

- γ_f – partial wind load coefficient;

- q_b – characteristic value of the wind velocity pressure depending on the structure location in the country, accounting for seasonal changes and the influence of prevailing winds (equivalent of q_k in Polish Standards);
 c_f – aerodynamic drag coefficient (equivalent of C in standard [10]);
 $c_s c_d$ – structural coefficient describing possible interactions of structural vibrations and turbulent wind effects (similar to β in standard [10]).

Figure 1 presents a comparison of wind load values in the function of chimney height. This includes a dimensionless parameter describing the load defined as:

$$w = 10^6 p / f_y \quad (8)$$

where:

- w – dimensionless parameter of wind load;
 p – wind pressure [Pa] calculated according to the guidelines in standards [6], [10] and [16], calculated according to formulas (5–7);
 f_y – yield strength of steel.

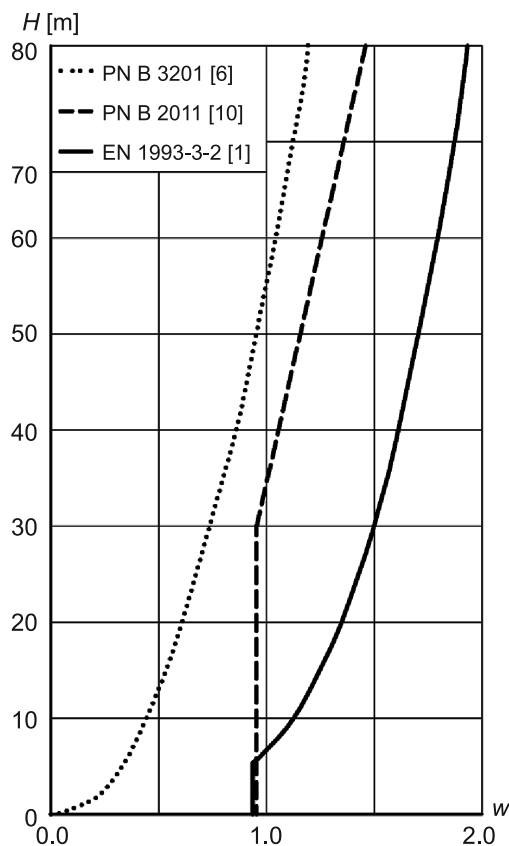


Fig. 1. Comparison of wind load according to various standards

The comparison was based on the following assumptions:

- climatic zone 1 of wind load
- industrial area, i.e. surrounding type *C* according to [10] and 4 according to [16],
- chimney diameter 4.0 m.

A significant change compared to previous standards is the need to account for structural imperfection. In the case of free-standing cantilever chimneys, this is treated as top deflection with the following value:

$$\Delta = (h / 500) \sqrt{(1 + 50 / h)} \quad (9)$$

where:

- h – chimney height (depending on the location of the symbol in the formula, its measurement unit is [m] or it is a dimensionless value).

4. Calculation example

A comparison of guidelines from the new and old standards was conducted for an 80 meters high cylindrical steel chimney. Originally, the chimney was located in Kraków Łęg Power Station [18]. The structure is presented in Fig. 2.

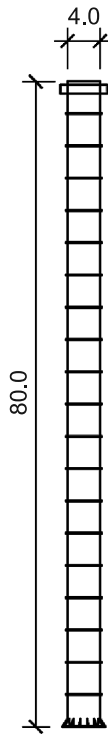


Fig. 2. The chimney

The calculation of the chimney was based on the following data and conditions:

- diameter $D = 4\,000$ mm, height $H = 80\,000$ mm;
- temperature impact on chimney operation and vortex load was omitted;
- location – Kraków;
- steel grade 1.4016 (H17);
- mechanical parameters – yield strength $f_y = 240$ MPa, fatigue limit $f_u = 430$ Mpa.

The chimney bearing structure is a cylindrical sheet metal shell. The assembly member is 4.00 m long. Conduits are connected with one another by flanged contact screws. The sheet metal core is 10–20 mm thick. The chimney was modelled (as the chimney in the Kraków Łęg Power Station in Cracow) with a variable shell thickness of 8–12 mm.

Safety factors were derived from EN standards. Calculations were based on EN standards. They used reliability class 2 and production class B. Additionally, a beam model was analysed according to the guidelines on standard [1].

Two models of structure were taken into consideration: a shell model and a bar model.

The chimney was modelled as a shell structure loaded with a dead load, a technological load, wind pressure and wind suction. The impact of imperfections was also considered in terms of concentrated force applied to the chimney top. It was established that the force value results in equivalent movement of the chimney top according to [1]. The values of wind pressure and suction were applied according to [16]. The distribution of pressure around the perimeter was aligned with the guidelines of standard [16]. The wind load coefficient for the beam structure with a circular section was assumed as 0.7.

The impact of flanges connecting conduits and the technological bridge on the shell stiffness was also accounted for. The initial calculations do not include the impact of the thermal effects of hot gases and the dynamic effects related to the wind load. The calculations were carried out in Algor software. Linear elastic analysis was used (LA according to [5]).

According to [17], the section class for elements with a circular section should be calculated as a ratio of diameter to wall thickness, which in the case of the analysed structure results in section class 4. As specified in [17], in such a case, the calculation process should be in line with [5]. With this chimney section, class 3 is possible only if 44 mm thick sheet steel is used, which is economically unreasonable.

In the beam model, wind pressure bending interacts with vertical forces buckling (dead load, technological load). Additionally, second-order effects should be accounted for by applying strict conditions to the condition of pure buckling and the increase of the bending moment value at the bottom of the cantilever.

In the case of the shell model, the chimney is calculated according to the requirements of standard [1]. This requires that in the bearing ultimate limit state, the following conditions are checked:

- static equilibrium;
- strength of its structural elements (i.e. plastic limit state = SL1 according to [5] and tensile resistance);
- overall stability;
- local buckling of its elements (limit state SL3 according to [5]);
- fatigue of its structural elements, including low-cycle fatigue (limit state SL4 according to [5]);

- failure of connections (bolted and welded joints).
- In the serviceability limit state, the evaluation is based on:
 - deformations or deflections in the along wind direction and/or in the cross-wind direction which adversely affect the appearance or effective use the structure;
 - vibrations, oscillations or sway which may cause alarm among bystanders;
 - deformations, deflections, vibrations, oscillations or sway which may cause damage to non-structural elements.

Checking conditions LS1, LS3 and LS4 according to standard [5] involves checking the following conditions:

$$\sqrt{[\sigma_{x,Ed}^2 + \sigma_{\theta,Ed}^2 - \sigma_{x,Ed} \sigma_{\theta,Ed} + 3(\tau_{x\theta,Ed}^2 + \tau_{xn,Ed}^2 + \tau_{\theta n,Ed}^2)]} / f_{eq,Rd} \leq 1.0 \quad (10)$$

$$(\sigma_{x,Ed} / \sigma_{x,Rd})^{k_x} - k_j (\sigma_{x,Ed} / \sigma_{x,Rd}) (\sigma_{\theta,Ed} / \sigma_{\theta,Rd}) + (\sigma_{\theta,Ed} / \sigma_{\theta,Rd})^{k_{\theta}} + (\tau_{\theta,Ed} / \tau_{\theta,Rd})^{k_{\tau}} \leq 1.0 \quad (11)$$

$$\Delta\sigma_E \gamma_{FF} < \Delta\sigma_R / \gamma_{Mf} \quad (12)$$

where:

- $\sigma_{i,Ed}$ – meridional, circumferential or shearing stress;
- k_i – local stability factors;
- $\sigma_{i,Rd}$ – critical stress at loss of stability;
- $\Delta\sigma_E$ – variable stress at fatigue;
- $\Delta\sigma_R$ – fatigue strength of notches according to standards [1] and [4].

5. Conclusions

The results of the beam model were analysed, including second-order effects. Results of shell model were analysed too. They were related to the actual chimney in the Kraków Łęg Power Station. The analysis results are presented in Table 5.

Table 5

Calculation results

Model, maximum shell thickness	Maximum effort		Sway/acceptable sway
	LS1	LS3	
Beam, 10 mm	0.692		0.375
Shell, 12 mm	0.378	4.108	0.178
Shell, 20 mm	0.222	0.762	0.112

The calculation results show that the conditions that were the most difficult to be met are connected with shell stability. Meeting the requirements regarding stability is only possible if the wall thickness reaches 10 mm in the upper part and 20 mm in the lower part, this results in an almost two-times increase of thickness as compared to the initial structure (8–12 mm).

Eurocode provisions are stricter than the old Polish Standards. Loads and actions from dust and ashes, imperfections, atmospheric icing, gas internal pressure, gas temperature,

outside temperature, temperature impact on steel creep and inner fire must be always taken into account, this is contrary to the old Polish Standards. The effects of this requirement are higher intensities of actions applied to the structure in the calculation process. The same, static action of wind has a larger value in the case of calculations according to Eurocode than with the old Polish Standards. According to there results, contemporary structures are more massive than older.

A few phenomena: the impact of gas temperature on corrosion and on the mechanical properties of steel, the impact of aggressive gases on the mechanical properties on steel, seismic effects, paraseismic effects, terrain deformation and ground settlement effects must be analysed according to few additional standards. The comparison between old and contemporary requirements is possible after more accurate analysis.

References

- [1] EN 1993-3-2:2006 Design of steel structures – Towers, masts and chimneys - Chimneys.
- [2] EN 1990:2002 Basis of structural design.
- [3] EN 1993-1-8:2005 Design of steel structures – Design of joints.
- [4] EN 1993-1-9:2005 Design of steel structures – Fatigue.
- [5] EN 1993-1-6:2007 Design of steel structures – Strength and stability of shell structures.
- [6] PN-93/B-03201 Steel structures – Chimneys – Static calculations and design (in Polish).
- [7] PN-90/B-03200 Steel structures – Static calculations and design (in Polish).
- [8] EN 13084-1:2007 Free standing chimneys – General requirements.
- [9] EN 1998-6:2005 Design of structures for earthquake resistance - Towers, masts and chimneys.
- [10] PN-77/B-02011 Static load calculations – Wind actions (in Polish).
- [11] PN-B-03204:2002 Steel structures – towers and masts – design and construction (in Polish).
- [12] PN-79/B-3204 Steel structures – masts and towers, radio and television – static calculations and design (in Polish).
- [13] PN-E05100-1:1998 Overhead electrical lines – design and construction (in Polish).
- [14] PN-B-03205:1996 Steel structures – support power lines – design and construction (in Polish).
- [15] Rykaluk K., *The wind load of steel towers*, Inżynieria i Budownictwo, 10/2003, 557-559 (in Polish).
- [16] EN 1991-1-4:2005 Actions on structures – General actions – Wind actions.
- [17] EN 1993-1-1:2005 Design of steel structures – General rules and rules for buildings.
- [18] Bogucki W. et al, *Guide-book for the designer of steel structures*, Arkady, Warszawa 1982 (in Polish).

MAREK PIEKARCZYK*, TOMASZ MICHAŁOWSKI*, DAWID KOWALCZYK*

EXAMPLES OF DESIGNING STEEL SHELL STRUCTURES ACCORDING TO EUROCODES

PRZYKŁADY PROJEKTOWANIA STALOWYCH KONSTRUKCJI POWŁOKOWYCH WEDŁUG EUROKODÓW

Abstract

The paper presents an analysis of the guidelines of the European standards on procedures for the calculation of shell structures. The analysis is illustrated with examples concerning three types of structures of the type i.e.: a chimney, a silo and a tank.

Keywords: steel structures, shell structures, chimney, silo, tank

Streszczenie

W artykule przedstawiono analizę wytycznych norm europejskich dotyczących procedur obliczeniowych konstrukcji powłokowych. Analiza zilustrowana została przykładami obliczeniowymi dotyczącymi trzech konstrukcji, czyli komin, silosu i zbiornika.

Słowa kluczowe: konstrukcje metalowe, konstrukcje powłokowe, komin, silos, zbiornik

DOI: 10.4467/2353737XCT.15.080.3880

* Prof. D.Sc. Ph.D. Eng. Marek Piekarczyk, Ph.D. Eng. Tomasz Michałowski, M.Sc. Eng. Dawid Kowalczyk, Chair of Metal Structures, Institute of Building Material and Structures, Civil Engineering Faculty, Cracow University of Technology.

1. Introduction

The chosen design examples of steel structures set up in the paper are all shells of revolution. That is why they should be designed according to the rules given in the standard PN-EN 1993-1-6 [1]. They belong however to three various types of buildings for which detailed regulations were also elaborated separately: for chimneys in the regulation PN-EN 1993-3-2 [2], silos in the regulation PN-EN 1993-4-1 [3] and tanks in PN-EN 1993-4-2 [4].

Before 2010 each of the three types of steel structures was designed according to the adequate object standard in the Polish project practice, ie chimneys – PN-93/B 03201 [5], silos for loose materials PN-B-03202: 1996 [6], cylindrical vertical tanks PN-B-03210: 1997 [7]. To each type of the structure corresponding Polish comprehensive monographs have been dedicated – for instance [8] and [9] for chimneys, [10] for silos and [11] for tanks.

The way in which wind actions on structures are estimated can be an illustration of differences between calculations for the three types of shells after “old” Polish and “new” European standards. Silos and tanks were calculated according to [12], chimneys according to [5]. The results of calculations according to different standards for a few cases of tower-type structures are presented in detail in [13]. For example, Fig. 1 shows

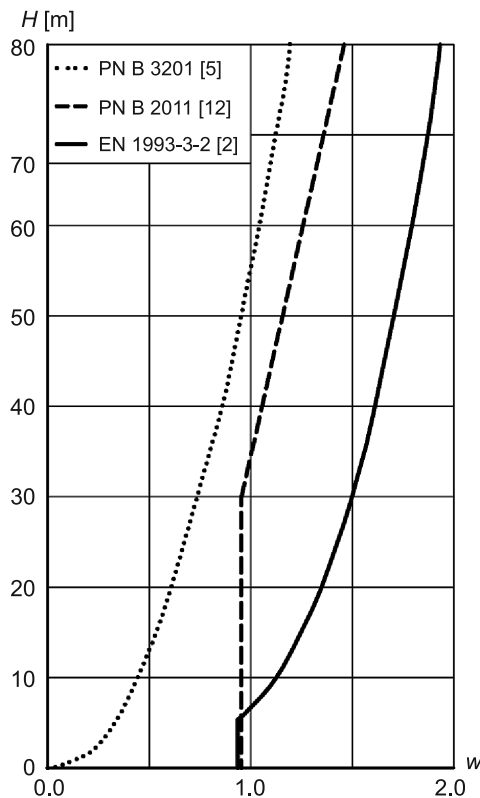


Fig. 1. Comparison of wind load according to various standards

a comparison of wind load values as a function of the chimney height H . This includes a dimensionless parameter describing wind action defined as:

$$w = 10^6 p / f \quad (1)$$

where:

- w – dimensionless parameter of wind load,
- p – wind pressure [Pa] calculated according to the guidelines in standards [12] and [14],
- f – yield strength of steel.

The above described comparison was based on the following assumptions:

- climatic zone 1 of wind load according to [12] and [14],
- industrial area, i.e. type C of the surroundings according to [12] and 3 according to [14],
- 4.0 m diameter of the structure.

The most essential change in comparison to the traditional “old” approach to the design procedures of the considered shell structures is the integration of the rules within the range of their strength and stability check as well as the uniform approach to their reliability. The latter is described in the standard [15]. The uniform approach to all the shell structures is also shown in standard [1] and described in the commentary to it [16, 17]. This uniform approach is based on the two most important rules:

1. Common approach to each structure according to EN 1990 [15];
2. Wide range of MES application to the calculation of shell structures.

The algorithm of calculations is presented in Table 1.

Table 1

Algorithm of calculations

Step of analysis	Number of Eurocode	Comments
1	EN 1990	General information on reliability of structures
2	EN 1991-1, EN 1991-4	Loads and actions
3	EN 1993-3-2, EN 1993-4-1, EN 1993-4-2	Specific requirements for chimneys, silos and tanks
4	EN 1993-1-6	Calculation of shell structures
5	other	Calculation of other parts of structures

2. Reliability of structures

Analyses of reliability should be performed according to the standards [2–4, 15] and [18]. For chimneys, the most important parameter is the reliability class (RC), for tanks it is a consequence class (CC). Two parameters must be taken into account for silos, i.e. an action assessment class (AAC) and a consequence class (CC). These classes are very important for the values of safety factors of actions and sets of their combinations (for chimneys and silos) and serviceability limit states (for chimneys), for the choice of method of structural

analysis (for tanks and silos). The method of classifying structures as well as the results of the qualifications are presented in Tables 2–9 for different shell structures.

Table 2

Reliability differentiation for chimneys [2]

Reliability class	Definition
1	Chimneys built in open countryside whose failure would not cause injury. Chimneys less than 16 m high in unmanned sites.
2	All normal chimneys at industrial sites or other locations that cannot be defined as class 1 or class 3.
3	Chimneys erected in strategic locations such as nuclear power plants or in densely populated urban locations. Major chimneys in manned industrial sites where the economic and social consequences of their failure would be very high.

Table 3

Partial factors for permanent and variable actions [2] (for chimneys)

Type of effects	Reliability class	Permanent actions	Variable actions
unfavourable	1	1.0	1.2
	2	1.1	1.4
	3	1.2	1.6
favourable	1, 2, 3	1.0	0.0
Accidental situations		1.0	1.0

Table 4

**Recommendations for maximum amplitudes of cross-wind vibrations [2]
(for chimneys)**

Reliability class	Limits to cross-wind vibration amplitude
1	0.15 D
2	0.10 D
3	0.05 D

where:

D – outer diameter.

Table 5

Reliability differentiation for tanks [4]

Reliability class	Definition
1	Agricultural tanks and tanks containing water.
2	Medium sized tanks with flammable or water-polluting liquids located in urban areas.
3	Tanks storing liquids or liquefied gases with toxic or explosive potential and large tanks with flammable or water-polluting liquids located in urban areas.

Table 6

Methods of analysis for tanks [4]

Consequence class	Circular shell tank structure	Rectangular box tank structure
1	Membrane theory with simplified formulas to describe local bending effects	Static equilibrium for membrane forces and beam theory for bending
2	Membrane theory with bending theory or numerical analysis (FEM)	An analysis based on linear plate bending and stretching theory
3	Numerical analysis (FEM)	An analysis based on nonlinear plate bending and stretching theory

Table 7

Reliability differentiation for actions in silos [18]

Action assessment class	Definition
1	Silos with a capacity below 100 tons.
2	All silos covered by standard [18] and not placed class in 1 or 3.
3	Silos with a capacity in excess of 10 000 tons or silos with a capacity in excess of 1000 tons in which any of the following design situations occur: a) eccentric discharge with $e_0/d_c > 0.25$ b) squat silos with top surface eccentricity with $e_t/d_c > 0.25$

Generally, for the higher number of action assessment class, the higher values of actions are used. Additionally, more complicated cases of combinations of actions must be analysed.

Table 8

Reliability differentiation for silos [3]

Consequence class	Definition
1	Silos with capacity between 10 and 100 tons.
2	All silos covered by standard [3] and not placed in class 1 or 3.
3	Ground supported silos or silos supported on a complete skirt extending to the ground with capacity in excess of 5000 tons or discretely supported silos with capacity in excess of 1000 tons or silos with capacity in excess of 200 tons in which any of the following design situations occur: a) eccentric discharge b) local patch loading b) unsymmetrical filling

Methods of analysis for silos [3]

Consequence class	Circular shell silos structure	Rectangular box silos structure
1	Membrane theory with simplified formulas to describe local bending effects	Static equilibrium for membrane forces and beam theory for bending
2	Membrane theory with bending theory or numerical analysis (FEM)	An analysis based on linear plate bending and stretching theory
3	Numerical analysis (FEM)	An analysis based on nonlinear plate bending and stretching theory

3. Shell structures in general

Standard [1] defines four basic limit states for steel shell structures and shows the methods that should be used in order to determine the values of stresses and cross-sectional forces in the given state according to the pattern outlined in Table 10.

Table 10

Methods (models) of analysis for each limit states of shells [1]

Limit state (name)	Method (model) of analysis
LS1 (plastic limit state)	Linear elastic analysis (LA), materially nonlinear analysis (MNA), geometrically and materially nonlinear analysis (GMNA)
LS2 (cyclic plasticity limit state)	Analysis LA or GNA, materially nonlinear analysis MNA or GMNA
LS3 (buckling limit state)	Analysis LA, linear elastic bifurcation analysis (LBA), materially nonlinear analysis MNA, geometrically and materially nonlinear analysis with imperfections GMNIA
LS4 (fatigue limit state)	Analysis LA or GNA with coefficients of stress concentration

In the above mentioned standards conditions for dimensioning the shell are specified in accordance with the used method of analysis for the chosen limit state. For instance, in the state LS1 (plastic limit) the following condition should be fulfilled:

$$\sigma_{Ed} \leq f_{yk} / \gamma_{M0} \quad (2)$$

where:

- σ_{Ed} – design value of a component of stress tensor or equivalent stress,
- f_{yk} – characteristic value of yield strength,
- $\gamma_{M0} = 1.0$,

while in the state LS3:

$$\sigma_{Ed} \leq \chi f_{yk} / \gamma_{m1} \quad (3)$$

where:

χ – coefficient of instability.

$\gamma_{M1} = 1.0$.

Acceptable types of analysis for shell structures are presented in detail in Table 11.

Table 11

Types of analysis for shell structures [1]

Types of analysis	Deformations	$\sigma \leftrightarrow \varepsilon$	Imperfections
Linear elastic shell analysis (LA)	Small	Linear	No
Linear elastic bifurcation analysis (LBA)	Small	Linear	No
Geometrically nonlinear elastic analysis (GNA)	Large	Linear	No
Materially nonlinear analysis (MNA)	Small	Nonlinear	No
Geometrically and materially nonlinear analysis (GMNA)	Large	Nonlinear	No
Geometrically nonlinear elastic analysis with imperfections included (GNIA)	Large	Linear	Yes
Geometrically and materially nonlinear analysis with imperfections included (GMNIA)	Large	Nonlinear	Yes

The choice of the appropriate calculation method for a given type of structure is made in accordance with the corresponding standard for silos and tanks with respect to the consequence class which in turn depends on the geometry of the structure and the conditions of its exploitation [3, 4]. In the case of chimneys [2], the method of analysis depends on the class of cross-section. Here, for classes 1–3 the shell is considered to be like a generalised beam with bending effects and possibly taking the II-range effects into account, whereas cross-sections of class 4 are treated like shells with use of a linear analysis LA.

4. Design examples of shell structures

Three structures are presented here for example: a steel chimney [19], a silo [20], a tank [21]. Views of structures and the results of FEM static analysis for these structures are presented in the tables and figures below. These were recommended to be published in full in [19].

Characteristics of analysed structures

Structure	Consequence class	Thickness [mm]	Grade of steel	FEM shell elements
Chimney in an electric power station	CC2	10–20	1.4401 stainless steel	Four-nodes
Silo constructed from flat sheets	CC2	6–12	S355	Four-nodes
Tank for storage of ammonia water	CC3	6	1.4301 stainless steel	Four-nodes

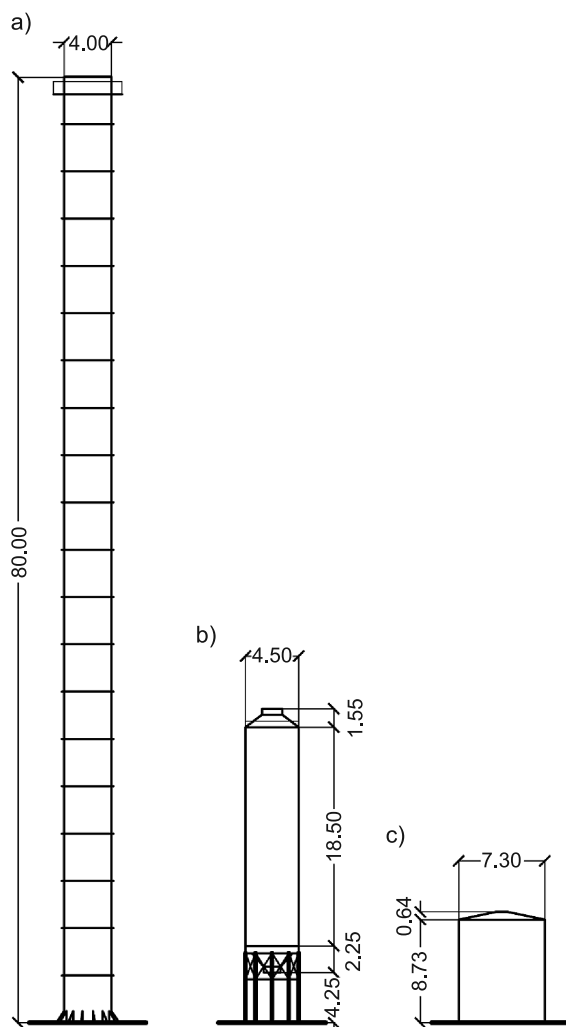


Fig. 2. Schemes of analysed structures: a) chimney, b) silo, c) tank

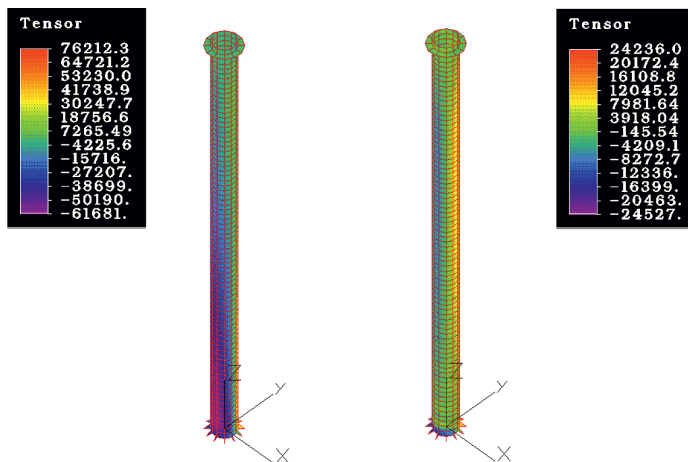


Fig. 3. Example design results for the chimney 80m high chimney for the pressure of wind velocity: σ_{HMH} [kPa], meridional stresses (left), circumferential stresses (right), LA analysis, (Algor [22])

Table 13

Results FEM for chimney

Limit state (condition)	Check
LS1 (1)	$0.220 < 1.0$
LS3 (2)	$0.760 < 1.0$

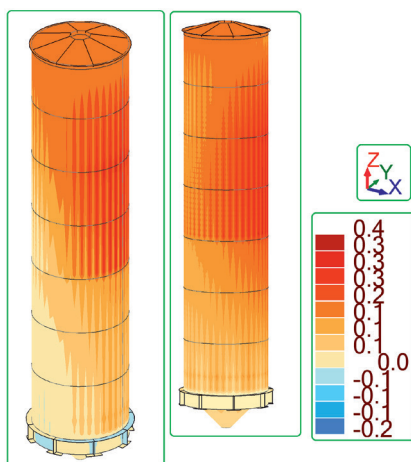


Fig. 4. Silo for wheat, FEM results, displacements u_x (left), general displacements (right) [cm], LA analysis, (Robot [23])

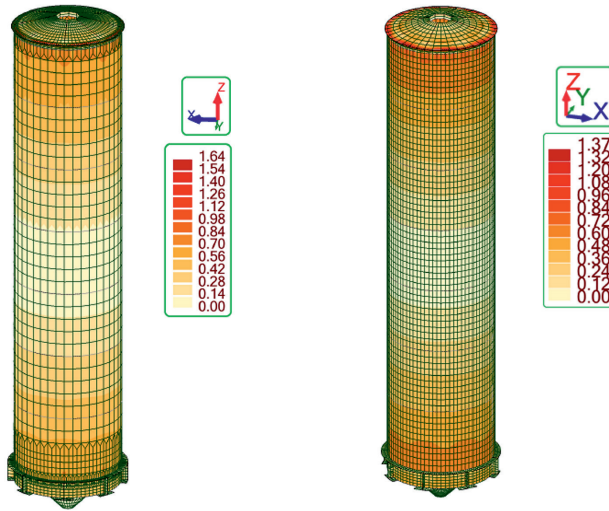
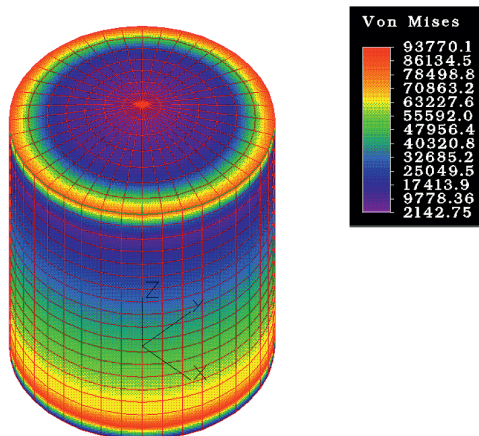


Fig. 5. Comparison of results from LA analysis (left) and GMNA analysis (right); dead weight, σ_{HMH} [MPa]

Table 14

Results FEM for silo

Limit state (condition)	Check
LS1 (1)	0.277 < 1.0
LS3 (2)	0.907 < 1.0



SVIEW 4.18 File:zbi LC 1/ 1 Vu= 7 Lo= 45 Lo= 45 R= 0

Fig. 6. Results of calculations (Algor [22]) for the most disadvantageous equivalent stress, LA analysis, [kPa]

Table 15

Results FEM for tank

Limit state (condition)	Check
LS1 (1)	$0.723 < 1.0$
LS3 (2)	$0.095 < 1.0$

Safety factors: for ammonia water $\gamma_F = 1.40$, other live loads $\gamma_F = 1.50$, for dead weight $\gamma_F = 1.35$, $\gamma_{M0} = 1.10$, $\gamma_{M2} = \gamma_{M5} = 1.25$, $\gamma_R = 1.05$, $k_{Fi} = 1.10$ (factor for actions for RC3).

5. Summary

The three design examples of special steel structures constructed from sheets with the cross-sections which are shells of revolution are presented. A uniform approach to assessing the reliability of the structures was adopted. The wind load was calculated according to Eurocode [14] in order that it provides the largest values for all the different standards. In all cases, the FEM as well as the algorithm described in standard [1] were effectively used for the analysis of the stress state (effort) and displacements of the shells.

References

- [1] EN 1993-1-6:2007 Design of steel structures – Strength and stability of shell structures.
- [2] EN 1993-3-2:2006 EN 1993-3-2:2006 Design of steel structures – Towers, masts and chimneys – Chimneys.
- [3] EN 1993-4-1:2007 Design of steel structures – Silos.
- [4] EN 1993-4-2:2009 Design of steel structures – Tanks.
- [5] PN-93/B-03201 Steel structures – Chimneys – Static calculations and design (in Polish).
- [6] PN-B-03202:1996 Steel structures – Silos for bulk materials – Static calculations and design (in Polish).
- [7] PN-B-03210:1997 Steel structures – Vertical cylindrical tanks for liquids – Design and erection (in Polish).
- [8] Rykaluk K., *Steel structures, chimneys, towers, masts*, Oficyna Wydawnicza Politechniki Wrocławskiej, Wrocław 2005 (in Polish).
- [9] Meller M., Pacek M., *Industrial chimneys*, Wydawnictwo Politechniki Koszalińskiej, Koszalin 2001 (in Polish).
- [10] Ziółko J., Włodarczyk W., Mendera Z., Włodarczyk S., *Special steel structures*, Arkady, Warszawa 1995 (in Polish).
- [11] Ziółko J., *Metal tanks for liquids and gases*, Warszawa 1986 (in Polish).
- [12] PN -77/B-02011 Static load calculations – Wind actions (in Polish).
- [13] Rykaluk K., *The wind load of steel towers*, Inżynieria i Budownictwo 10/2003, 557-559 (in Polish).
- [14] EN 1991-1-4:2005 Actions on structures – General actions – wind actions.
- [15] EN 1990:2002 Basis of structural design.
- [16] ECCS, *Buckling of steel shells. European Design Recommendations*, 5th edition, 2008.

- [17] Rotter M., *Guide for the economic design of circular metal silos*, Spon Press, London 2001.
- [18] EN 1991-4:2006 Actions on structures – Silos and tanks.
- [19] Piekarczyk M., Michałowski T., Kowalczyk D., *Examples of design steel shell structures according to Eurocodes*, proc. of Conference ZK 2014 Metal Structures, Kielce University of Technology, 147-150 (in Polish).
- [20] Kowalczyk D., *Design of steel silo with flat sheets, made in consequence classes CC2*, Master thesis, thesis supervisor T. Domański, Politechnika Krakowska, Kraków 2013 (in Polish).
- [21] Gwóźdź M., Michałowski T., *Basis of reliability of welded steel tanks for liquids and liquefied gases*, Przegląd spawalnictwa, 3/2012, 3-10 (in Polish).
- [22] Błazik-Borowa E. et al., *Examples of solutions of structural mechanics problems using a system Algor*, IZT, Lublin 2000 (in Polish).
- [23] Pazdanowski M., *Calculation program "Robot" in examples*, CUT, Kraków 2011 (in Polish).

WOJCIECH POLITALSKI*

THE LOADING PATTERN'S INFLUENCE ON THE STRESS INCREMENT IN PRESTRESSING STEEL AND BENDING MOMENT RESISTANCE IN MULTI-SPAN MEMBERS POST-TENSIONED WITH UNBONDED TENDONS

WPŁYW SCHEMATU OBCIĄŻEŃ NA PRZYROST NAPRĘŻEŃ W STALI SPRĘŻAJĄCEJ ORAZ NOŚNOŚĆ NA ZGINANIE W ELEMENTACH WIELOPRZĘSŁOWYCH SPRĘŻONYCH CIĘGNAMI BEZ PRZYCZEPNOŚCI

Abstract

During the design process of members post-tensioned with unbonded tendons, deformations of the whole structure between anchorages, having impact on ultimate value of prestressing force, shall be considered. The conducted researches enabled the separation of several parameters influencing the stress increase in unbonded tendons – i.a. the loading pattern in multi-span members. This paper presents selected codes provisions and theoretical researches describing this factor. Values received from analytical calculations are shown and compared.

Keywords: design process, stress increase in unbonded tendons, multi-span members

Streszczenie

Podczas projektowania elementów sprężonych cięgnami bez przyczepności należy wziąć pod uwagę odkształcenia całej konstrukcji pomiędzy zakotwieniami mające wpływ na graniczną wartość siły sprężającej. W przeprowadzonych badaniach wyodrębniono kilka parametrów wpływających na przyrost naprężeń w cięgnach bez przyczepności – m.in. schemat obciążeń. Artykuł przedstawia wybrane przepisy normowe i podejścia teoretyczne opisujące ten wskaźnik. Zaprezentowano i porównano jego wartości otrzymane z obliczeń teoretycznych.

Słowa kluczowe: projektowanie, przyrost naprężeń w cięgnach, elementy wieloprzęsłowe

DOI: 10.4467/2353737XCT.15.081.3881

* Ph.D. Eng, Wojciech Politalski, Institute of Building Materials and Structures, Faculty of Civil Engineering, Cracow University of Technology.

1. Introduction

Knowledge of cross-section internal forces is required for the estimation of bending moment resistance; thus, compression forces in concrete and ordinary reinforcement, tension forces in ordinary and prestressing reinforcement. For this purpose, strain compatibility analysis, strains-stresses relationships for concrete and steel and equilibrium equations introduced both in Polish Code [3] and Eurocode 2 [2] can be used. However, problems connected with establishing the prestressing force value in unbonded tendons are encountered. Prestressing reinforcement stresses can be described using the equations:

– EC2 notation [2]

$$\sigma_{pmt} = \sigma_{pm\infty} + \Delta\sigma_{p,ULS} \quad (1a)$$

– ACI 318M-14 notation [1]

$$f_{ps} = f_{se} + \Delta f_{ps} \quad (1b)$$

where:

- σ_{pmt}, f_{ps} – stress in tendons at ultimate,
- $\sigma_{pm\infty}, f_{se}$ – effective prestress in tendons,
- $\Delta\sigma_{p,ULS}, \Delta f_{ps}$ – stress increase in unbonded tendons at ultimate.

Although effective prestress determination can be performed with limited effort, stress increase in unbonded tendons due to external loading is not such an easy task. The encountered problem is caused by the fact that strains increase in unbonded tendons has rather global than local character in comparison with bonded tendons. Ideal bond assumption between concrete and prestressing reinforcement, which could be taken in case of bonded tendons, leads to the same strains changes in prestressing reinforcement and concrete at the tendon's level. On the other hand, neglecting friction between the prestressing reinforcement and the sheath in the case of unbonded tendons results in the same value of stresses along the tendon. Therefore, strain changes in prestressing reinforcement are equal to mean value of strain changes in concrete at tendon's level between anchorages.

Thanks to both theoretical and experimental research, several parameters influencing stress increase in unbonded tendons were distinguished. These are: concrete compressive strength, span-to-depth ratio, type of loading, ordinary and prestressing reinforcement ratios and finally, the loading pattern in the case of multi-span members. A large majority of them are presented in a previous article dealing with stress increase in unbonded tendons at ultimate [10].

2. Codes provisions

Recommendations regarding stresses in unbonded tendons at ultimate could be encountered for the very first time in ACI 318 Code 1963 edition. Due to the small number of tests and corresponding lack of proper knowledge concerning these types of structures, the following very simple and conservative equation was proposed:

$$f_{ps} = f_{se} + 105 \text{ [MPa]} \quad (2)$$

The increasing amount of tests' data and theoretical researches conducted over dozens of years has led to the introduction of three parameters to the equations describing stress increment in unbonded tendons at ultimate. These are: concrete compressive strength f'_c , prestressing reinforcement ratio ρ_p and span-to-depth ratio l_{eff}/d_p . Currently used equations are gathered in Table 20.3.2.4.1 of ACI 318-14 [1]. Equation (3) is used for calculating stress in unbonded tendons at ultimate for members with span-to-depth ratio not greater than 35 ($L/d_p \leq 35$). Equation (4) is valid for more slender members.

$$f_{ps} = f_{se} + 70 + \frac{f'_c}{100 \cdot \rho_p} \text{ [MPa]} \quad (3)$$

with limitations $f_{ps} \leq f_{se} + 420 \text{ MPa}$; $f_{ps} \leq f_{py}$ i $f_{se} \geq 0.5 f_{pu}$

$$f_{ps} = f_{se} + 70 + \frac{f'_c}{300 \cdot \rho_p} \text{ [MPa]} \quad (4)$$

with limitations $f_{ps} \leq f_{se} + 200 \text{ MPa}$; $f_{ps} \leq f_{py}$ i $f_{se} \geq 0.5 f_{pu}$.

In chapter 5.10 of Eurocode 2 entitled 'Prestressed members and structures', recommendations regarding such types of structures are gathered. The most crucial facts concerning the above mentioned matter included in paragraph 5.10.8 are as follows:

- for prestressed members with permanently unbonded tendons, it is generally necessary to take the deformation of the whole member into account when calculating the increase of the stress in the prestressing steel,
- if no detailed calculation is made, it may be assumed that the increase of the stress from the effective prestress to the stress in the ultimate limit state is $\Delta\sigma_{p,ULS}$ with the indication that the recommended value should equal 100 MPa,
- if the stress increase is calculated using the deformation state of the whole member, the mean values of the material properties should be used. The design value of the stress increase $\Delta\sigma_{pd} = \Delta\sigma_p \cdot \gamma_{\Delta P}$ should be determined by applying partial safety factors $\gamma_{\Delta P, sup}$ and $\gamma_{\Delta P, inf}$ respectively. The recommended values for $\gamma_{\Delta P, sup}$ and $\gamma_{\Delta P, inf}$ are 1.2 and 0.8 respectively. If linear analysis with uncracked sections is applied, a lower limit of deformations may be assumed and the recommended value for both $\gamma_{\Delta P, sup}$ and $\gamma_{\Delta P, inf}$ is 1.

Additionally, in chapter 7.2 Eurocode recommends that the mean value of the stress in prestressing tendons should not exceed $0.75 f_{pk}$.

Polish Code [3] (significantly based on Eurocode 2) does not contain different information regarding calculation of stress increase in the unbonded tendons. Recommendations concerning this type of prestressing are described in paragraph 7.1.10 entitled 'Structures post-tensioned without bond'. These recommendations are as follows:

- prestressing force value at Ultimate Limit State equals the design value of the force in the tendon enlarged by the mean increase of the concrete strain along the tendon's duct,

- it is assumed that the stress increase in the internal unbonded tendons equals 100 MPa for a single span length. In the case of a higher number of spans, this value should be reduced considering amount of spans,
- the number of tendons in continuous slabs should be chosen in such a way that releasing prestress in two adjacent tendons will not lead to the destruction of the construction,
- in the case of a single tendon failure, the redistribution of internal forces should be assured by ordinary reinforcement.

Moreover in chapter 7.1.2, Polish Code recommends that the mean value of the stress in prestressing tendons should not exceed $0.65 f_{pk}$.

The above review of codes which are used in Poland during the design process indicates their conservativeness with regards to ULS of structures post-tensioned with unbonded tendons. The constant value equal to 100 MPa is given both in Polish Code [3] and Eurocode 2 [2], with no differentiation regarding the type of structures (beams, slabs, tanks etc.). This conforms to the state of art described by the ACI Code from 1963. Even though the Polish Code provides stress reduction necessity in the case of continuous members, it does not specify exact means to be taken in this regard. Although ACI Code [1] takes into account three parameters influencing stress increase in unbonded tendons, the loading pattern is not considered among them. Factors distinguished during regression analysis were calculated based on tests' researches both for single and multi-span members.

3. Theoretical researches

Description trials of the above mentioned phenomenon were conducted by various authors. Two trends could be emphasised among the proposed theories. The first trend introduces the prestressing reinforcement strain reduction factor which allows conducting calculations in a similar way as for members post-tensioned with bonded tendons [8, 11]. The second one refers to plastic hinge length which occurs at ultimate [4–7]. Only theories considering the loading pattern as a parameter used for estimating stress increase in unbonded tendons are described below.

3.1. Naaman et al.

Strain reduction factor defined as mean strain increase in unbonded tendons to strain increase in equivalent bonded tendons in critical cross-section was introduced by Naaman. This is expressed by the equation below:

$$\Omega_u = \frac{(\Delta\varepsilon_{psu})_{av}}{(\Delta\varepsilon_{psb})_m} = \frac{(\Delta\varepsilon_{psu})_{av}}{(\Delta\varepsilon_{cps})_m} \quad (5)$$

where:

- $(\Delta\varepsilon_{psu})_{av}$ – average strain increase in unbonded tendons beyond ε_{pe} ,
- $(\Delta\varepsilon_{psb})_m$ – maximum strain increase in bonded tendons beyond ε_{pe} ,
- $(\Delta\varepsilon_{cps})_m$ – maximum strain increase in concrete at the level of the tendon.

During regression analysis, two parameters were taken into consideration: type of loading (one-point loading, third-point loading and uniformly distributed loading) and span-to-depth

ratio varying within the limits of 7.8 to 45 – this covers the majority of commonly used beams and slabs. The best convergence between test results and analytical calculations was obtained for the following values of Ω_u :

$$\Omega_u = \frac{2.6}{\left(\frac{L}{d_{ps}}\right)} \quad \text{for one-point loading} \quad (6)$$

$$\Omega_u = \frac{5.4}{\left(\frac{L}{d_{ps}}\right)} \quad \text{for third-point or uniformly distributed loading} \quad (7)$$

Equation describing the value of stress in unbonded tendons at ultimate:

$$f_{ps} = f_{pe} + \Omega_u \cdot E_{ps} \cdot \varepsilon_{cu} \cdot \left(\frac{d_{ps}}{c} - 1\right) \cdot \frac{L_1}{L_2} \quad (8)$$

where:

- E_{ps} – prestressing steel modulus of elasticity,
- ε_{cu} – ultimate compressive strain in the concrete,
- d_{ps} – effective depth of a cross-section,
- c – concrete compressive stress block depth,
- L_1 – sum of spans lengths under loading,
- L_2 – tendon length between anchorages.

3.2. Harajli et al.

In one of the first papers, Harajli [4] connected stress increase in unbonded tendons with the number and length of plastic hinges which occur at ultimate. After few operations, plastic hinge length L_0 could be expressed as a function of loading type and span-to-depth ratio described by the equation below:

$$L_0 = d_p \left[\frac{L}{d_p} \cdot \left(\frac{0.95}{f} + 0.05 \right) + 1 \right] \quad (9)$$

where:

- $f = \infty$ – for one-point loading,
- $f = 6$ – for uniformly distributed loading,
- $f = 3$ – for third-point loading.

In equation (11), which describes value of stress increment in unbonded tendons, plastic hinge length was expressed by usage of the γ parameter (10). Additionally, by means of regression analysis, two factors α and β (depending on type of loading) were introduced.

$$\gamma = \left[1 + \frac{1}{\frac{L}{d_p} \cdot \left(\frac{0.95}{f} + 0.05 \right)} \right] \cdot \frac{n_0}{n} \quad (10)$$

$$f_{ps} = f_{pe} + \gamma \cdot f_{pu} \cdot \left(\alpha - \beta \cdot \frac{c}{d_p} \right) \quad (11)$$

where:

- $\alpha = 0.10; \beta = 0.18$ – for one-point loading ($f = \infty$),
- $\alpha = 0.25; \beta = 0.44$ – for uniformly distributed loading ($f = 6$),
- $\alpha = 0.40; \beta = 0.70$ – for third-point loading ($f = 3$),
- n_0 – number of spans under loading,
- n – total number of spans.

In consecutive paper [5] plastic hinge length was expressed as a function of compression zone depth c and type of acting loading (12). The stress increment in continuous members could be calculated as a variable of plastic hinges number n_p and length L_p (13) – its form is described by equation (14) in which compression zone depth c_y is counted by assuming yield strength both in ordinary and prestressing reinforcement (15).

$$L_p = \left(\frac{20.7}{f} + 10.5 \right) \cdot c \quad (12)$$

$$\Delta f_{ps} = E_{ps} \varepsilon_{cu} \left(\frac{d_p - c}{c} \right) \cdot \frac{n_p \cdot L_p}{L} \quad (13)$$

$$f_{ps} = f_{pe} + \phi_{ps} E_{ps} \varepsilon_{cu} \left(\frac{d_p - c_y}{L / n_p} \right) \cdot \left(\frac{20.7}{f} + 10.5 \right) \leq f_{py} \quad (14)$$

$$c_y = \frac{A_{ps} f_{py} + A_s f_y}{0.85 \beta_1 f'_c b} \quad (15)$$

where:

- ϕ_{ps} – partial safety factor,
- n_p – number of formed plastic hinges at ultimate,
- A_{ps} – prestressing reinforcement area,
- f_{py} – yield strength of prestressing reinforcement,
- A_s – ordinary reinforcement area,
- f_y – yield strength of ordinary reinforcement,
- β_1 – factor in the Whitney stress block,
- b – width of concrete compressive stress block.

Figure 1 shows differences in calculations of the loading pattern factor for two- and three-span members according to equations (8), (10) and (14). It should be pointed out that in all

cases, expressions L_1/L_2 , n_0/n and n_p/n are equal to 1 for simply supported beams. It can be observed that failure mechanism analysis by considering number of plastic hinges at ultimate enables to obtain greater values of loading pattern factor. Another benefit is that it takes into account and differentiates which span is loaded – the external or the internal. It should be emphasised that applying some loading patterns could lead to a value greater than 1 which is assumed for simply supported members.

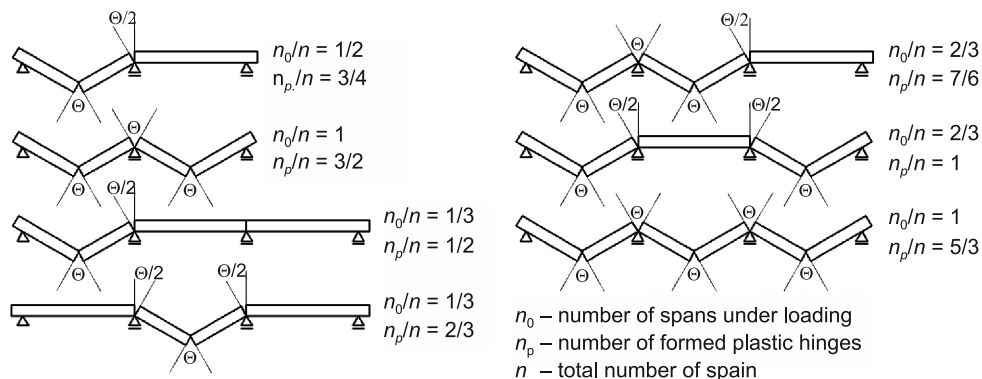


Fig. 1. Load pattern factor values – two- and three-span members

Some discrepancies can be found in over-mentioned theory. In (14) factor f which depends on loading type expresses only one plastic hinge length. It should be added that plastic hinge length might differ in span where different types of loading could be acting ($f = 3, 6$ or ∞) and at support where reaction should be rather associated with one-point loading ($f = \infty$).

The next paper [6] deals with these doubts by introducing distinction for plastic hinges formed in spans n_p^+ and at supports n_p^- . Both of these are connected and expressed by N_p factor (16). Equation (17) for calculating the stress increase in unbonded tendons at ultimate is a modification of the former equation (14).

$$N_p = \left(\frac{20.7}{f} + 10.5 \right) \cdot n_p^+ + 10.5 \cdot n_p^- \quad (16)$$

$$f_{ps} = f_{pe} + \frac{\phi_{ps} \cdot N_p \cdot E_{ps} \cdot \varepsilon_{cu}}{L / d_p} \cdot \left[1 - \frac{c_y}{d_p} \right] \leq 0.95 f_{py} \quad (17)$$

The method of calculating the N_p factor in accordance with equation (16) is presented in Fig. 2. The numbers of plastic hinges in spans n_p^+ and at supports n_p^- are presented. Moreover, two values of this factor which depend on the type of loading are presented for one-point loading (1P) and uniformly distributed loading (q) respectively. It is worth emphasising that this value for simply supported beams is 10.5 and 14 accordingly.

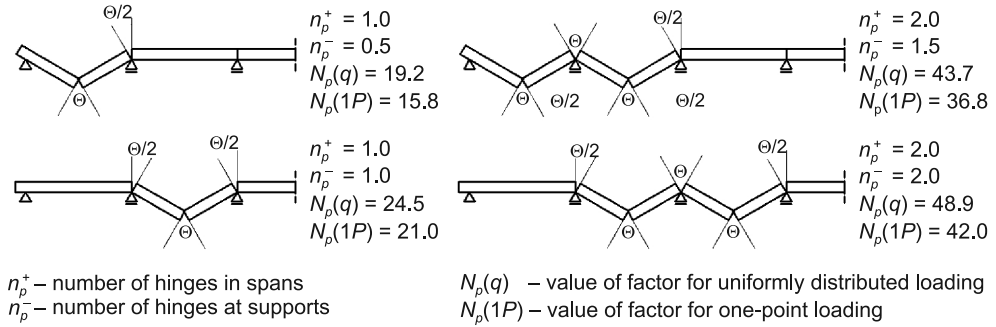


Fig. 2. Load pattern factor calculation with span and support hinge distinction taken into account

The following assumptions and limitations regarding the formation of plastic hinges are introduced:

- all plastic hinges behave similarly i.e. concrete compressive block depth c , depth and area of prestressing reinforcement d_{ps} and A_{ps} and ordinary reinforcement d_s and A_s are the same or very similar in all spans and support cross-sections,
- the section is rectangular or has rectangular section behaviour,
- stress increase at ultimate above the effective prestress Δf_{ps} is assumed to be not greater than $(0.95f_{py} - f_{se})$ – this ensures that the stress in tendons will not reach yield strength of prestressing reinforcement.

4. Conclusions

The above presented code recommendations treat unbonded tendons stress increase in continuous members in a superficial manner. ACI Code design equations for calculating stress increase do not make distinctions between simply supported and continuous members. The opportunity to achieve lower values of stress increase in multi-span members compared to simply supported elements in the case of loading which does not act at all spans simultaneously is disregarded by EC 2. Even though such a possibility is mentioned in Polish Code, no detailed provisions are given.

Due to this fact, directions for solving the problem of stress increment in multi-span unbonded members are searched and can be successfully found in theories proposed by various authors. All of the above presented equations in continuous members are expansions of equations derived firstly for simply supported members. Hence, the loading pattern factor for simply supported beams is equal to 1.

Table 1 contains a comparison of parameters needed to calculate the loading pattern factor utilising equations (10, 14 and 16) for members for which the span number is not greater than 3. Span names are signed with first alphabet letters as shown in Fig. 3. Due to symmetry and assumption that all spans lengths are equal not all combinations are being considered (e.g. in three-span member separate loading of external spans A and C, external and internal spans A+B and B+C will produce the same value of loading pattern factor).

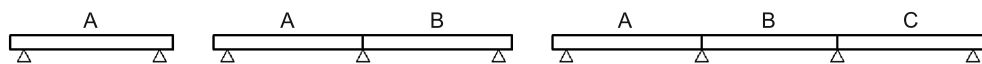


Fig. 3. Span nomenclature – simply supported, two-span and three-span members

Table 1

Loading pattern factor value for simply supported, two-span and three-span members

Type of member	One-span	Two-spans		Three-spans				
	A	A	A+B	A	B	A+B	A+C	A+B+C
Total number of spans n	1	2		3				
Number of loaded spans n_0	1	1	2	1	1	2	2	3
Value of factor n_0/n – eq. (10)	1	1/2	1	1/3	1/3	2/3	2/3	1
Number of plastic hinges n_p	1	1 1/2	3	1 1/2	2	3 1/2	3	5
Value of factor n_p/n – eq. (14)	1	3/4	1 1/2	1/2	2/3	1 1/6	1	1 2/3
Number of plastic hinges n_p^+	1	1	2	1	1	2	2	3
Number of plastic hinges n_p^-	0	1/2	1	1/2	1	1 1/2	1	2
$N_p(1P)$ value – eq. (16) $f = \infty$	10.5	15.8	31.5	15.8	21.0	36.8	31.5	52.5
$N_p(q)$ value – eq. (16) $f = 6$	14.0	19.2	38.4	19.2	24.5	43.7	38.4	62.9
Factor $N_p(1P)/(n \cdot N_p(1 \text{ span}))$	1	3/4	1 1/2	1/2	2/3	1 1/6	1	1 2/3
Factor $N_p(1q)/(n \cdot N_p(1 \text{ span}))$	1	2/3	1 3/8	1/2	3/5	1	1	1 1/2

Observation of loading pattern factor values gathered in Table 1 leads to the following conclusions regarding two- or three-span members:

- in the case of only one span loaded stress increase in unbonded tendons will be lower than that calculated for simply supported member. This effect is greater for three-span than for two-span members; therefore, for members containing additional spans, this phenomenon will intensify,
- in the case of all spans loaded in two-span or at least two spans loaded in three-span, member stress increase in unbonded tendons will be greater or at the very least, the same as for simply supported members. Once again, this effect is greater for three-span than for two-span members; therefore, for members containing additional spans this phenomenon will intensify,
- loads acting in internal spans give greater values of load pattern factor than in the case of external span loading – this is caused by a higher number of formed plastic hinges.

Usually, when designing ordinary reinforced structures or structures post-tensioned with bonded tendons, we get into the habit of checking resistance in crucial cross-sections using loading patterns which give maximum bending moments. In the case of three-span members, the maximum moment in span A occurs when spans A and C are loaded simultaneously. The maximum moment at internal support appears when spans A and B (or B and C) are loaded simultaneously.

The design of multi-span structures post-tensioned with unbonded tendons could be different to the one described in the above scheme. In some cases, Ultimate Limit State could

be reached by different loading patterns; for example, both span and support bending moments caused by loading only one exterior span (A) would be lower than loading both exterior spans (A+C) and exterior and interior span (A+B) respectively. It should be emphasised that stress increase in unbonded tendons which has an influence on the bending moment resistance would also be lower. In some cases, loading of only one span could result in the bending resistance reduction being greater than the decrease of bending moment produced by external loading. It could be anticipated that this effect would be greater for members with a higher number of spans. Ultimate Limit State would not be reached by a sophisticated loading pattern but for simple scheme where one, external span is loaded.

References

- [1] Building Code Requirements for Structural Concrete (ACI 318M-14).
- [2] PN-EN 1992-1-1:2004 Eurokod 2: Projektowanie konstrukcji z betonu – Część 1: Reguły ogólne i reguły dla budynków (Eurocode 2: Design of concrete structures – Part 1-1: General rules and rules for buildings).
- [3] PN-B-03264:2002 Konstrukcje betonowe, żelbetowe i sprężone. Obliczenia statyczne i projektowanie (Plain, reinforced and prestressed concrete structures. Analysis and structural design).
- [4] Harajli M., Hijazi S., *Evaluation of the Ultimate Steel Stress in Partially Prestressed Concrete Members*, PCI Journal, Vol. 36, No. 1 1991, 62-82.
- [5] Harajli M., *On the Stress in Unbonded Tendons at Ultimate: Critical Assessment and Proposed Changes*, ACI Structural Journal, Vol. 103, No. 6, 2006, 803-812.
- [6] Harajli M., *Tendon Stress at Ultimate in Continuous Unbonded Post-Tensioned Members: Proposed Modification of ACI 318, Eq. (18-4) and (18-5)*, ACI Structural Journal, Vol. 109, No. 2, 2012, 183-192.
- [7] Lee L.H., Moon J.H., Lim J.H., *Proposed Methodology for Computing of Unbonded Tendon Stress at Flexural Failure*, ACI Structural Journal, Vol. 96, No. 6, 1999, 1040-1048.
- [8] Naaman A., Alkhairi F., *Stress at Ultimate in Unbonded Post-Tensioning Tendons: Part II – Proposed Methodology*, ACI Structural Journal, Vol. 88, No. 6, 1991, 683-692.
- [9] Politalski W., *Przyrost naprężeń w wewnętrznych cięgnach bez przyczepności w betonowych, sprężonych elementach zginanych*, Rozprawa doktorska (*Stress increase in internal unbonded tendons in prestressed concrete flexural members. Doctoral thesis*), July 2015.
- [10] Seruga A., Politalski W., *Graniczne naprężenia stali sprężającej w elementach zginanych sprężonych cięgnami bezprzyczepnościowymi*, Czasopismo Techniczne, 1-B/2008, 109-133.
- [11] Yang K. H., Kang H.-K., *Equivalent Strain Distribution Factor for Unbonded Tendon Stress at Ultimate*, ACI Structural Journal, Vol. 108, No. 2, 2011, 217-226.

KATARZYNA RZESZUT*, MACIEJ SZUMIGAŁA*, ŁUKASZ POLUS*

SELECTED ASPECTS OF THE PROPER APPLICATION OF STRUCTURAL MATERIALS IN TERMS OF CORROSION

WYBRANE ASPEKTY POPRAWNEGO STOSOWANIA MATERIAŁÓW KONSTRUKCYJNYCH W WARUNKACH KOROZJI

Abstract

In this paper, the problem of corrosion in structural elements made of materials which are considered as corrosion resistant is discussed. The paper presents an analysis of the reasons for corrosion damage to structural elements used in civil engineering. The main aim of the work was to identify the potential causes of corrosion and to formulate recommendations that allow the selection of the best structural material properties in order to counteract the negative impact of the corrosive environment. For this purpose, stainless steel ventilation duct corrosion in an indoor swimming pool hall is analysed. An assessment of the nature of the reasons for the potential damage of ventilation ducts is performed based on macroscopic inspection. This allowed the determination of the type and nature of the existing corrosion of stainless steel. The analysis of the results of the chemical composition of the material provided by the gravimetric method and the results of the corrosion products report provided further information. Based on its conclusions, recommendations in order to avoid this type of corrosion in aggressive indoor swimming pool environments are formulated. Next, the problem of corrosion of aluminium in contact with steel in new aluminium and concrete composite structures which consist of an aluminium beam, steel trapezoidal sheeting and a concrete slab is analysed. Moreover, recommendations in order to avoid this type of corrosion are formulated. The presented analyses can be a valuable source of information on corrosion and protection methods in specific cases of building structures.

Keywords: stainless steel, aluminium, aluminium and concrete composite structures

Streszczenie

W artykule poruszono problem korozji w elementach konstrukcyjnych wykonanych z materiałów uznawanych za odporne na korozję. Artykuł zawiera analizę przyczyn niszczenia elementów konstrukcyjnych wskutek korozji. Główny cel pracy to określenie potencjalnych przyczyn korozji i sformułowanie zaleceń, które pozwolą wybrać najlepsze właściwości materiału w celu przeciwdziałania korozyjnemu środowisku. W tym celu poddano analizie skorodowane przewody wentylacyjne zamontowane w krytej pływalni. Ocena charakteru potencjalnych przyczyn uszkodzeń kanałów wentylacyjnych była wykonana w oparciu o badania makroskopowe. To pozwoliło określić typ i naturę korozji w stali nierdzewnej. Analiza składu chemicznego materiału otrzymana z badania metodą grawimetryczną oraz wyniki raportu o produktach korozji dostarczyły dodatkowych informacji. W oparciu o powyższe sformulowano wnioski i zalecenia, w jaki sposób uniknąć tego typu korozji w agresywnym środowisku występującym w krytej pływalni. Następnie przeanalizowano problem korozji aluminium w kontakcie ze stalą w nowych aluminiowo-betonowych konstrukcjach zespolonych, które składają się z: aluminiowej belki, stalowej trapezowej blachy i betonowej płyty. Ponadto sformulowano zalecenia, w jaki sposób uniknąć korozji w tych konstrukcjach. Zaprezentowane analizy mogą być cennym źródłem informacji na temat korozji i metod jej zapobiegania w konkretnych budynkach.

Słowa kluczowe: stal nierdzewna, aluminium, aluminiowo-betonowe konstrukcje zespolone

DOI: 10.4467/2353737XCT.15.082.3882

* Ph.D. Katarzyna Rzeszut, D.Sc. Ph.D. Maciej Szumigała, M.Sc. Łukasz Polus, Institute of Structural Engineering, Faculty of Civil Engineering and Environmental Engineering, Poznan University of Technology.

1. Introduction

Stainless steels and aluminium are widely used in civil engineering applications. Stainless steels cover a wide range of steel types and grades which characterise high resistance against corrosion or oxidation [10]. Stainless steels are iron alloys with a minimum of 10.5% chromium and with other alloying elements such as nickel, molybdenum, titanium, copper and carbon. These alloying elements enhance the properties of the material, the most important being its strength and corrosion resistance. The influence of chemical composition and temperature on the physical properties of austenitic stainless steel is presented in [2]. The present paper discusses the temperature influence on mechanical properties, such as tensile strength, fatigue and creep. Mechanisms to strengthen the austenitic stainless steels by appropriate thermo-mechanical treatments are analysed and the fact that the selection of a particular grade of stainless steel must meet the corrosion resistance requirements for a specified application or environment is highlighted. The problem of stainless steel corrosion is widely discussed in literature. The uniform corrosion aspect of austenitic stainless steels in various corrosive environments is reviewed in [12]. Ningshen and Kamachi Mudali discussed the application of existing and advanced austenitic alloys for various chemical media and the various testing techniques employed for assessing uniform corrosion. The pitting corrosion of austenitic stainless steels is studied in [7], this takes into account the influence of alloy composition, microstructure, cold working, grain size and different parameters of environments. The susceptibility of annealed and unannealed AISI 444 ferritic stainless steel to pitting and crevice corrosion is analysed in [1]. It was found that annealing does not improve the resistance to pitting and crevice corrosion. The problem of stainless steel corrosions became most important in the case of application in indoor swimming pool buildings. Highly aggressive conditions result from the particular atmospheric circumstances in such buildings and this decreases corrosion resistance. Common reasons for stainless steel corrosion in indoor pools are presented in [4]. Houska and Fritz pointed out that chlorine-based chemicals used to disinfect pool water produce chloramines which are passed into the atmosphere and deposited on metal surfaces causing the corrosion problems. The corrosion rate varies with temperature and humidity level and may result in the damage of swimming pool equipment or main structural element collapse. It was found that usually, collapses are caused by stress corrosion cracking (SCC) of stainless steel load bearing elements subjected to tensile stress. According the European Standard recommendations [15], several austenitic steels are suitable for many applications in indoor and outdoor swimming-pools. The investigation conducted in [5] confirms that stainless steel 1.4547 shows the best performance and resistance to stress corrosion cracking compared to the other tested stainless steels. Nevertheless, even this kind of stainless steel can be susceptible to SCC if deposits of chloride salts and very specific relative humidity for these salts in combination with the temperature exceed the limit value. In [13], results of metallographic investigations of indoor pool ventilation ducts made of stainless steel type 1.4301 were presented. It was found that the corrosive degradation of this steel occurred as a pitting corrosion in a chloride medium in the form of pinholes and micro-cracking.

Aluminium structures are considered as corrosion resistant material as well as stainless steels [3]. Corrosion resistance is one of the most important features of aluminium [8].

However, aluminium may corrode in some cases. The problem of aluminium corrosion is widely discussed in [9]; the author pointed out that aluminium is resistant to atmospheric corrosion thanks to inert aluminium oxide film being insoluble in water and this blocks further oxidation. Corrosion resistance of aluminium depends on chemical composition, the fabrication process, heat treatment and the stress field. What is important is that usually, corrosion does not reduce the safety of aluminium structures, but only decreases the aesthetics of the structures. Mazzolani in [12] presented the influence of alloy additions to pure aluminium on corrosion resistance and proposed systems which may protect the surface of the metal. He described types of corrosion of aluminium (surface, concentrated, intergranular, lamellar, stress, and corrosion by contact) and he particularly focused on corrosion of aluminium in contact with steel. He also pointed out that the contact aluminium with a humid and corrosive environment should be limited. Aluminium should be separated from concrete, mortar, timber and bricks. A similar suggestion is presented in [11]. He suggested coating aluminium with bitumen to separate it from concrete. In his opinion, the pure aluminium exhibited the highest corrosion resistance. Aluminium is dissolved by fluorine, sodium hydroxide and potassium hydroxide. Hydrochloric acid, copper and bromine are very corrosive for aluminium. Aluminium corrodes in seawater, sea air, industrial air, and when in contact with steel, lead, copper and mercury. Aluminium does not corrode in contact with zinc, cadmium and stainless steel. Furthermore, aluminium does not corrode in aluminium and iron Alfin brake drums thanks to accurate connection of both materials. Mromliński underlined that corrosion intensity decreases rapidly after two years. Jasiczak and Hajkowski suggested using aluminium at a pH of between four and nine [6] and checking the possibility of corrosion using the Pourbaix diagram [17]. Siwowski described an example of corrosion of aluminium in contact with steel in an aluminium bridge deck [19]. The aluminium bridge deck corroded because of contact aluminium with steel rivets.

2. Corrosion of stainless steel

The first part of the paper covers an analysis of the corrosion of stainless steel that was carried out on the example of ventilation ducts installed in the pool hall of The Centre for Tourism and Recreation [18].

2.1. Macroscopic assessment of installed ventilation ducts

The macroscopic assessment of the current state of ventilation ducts allowed determining the nature of reasons for potential damage. It was recognised that several types of damage and corrosion had occurred within the ventilation ducts mounted over the basin of the pool. One of these was pitting corrosion, which occurs when the atmosphere contains chlorides and the passive layer of stainless steel is locally damaged. In the analysed sample, the pitting corrosion occurs in the form of pinholes and micro-cracks (Fig. 1).

The rate of this type of corrosion significantly increases at elevated temperatures. A corrosion cavity develops and can lead to the complete perforation of the metal sheet.

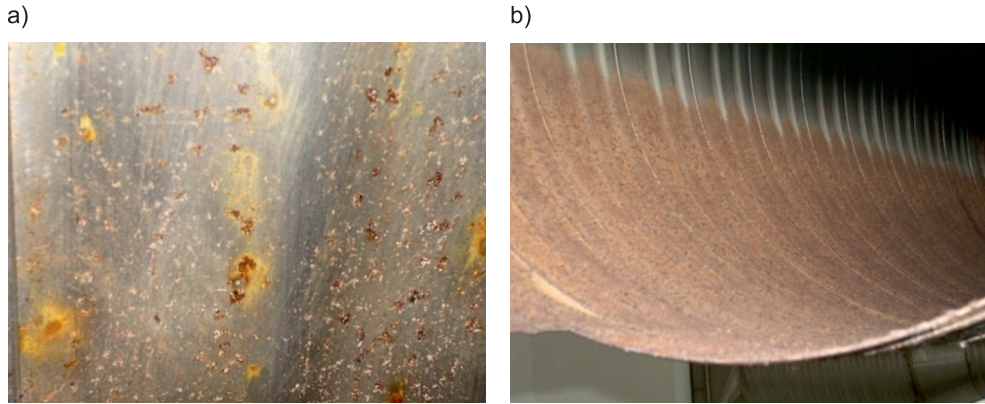


Fig. 1. Pitting corrosion: a) visible micro-cracking and pinholes; b) deposits of corrosion on the surfaces of ventilation ducts [18]

Stress corrosion cracking (SCC) in the form of layers of light and rust deposits on the fold line of the sheet is presented in Fig. 2a. One can observe linearly placed local pitting corrosion as a consequence of tensile stresses due to cold-rolling. Stress corrosion cracking occurred with the equipment exposed to swimming pool atmospheres and arises due to the combination of the mechanical load and the corrosive environment with free chloride ions. It is worth noting that the SCC process is usually difficult to detect before cracking occurs because it develops inside the material among the crystals. Therefore, designers should keep in mind that this corrosion is present in members subjected to tensile stress, as a result of external load action or in the form of residual stresses due to welding, cold rolling or deep forming.

Another type of corrosion detected in the analysed vent ducts was crevice corrosion. This type of corrosion appears when the pH reaches a critical value called the ‘depassivation

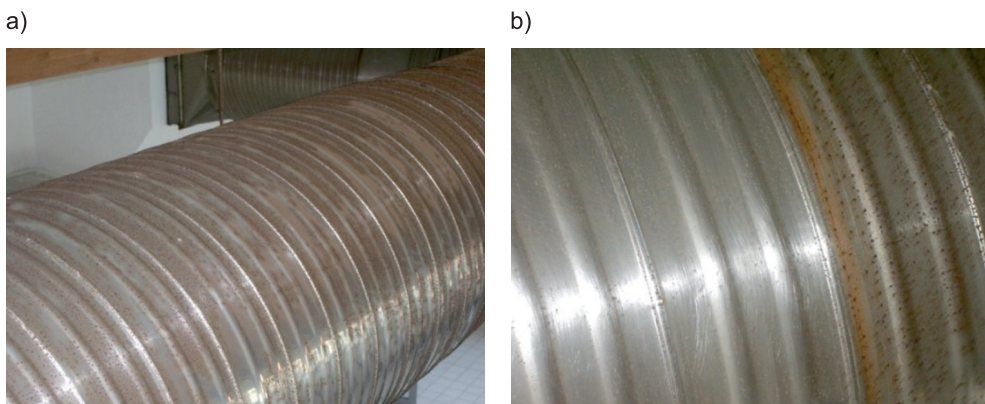


Fig. 2. a) example of stress corrosion cracking due to cold rolling; b) example of crevice corrosion [18]

pH'. It develops at the region within a crevice which promotes the accumulation of chemical deposits. Crevice corrosion associated with the presence of gaps within a connection is presented in Fig. 2b.

2.2. Analysis of the chemical composition

Analysis of chemical composition of material and corrosion products was performed based on results supplied by the contractor. The chemical composition was conducted by the gravimetric method (Table 1).

Table 1

Chemical composition of material [18]

Chemical element	Tested sample (vent duct) [%]	X2CrNiMo17-12-2 (1.4404) (PN EN 10088-1:2007) [%]
C	0.03	0.03
Si	0.028	1.00
Mn	1.90	2.00
P	0.025	0.045
S	0.015	0.15
Cr	16.80	16.5–18.5
Ni	10.00	10.0–13.0
Mo	2.35	2.0–2.5

It was found that the material of vent ducts installed in the swimming pool corresponds to the stainless steel grade X2CrNiMo17-12-2 (1.4404) according to [14]. Based on the analysis of the chemical composition of the steel sample, it can be concluded that the content of the Cr and Ni is placed in the lower limits of the range referred to in [14], while the carbon content reaches an upper limit. As is well known, a low content of Cr and Ni can influence the reduction in corrosion resistance. Furthermore, in environments containing spray steam and free chlorine ions, the risk of corrosion increases significantly. Particular attention should be paid to the very high content of chlorine that was found during the analysis of the chemical composition of corrosion products (Table. 2). The content of Cl reaches approx. 35% in the worst place.

Table 2

Chemical composition of corrosion products [18]

Chemical element [%]	O	Al	Si	Cl	Ca	Cr	Fe	Ni	K	Mn
place 1	18.14	1.23	3.22	24.09	5.26	4.49	29.55	14.04	–	–
place 2	22.07	4.89	12.68	34.65	6.41	1.76	6.62	10.30	0.63	–
place 3	16.25	0.24	0.44	20.25	4.56	9.43	27.92	17.55	–	3.37

3. Corrosion of aluminium in aluminium and concrete composite structures

In the second part of the paper, corrosion of aluminium in contact with steel in aluminium and concrete composite structures is analysed. Electromechanical corrosion occurs when aluminium is in contact with another metal with a liquid between two metals and a voltaic pile is established. This type of corrosion is widely discussed in [9]. The contact voltage of steel with respect to aluminium is 850 mV. Note that aluminium may corrode in contact with steel because aluminium has a lower voltage than steel. For this reason, it is necessary to separate steel from aluminium. Steel and aluminium may be separated using insulating materials like elastomeric tape, rubber or zinc plating. Steel bolts should be galvanised or electroplated. An example of insulating steel from aluminium is presented in Fig. 3. Insulating material should extend beyond the contact area.

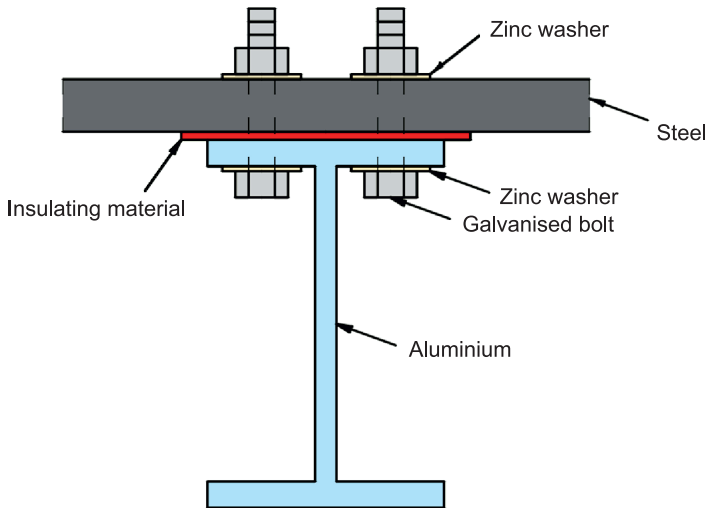


Fig. 3. Insulating steel from aluminium

Aluminium and concrete structures are a type of composite structures which consists of an aluminium beam, a concrete slab, steel sheeting and connectors [16] (Fig. 4).

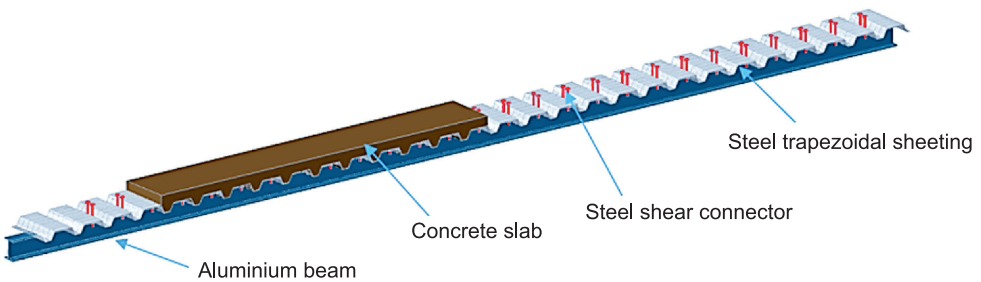


Fig. 4. An aluminium and concrete composite beam

A connection an aluminium beam with a concrete slab using special connectors is a quite new solution. Aluminium and concrete structures may be used in durable constructions. For this reason, they should be corrosion resistant. The aluminium beam is joined with the concrete slab using a steel shear connector [20] which should be galvanised to avoid corrosion of the aluminium (Fig. 5).

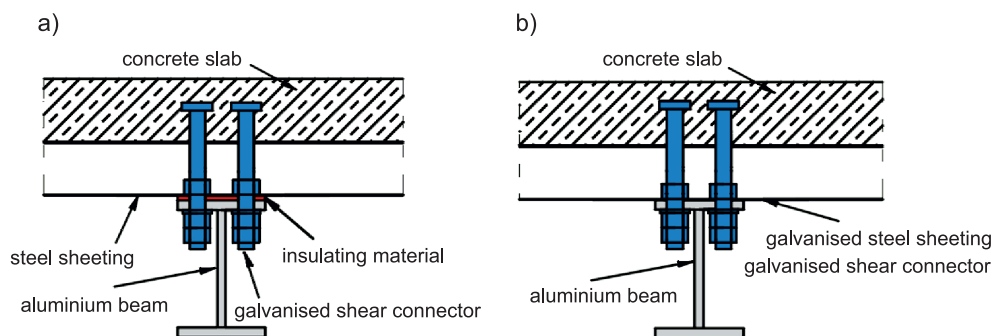


Fig. 5. A corrosion protection of the aluminium beam: a) when steel sheeting is not galvanised; b) when steel sheeting is galvanised

When steel sheeting is not galvanised, an insulating material should be applied between the aluminium flange and the steel sheeting, for example, elastomeric tape. When steel sheeting is galvanised, insulating material is unnecessary. Fresh concrete is separated from aluminium by the galvanised steel sheeting.

4. Conclusions

Based on the presented examples, it can be concluded that stainless steel is susceptible to stress corrosion cracking in aggressive environments as deposits of chloride salts and very specific relative humidity in combination with the temperature. This is particularly dangerous in the case of load bearing members subjected to tension stresses which are not cleaned. The lack of maintenance of ventilation ducts with condensed water and cleaning agents without chlorine, results in local damage to the passive layer of stainless steel and causes pitting corrosion. Another mistake is the use of corrugated metal sheet, because cold-rolling provides relatively high residual stresses. Moreover, the folds disturb easy cleaning to remove the accumulation of aggressive chloride. As a consequence, the rapid develop of stress corrosion cracking is observed. In conclusion, the application of stainless steel grade 1.4404 for vent ducts in the swimming pool was an inappropriate choice. To ensure the proper design of this type of structural member, the designers should follow the recommendation contained in the relevant norms. In the example, according to the PN-EN 1993-1-4 [15] in swimming pool's corrosive chloride environment, ventilation ducts should be designed with the following grades of steel: austenitic steels alloyed, 1.4439/X2CrNiMoN17-13-5 or 1.4539/X1NiCrMoCu25-20-5, 1.4547/X1CrNiMoCuN20-18-7 or 1.4529/X1NiCrMoCuN25-20-7 and ferritic-austenitic (duplex) 1.4462/X2CrNiMoN22-5-3. Designers should also consider the alternative method

which is based on zinc coating technology. This solution is widely used as anti-corrosion protection of steel structures. It is characterised by ease of implementation, its relatively low cost and high efficiency. The zinc layer provides anodic protection which is quite effective in case of negative impact of corrosive environment.

In the case of aluminium, it was proposed that it is one of the best materials used in building construction in terms of corrosion resistance. However, as with stainless steel it may corrode when it is used incorrectly. Corrosion does not usually decrease the safety of aluminium structures, but only damage the aesthetics of the structures. What is more, corrosion intensity may decrease rapidly after two years. Aluminium and concrete structures are a fairly new structural solution. They may be used in durable structures and they should be corrosion resistant. Therefore, designers should keep in mind that aluminium may corrode in contact with steel, because aluminium has a lower voltage than steel. Steel shear connectors in aluminium and concrete composite structures should be galvanised to avoid the corrosion of aluminium in contact with steel. When steel sheeting is not galvanised, an insulating material should be applied i.e. elastomeric tape between the aluminium flange and the steel sheeting.

Financial support from the DS grant 11-405/2015 is kindly acknowledged.

References

- [1] Bitondoa C., Bossioa A., Monettaa T., Curionib M., Belluccia F., *The effect of annealing on the corrosion behaviour of 444 stainless steel for drinking water applications*, Corrosion Science, Vol. 87, 2014, 6-10.
- [2] George G., Shaikh H., *Introduction to Austenitic Stainless Steels*, Corrosion of Austenitic Stainless Steels, Mechanism, Mitigation and Monitoring, [in:] Woodhead Publishing Series in Metals and Surface Engineering, 2002, 1-36.
- [3] Gwózdź M., *Project problems of contemporary aluminium structures*, Czasopismo Techniczne, 4-A/2007, 281-286 (in Polish).
- [4] Houska C., Fritz J., *Successful Stainless Swimming Pool Design*, British Stainless Steel Association, Construction Specifier Magazine, 2005, 1-9.
- [5] Iversen A., Prosek T., *Atmospheric stress corrosion cracking of stainless steels in swimming pool environments*, Proceedings of European Stainless Steel Conference, 2008, 49-56.
- [6] Jasiczak J., Hajkowski M., *Corrosion susceptible elevations made with aluminium plates working in treatment's plant environment*, Ochrona Przed Korozją, 5s/A, 2008, 79-85 (in Polish).
- [7] Kamachi Mudali U., Pujar M.G., *Pitting Corrosion of Austenitic Stainless Steels and Their Weldments*, Corrosion of Austenitic Stainless Steels, Mechanism, Mitigation and Monitoring, A volume in Woodhead Publishing Series in Metals and Surface Engineering, 2002, 74-105.
- [8] Mazzolani F.M., *Aluminium Alloy Structures*, E & FN SPON, an imprint of Chapman&Hall, London 1995.
- [9] Mazzolani F.M., *Aluminium Structural Design*, Springer-Verlag Wien GmbH, Wien 2003.
- [10] Mietz J., Isecke B., *Stainless steels for applications in civil engineering*, Stainless Steel World Conference, 2001, 334-339.
- [11] Mromliński R., *Aluminium structures*, Arkady, Warszawa 1975 (in Polish).

- [12] Ningshen S., Kamachi Mudali U., *Uniform Corrosion of Austenitic Stainless Steels*, Corrosion of Austenitic Stainless Steels, Mechanism, Mitigation and Monitoring, A volume in Woodhead Publishing Series in Metals and Surface Engineering, 2002, 37-73.
- [13] Ozgowicz W., Kalinowska-Ozgowicz E., Lesz S., *Ventilation ducts of an indoor swimming-pool – materials and technology possibilities*, Rynek Instalacyjny 10, 2013 (in Polish).
- [14] PN EN 10088-1:2007 Stale odporne na korozję, Gatunki stali odpornych na korozję, Polski Komitet Normalizacyjny (in Polish).
- [15] PN-EN 1993-1-4:2007 Projektowanie konstrukcji stalowych, Część 1–4: Reguły ogólne, Reguły uzupełniające dla konstrukcji ze stali nierdzewnych, Polski Komitet Normalizacyjny (in Polish).
- [16] Polus Ł., Szumigała M., *A numerical analysis of the resistance and stiffness of the aluminium and concrete composite beam*, Civil and Environmental engineering reports, CEER 15 (4), 2014, 99-112.
- [17] Pourbaix M., *Wykłady z korozji elektrochemicznej*, Polish Scientific Publishers, Warszawa 1978. (in Polish)
- [18] Rzeszut K., *Expert report on the causes of ventilation ducts corrosion in indoor swimming pool environments*, Poznan University of Technology, Poznań 2011 (in Polish).
- [19] Siwowski T., *Aluminium bridge decks*, Technical University of Rzeszów Publisher, Rzeszów 2008 (in Polish).
- [20] Szumigała M., Polus Ł., *A numerical modelling of the load capacity of the shear connector to aluminium and concrete structures*, II International Polish-Ukrainian Scientific-Technical Conference Current Problems of Metal Structures, Gdańsk, 27–28 November 2014, 221-224.

KAMIL SŁOWIŃSKI*, WALTER WUWER**

EXPERIMENTALLY AND ANALYTICALLY BASED SHAPING OF A BUILT-UP COMPRESSION BAR WITH DEFORMABLE JOINTS OF THE BRANCHES

KSZTAŁTOWANIE NA DRODZE DOŚWIADCZALNEJ I ANALITYCZNEJ ŚCISKANEGO PRĘTA ZŁOŻONEGO Z ODKSZTAŁCALNYMI POŁĄCZENIAMI GAŁĘZI

Abstract

This paper presents the course and results of a research programme aimed at the determination of the design buckling resistance of an axially compressed RHS column strengthened using two shorter U-sections. Connections of the tube and the channel branches were fabricated using BOM blind fasteners. Results of the experimental tests demonstrated the satisfactory efficiency of the performed strengthening of the tubular bar. Parametric analyses performed based on the validated theoretical model allowed the identification of the key factors influencing the effectiveness and economic efficiency of the strengthening process.

Keywords: strengthening, buckling, built-up bars, flexible lap joints

Streszczenie

W artykule przedstawiono przebieg i wyniki programu badawczego, którego celem było określenie obliczeniowej nośności wyboczeniowej ściskanego osiowo pręta o przekroju rurowym prostokątnym, wzmocnionego za pomocą dwóch krótszych gałęzi ceowych. Połączenia gałęzi rurowej i ceowych wykonano przy użyciu łączników jednostronnych BOM. Wyniki badań wykazały zadowalającą skuteczność wzmocnienia. Analizy parametryczne wykonane przy użyciu modelu teoretycznego umożliwiły identyfikację kluczowych czynników wpływających na skuteczność i efektywność ekonomiczną procesu wzmocnienia.

Słowa kluczowe: wzmocnianie, wyboczenie, pręty złożone, podatne połączenia zakładkowe

DOI: 10.4467/2353737XCT.15.083.3883

* Ph.D. Eng. Kamil Słowiński, Department of Geomechanics, Civil Engineering and Geotechnology, Faculty of Mining and Geoengineering, AGH University of Science and Technology.

** Ph.D. D.Sc. Assoc. Prof. Walter Wuwer, Faculty of Architecture, Civil Engineering and Applied Arts Faculty, Katowice School of Technology.

1. Introduction

Steel hollow sections are widely used in the building industry, mainly due to their beneficial strength parameters. An extensive area of application for tubular sections are lightweight roof lattice girders (Fig. 1). If a building changes its function and the loads increase, a problematic issue may be the strengthening of the tubular bars of the truss, e.g. axially compressed diagonals made from rectangular hollow section (RHS), (Fig. 1). In addition, postulates of sustainable development in building require the strengthening process to be characterized by low energy expenditure.



Fig. 1. Lattice girders made from closed and open steel sections

Currently, a rapid development of methods of strengthening tubular bars using CFRP composites, which are glued to the walls of the strengthened bar, may be observed [1–4]. However, it should be noted that the process of strengthening using CFRP composites requires substantial amounts of work, mainly due to the necessity to ensure good adhesion of the composite to the surface of the strengthened element [5]. Another popular method to improve the stability conditions of the member in compression consists of welding shorter steel strengthening branches to the strengthened bar [6]. However, welding, due to it being an energy consuming process, does not fit into the framework of a sustainable building. The application of bolted joints – with the desired structural properties – is limited to the joint with access from both sides. The use of easy to install, self-tapping and self-drilling screws, blind rivets or innovative blind fasteners [7, 8] is, in turn, limited due to their low shear resistance and thus, there is a need to use a large number of fasteners in the fastening. These fasteners are therefore used mainly in the connections of walls of thickness not exceeding 3 mm [9–13]. Against this background, the attention may be paid to the blind fasteners BOM (blind, oversize, mechanically locked) [14] having the shear resistance comparable to the bolts of grade 10.9. BOM fasteners are mainly used in the automobile industry and occasionally in civil engineering (Fig. 2). The works of Wuwer [15–17]

and Swierczyna [18–20] revealed that BOM fasteners may be used as an alternative to standard bolts in the lap joints in the nodes of the lightweight latticed frames made from both open and closed steel sections. The tests revealed significant reserves in the strength, stiffness and ductility of the studied connections working in the bearing. It should be noted that the bearing action in connections was not taken into account in existing applications of the BOM fasteners.

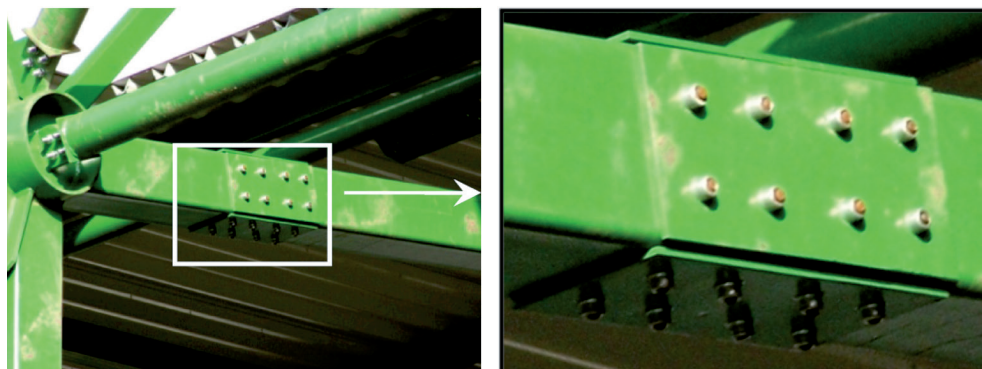


Fig. 2. Splice with blind fasteners BOM in the bottom chord of the truss made of tubular sections

The research performed by Wuwer and Swierczyna provided the basis to initiate a research programme aimed at the experimental and analytical study of axially compressed bars made from RHS, symmetrically strengthened by two shorter channel branches [21]. The article presents the results of experimental and theoretical studies that provide answer to the question of whether blind fasteners (BOM) may be an effective alternative to standard bolts in joints of walls of strengthened tubular bars and strengthening branches of open cross-sections.

2. Investigation programme

Within the first stage of the research programme, experimental tests of single lap joints with BOM fasteners in shear had been foreseen. The tests were aimed at the determination of the basic structural properties of the joints in working conditions similar to those for the connections of the branches in the built-up bars (intended for research in the second stage of the research programme).

The second stage of the programme covered tests of five identical columns in compression, composed of interconnected: tubular bar and two shorter strengthening branches. The aim of the study was to determine the buckling resistance of the observed built-up bars with connections of the branches made using BOM fasteners.

The third stage of the study incorporated the verification of the theoretical model describing the structural behaviour of the tested built-up bars.

Finally, the fourth stage included parametric analyses performed based on the validated theoretical model. The purpose of the analyses was to identify the key factors influencing the effectiveness and economic efficiency of the strengthening process.

3. Inventory of steel sections and material tests

An inventory of sections RHS100×60×4 and U30/60/30×4, intended for installation in test elements was performed prior to the experimental tests. Measurements of the cross-sectional geometry of the RHS revealed for the webs (side B and C in Fig. 3) both bow imperfections of a maximum value of 0.5 mm towards the interior of the cross-section and the difference in the thickness t (Fig. 4). The basic geometrical properties for the sections are presented in Table 1.

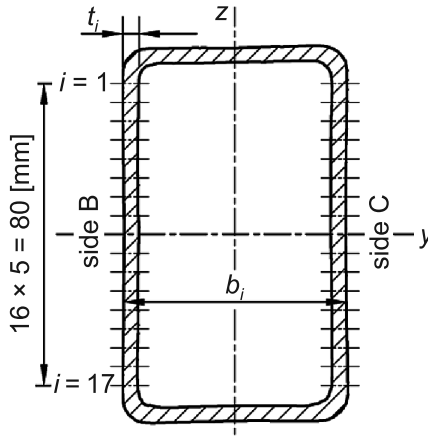


Fig. 3. Cross-section of RHS100×60×4 with measurement points

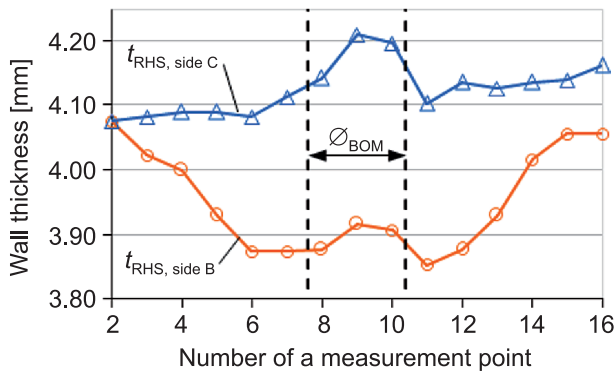


Fig. 4. Distribution of thickness of the walls B and C for RHS100×60×4

Table 1

Cross-sectional properties of sections

Section	A [cm ²]	t [mm]	$t_{\text{RHS,side B}}$ [mm]	$t_{\text{RHS,side C}}$ [mm]
RHS100×60×4	12.27	4.12	4.06	4.16
U30/60/30×4	4.27	3.98	–	–

For the material tests, four rectangular pieces were extracted from the webs of the tube as well as the channel section (Fig. 5). The destination shape of the specimens, according to [22], was obtained using the water jet cutting method. Tensile tests were performed using the Zwick Z/100 machine (Fig. 6). Measured mechanical properties of the specimens, determined according to [22], are presented in Table 2.

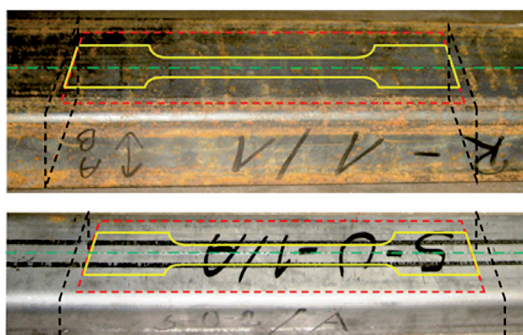


Fig. 5. Locations for the extraction of specimens from tubular (above) and channel (below) sections

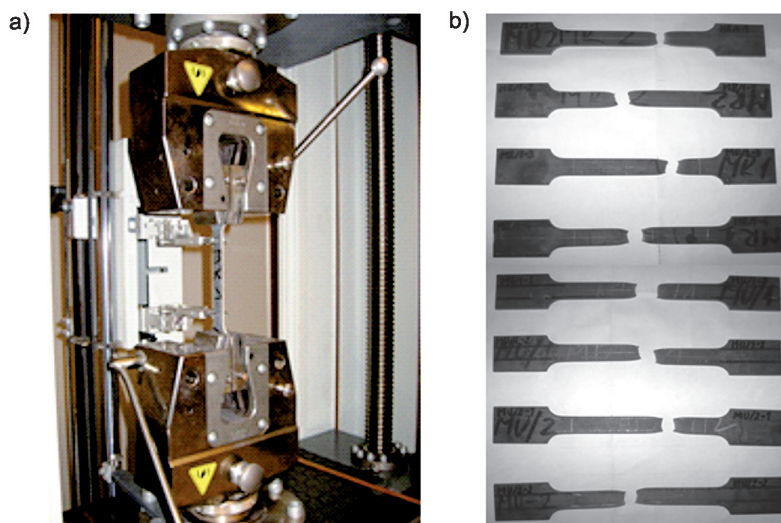


Fig. 6. Tensile tests: a) test set-up, b) specimens after tests

Tensile tests results

Section	Steel	R_{elt} [MPa]	R_{el} [MPa]	R_m [MPa]	E [MPa]
RHS100×60×4	S355J2H	402.63	372.23	528.45	203874.5
	standard deviation	6.11	1.99	2.72	3992.38
U30/60/30×4	S355	407.11	392.47	545.96	189928.7
	standard deviation	7.92	9.85	2.49	6398.23

4. Shear tests of joints

4.1. Construction of test elements

The experimental tests covered six identical test elements subjected to axial tension. Each of the elements was composed of RHS100×60×4 and two branches U30/60/30×4 (Fig. 7). The abutting walls of the sections were interconnected using two BOM-R16-4 fasteners [14] (Fig. 8). The specimens were equipped with short sections of the tube and the channels, in order to increase the bearing capacity of the anchorage in the testing machine (Fig. 7).

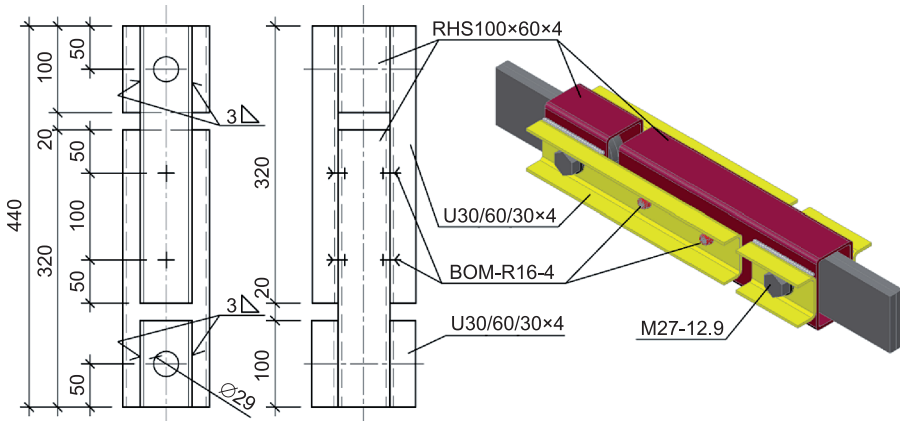


Fig. 7. Construction and dimensions (in millimetres) of test elements



Fig. 8. BOM-R16-4 fastener

4.2. Assembly of test elements

The BOM-R16-4 fasteners were installed in drilled holes with a nominal diameter of 14 mm. The measurement performed before installation revealed positive deviations of diameters with values of up to 9.5% of the nominal diameter. Installation of the BOM fasteners was performed using the installation tool (Fig. 9) which upsets the sleeve of the fastener, forming a head on the blind side and the locking groove on the accessible side (Fig. 10) [14].



Fig. 9. Merging the channel section with the tubular section

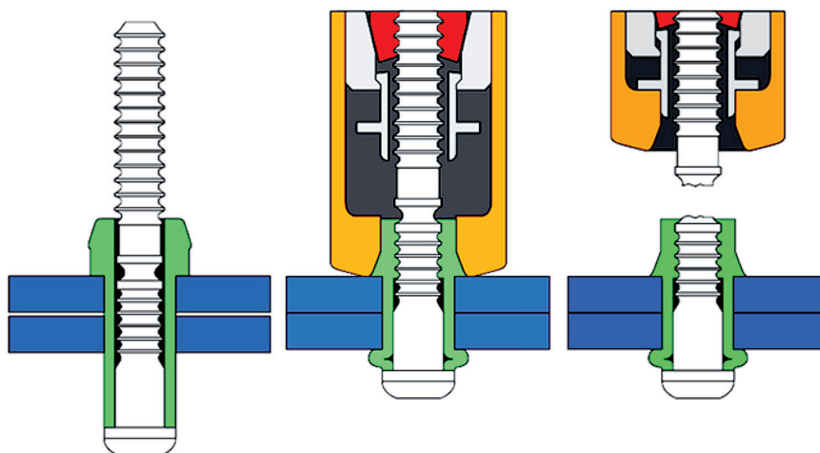


Fig. 10. Installation sequence of a BOM fastener [14]

4.3. Test procedure and measurement equipment

The test elements were subjected to axial tension in a hydraulic testing machine (Fig. 11). The load was applied in increments of 1 kN/min until the occurrence of significant deformations in the fastening, after which the test elements were unloaded.

By using four electronic displacement transducers (DT) (Fig. 11), the mutual displacements of the walls of the interconnected tube and the channel section were measured (two DTs were applied for each of the two connections).

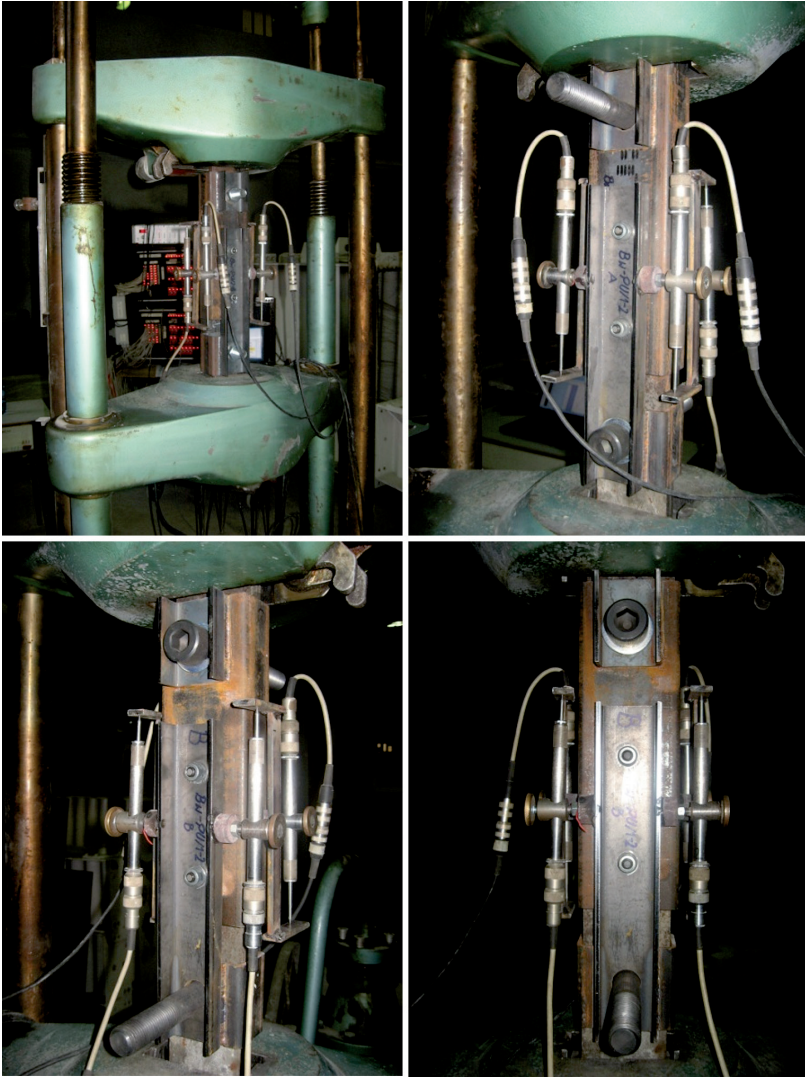


Fig. 11. Shear test set-up

4.4. Shear test results

4.4.1. Static equilibrium paths and failure modes

Fig. 12 shows the measured relationships between the shear force F acting on a single fastener (one-fourth of the tension force loaded the tested element) and the deformation v on the load direction. The magnitudes of the deformation v are the average values from the results of measurements recorded for each of the six tested elements, labelled as S-1 to S-6. As can be seen (Fig. 12), in the first phase of loading, i.e. for $F \leq 45$ kN, relationships

$F - v$ remained essentially linear. With increasing load, the gradual degradation of joint stiffness accompanied by tilting of the fasteners on the load direction was observed. Above the level of the shear force $F \approx 60$ kN, a significant increase in deformation v was recorded. This increase was accompanied by further tilting of fasteners, noticeable plastic ovalisation of holes and also, permanent deformations of the interconnected walls from the contact plane (Fig. 13). The specimens were unloaded at the deformation level $v \approx 15$ mm (Fig. 12).

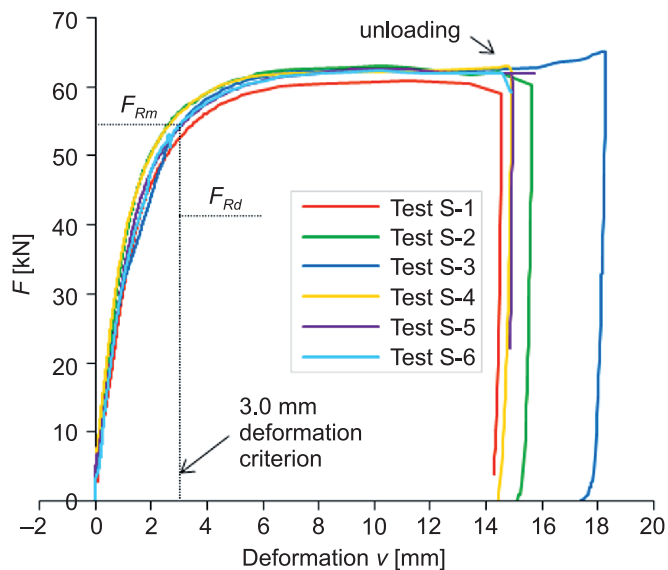


Fig. 12. Relationships $F - v$ for tested elements (average for two connections)



Fig. 13. Typical failure mode of the specimen after unloading

4.4.2. Design bearing resistance of connections

The design bearing resistance of the tested connections (1) in accordance with [23] was determined based on the deformation criterion of 3 mm by calculating: the characteristic resistance (2), the mean value (3) and the adjusted value (4), and also standard deviation (5), using the formulae:

$$F_{Rd} = \frac{F_{Rk}}{\gamma_M}, \quad (1)$$

$$F_{Rk} = F_{Rm} - k \cdot s, \quad (2)$$

$$F_{Rm} = \frac{F_{R,adj,1} + F_{R,adj,2} + \dots + F_{R,adj,n}}{n}, \quad (3)$$

$$F_{R,adj,i} = \frac{F_{R,obs,i}}{\mu_R}, \quad (4)$$

$$s = \sqrt{\frac{1}{n-1} \sum_{i=1}^n (F_{R,adj,i} - F_{Rm})^2}, \quad (5)$$

where:

- k – characteristic fractile factor according to [24],
- n – number of test elements,
- $F_{R,obs,i}$ – measured test result for test i ,
- γ_M – partial factor for resistance according to [23] and [25],
- μ_R – adjustment coefficient (calculations were performed for the measured values).

The results of the statistical evaluation according to formulae (1)–(5) are shown in Table 3.

Table 3

Results of statistical evaluation for design resistance F_{Rd}

F_{Rm} [kN]	s [kN]	k	μ_R	F_{Rk} [kN]	γ_M	F_{Rd} [kN]
54.59	1.37	2.18	1.0	51.61	1.25	41.3

For the measured relationships $F - v$, using the least squares method, the resulting analytical curve was determined of the form (Fig. 14):

$$F = 62.29(1 - e^{-0.7391 v}). \quad (6)$$

For the resulting curve, the instantaneous stiffness k_v corresponding to deformation: $v = 1$ mm – assumed as an upper boundary of the elastic action of the fastening, and $v = 3$ mm – according to the adopted deformation criterion, were developed (Table 4, Fig. 14). Based on the obtained results, it may be concluded that due to the relatively high degradation of stiffness k_v , the tested fastenings were strenuous at the plastic range at the level of deformation $v = 3$ mm.

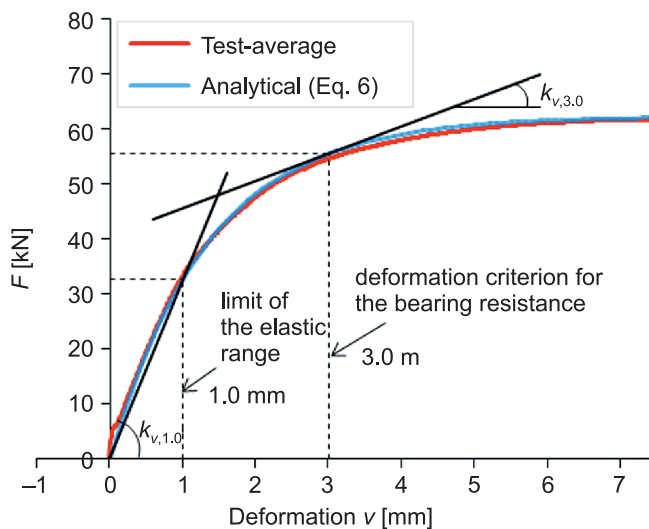


Fig. 14. Instantaneous stiffness of fastening at the level of deformation:
 $v = 1.0$ mm and $v = 3.0$ mm

Table 4

Instantaneous stiffness for tested fastening

	$k_{v,1.0}$	$k_{v,3.0}$
[kN/mm]	32.54	5.01
[%]	100%	15.4

4.4.3. Assessment of results

Fig. 15 shows the bi-linear relations $F - v$ determined for the tested connections with fasteners BOM-R16-4 and analogous connections with bolts M16 of grade 8.8. The bearing resistance and the stiffness of the bolted connection was established according to [25] (Table 5). As it can be seen, connections with BOM fasteners provide greater stiffness than

Table 5

**Design stiffness for connections with BOM fasteners
and M16 standard bolts according to [25]**

Fastener	Bolt M16-8.8	BOM-R16-4
k_v [kN/mm]	19.75	28.07
[%]	100	142.1
F_{Rd} [kN]	64.4	41.3
[%]	100	64.1

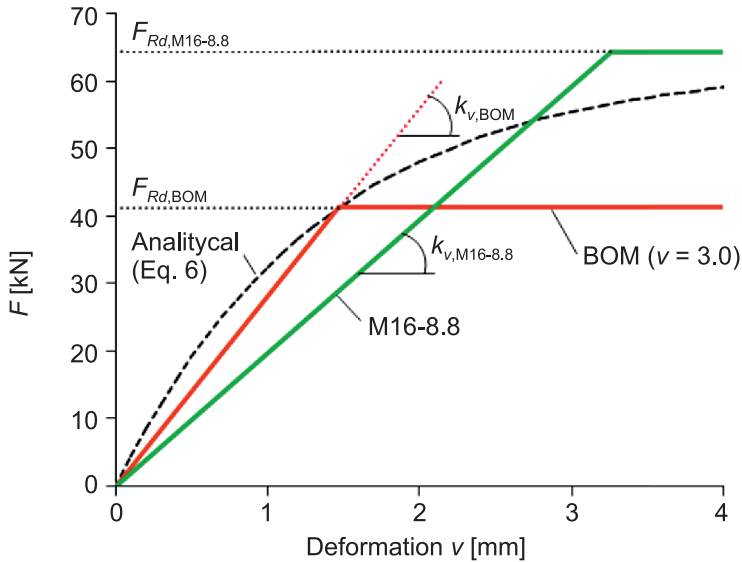


Fig. 15. Bi-linear relationships $F-v$ for connections with BOM fasteners and M16-8.8 bolts

the bolted connections. It should be noted that the relationship $F-v$ for the bolted connection does not include a possible slip in the fastening (for connections with BOM fasteners, the slip does not occur [21]). However, it can be seen that design bearing resistance of the connections with BOM fasteners is noticeably smaller than those for bolted connections.

5. Tests of built-up columns

5.1. Construction of test elements

The second stage of the research programme covered tests of five identical three-branched, pin-ended columns subjected to axial compression. The main bar (intended for strengthening) to which the compressive force was applied at the ends was made from RHS100×60×4 with a length of 3000 mm (Fig. 16). Each of the two channel branches U30/60/30×4 (foreseen as strengthening branches) with a length of 2960mm was connected with a main tubular bar using eight BOM-R16-4 fasteners, uniformly spaced at 408mm (Fig. 16). Installation of the



Fig. 16. Three-branched column foreseen for test (before installation of BOM fasteners)

fasteners was performed using the installation tool (Fig. 17) – previously, this was also used for the assembly of specimens for shear tests. Pinned-end conditions and the axial transfer of compressive force to the column was provided by – performed with high precision – end fixtures (Fig. 18). The buckling length of the tested elements placed on the test stand was $L = 3139$ mm.



Fig. 17. Assembly of the branches of the built-up column

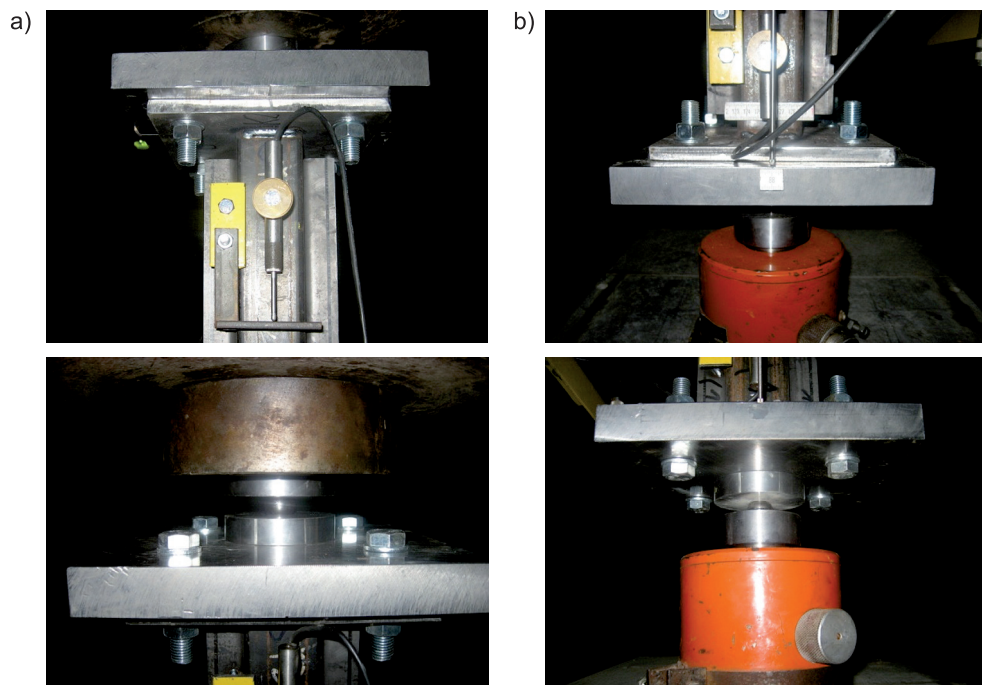


Fig. 18. End fixtures for tested columns: a) upper head, b) bottom head

5.2. Test procedure

The compression tests were performed using a hydraulic testing machine with loads range up to 1000 kN (Fig. 19a). The axial load was applied in increments of 10 kN/min [26], until the failure of the tested elements. During the test, strains of the walls of the tubular main bar were measured using stain gauges. Furthermore, by means of electronic displacement transducers (DT), the following measurements were recorded:

- lateral deflections normal to both principal axes of the built-up cross-section (at quarter points of the tested column), (Fig. 19b, c);
- mutual displacements between the interconnected walls of the tubular bar and channel branches (in the axis of each connection), (Fig. 19c);
- overall column shortening (Fig. 19d).

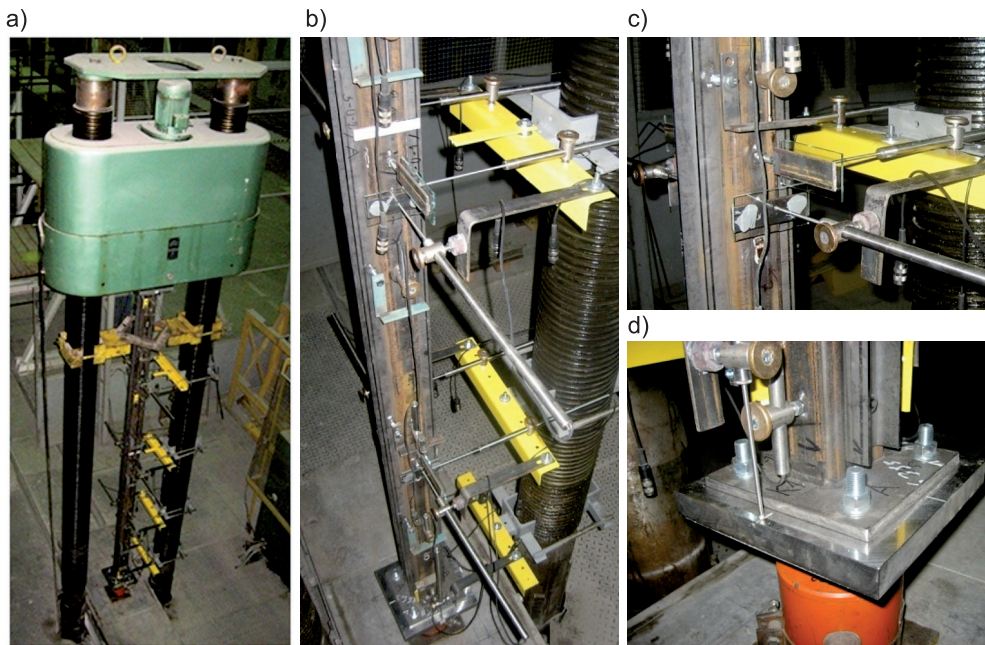


Fig. 19. Column test set-up: a) general view; b) and c) arrangement of DTs for measurement lateral deflections of the column and displacements between interconnected sections, respectively; d) instrumentation for recording overall shortening of the column

5.3. Column test results

5.3.1. Failure mode

The destruction of all the tested elements, labelled as Bz-1 to Bz-5, was as a result of their flexural buckling (Fig. 20) around the z axis of the built-up cross-section (Fig. 16). Figure 21 summarises the achieved relationships between the loaded axial force N and the

lateral deflection u_y (Fig. 21a) or u_z (Fig. 21b), i.e. measured in the xy plane or xz plane (Fig. 16) at the mid-length of the column (Fig. 19c).

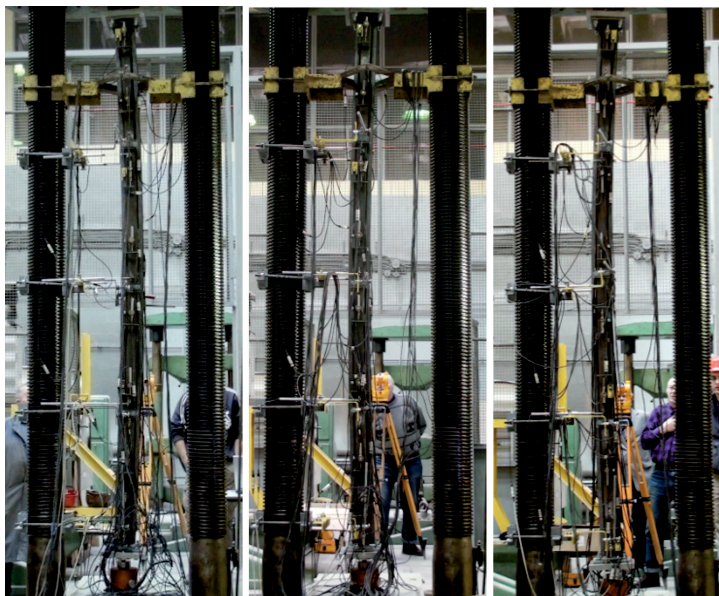


Fig. 20. Typical failure model of tested columns

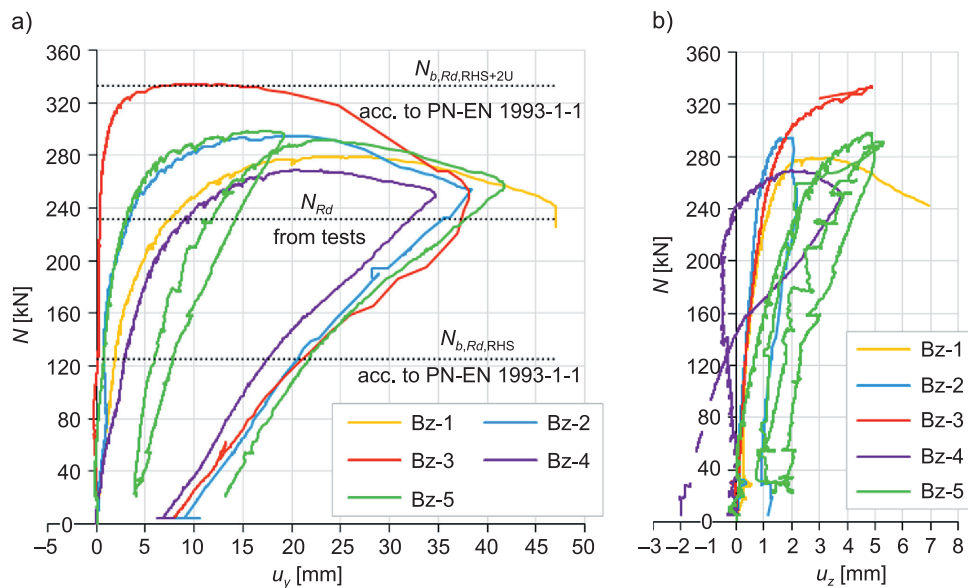


Fig. 21. Measured relationships load-lateral deflection: a) $N - u_y$, b) $N - u_z$

5.3.2. Design buckling resistance of built-up columns

It was assumed that for each tested column, the design criterion for the ultimate capacity will be determined by the lowest value of the axial force N , which is accompanied by:

- achievement of the buckling strength (N_{ult}) or
- yielding in extreme fibres of cross-section of the tubular main bar (N_{pl}) or
- achievement of the design bearing resistance by any connection of the branches.

The value of the N_{pl} was calculated based on the state of normal stresses in the most strenuous point along the length of the tubular bar. The normal stresses were calculated as the sum of the residual stresses, in accordance with [27] and the stresses determined on the basis of the strain gauge measurements. For each test element, the first yielding occurred in the walls of the tubular cross-section, on the concave side of the deflected (buckled) column, usually at the axis of the joint which was the nearest to the column's mid-point. The measured values of forces N_{ult} and N_{pl} are summarised in Tables 6 and 7. For the group of test elements, the average values of compressive stresses in the tubular cross-section under the load $N = N_{ult}$ constituted from 79% (in element Bz-4) to 93% (in element Bz-3) of the upper yield strength R_{eH} for the RHS material (Table 2).

The design buckling resistance N_{Rd} for tested columns was statistically determined based on the values of load N_{pl} (Table 7, Table 8), using equations (1) to (6) – in the formulae, symbol F was replaced with symbol N . The calculation results are presented in Table 9. As can be seen, the achieved design buckling resistance N_{Rd} constitutes approx. 185% of the buckling resistance of the tubular bar only, according to [28] (Fig. 21a). At the same time, the calculated resistance N_{Rd} constitutes approx. 70% of the buckling resistance of the theoretical built-up column with equal lengths of the three perfectly rigid interconnected branches, according to [27] (Fig. 21a). It should be noted that for each tested element, shear forces acting in the joints of the branches were lower than the design bearing resistance of those joints [21].

Table 6

Ultimate load N_{ult} for tested columns

Specimen	Bz-1	Bz-2	Bz-3	Bz-4	Bz-5
Measured value N_{ult} [kN]	278.85	294.6	333.81	269.11	298.48
Average value N_{Rm} [kN]	294.97				
Standard deviation s [kN]	24.75				
Coefficient of variation V	0.084				

Table 7

Load N_{pl} for tested columns

Specimen	Bz-1	Bz-2	Bz-3	Bz-4	Bz-5
Measured value N_{pl} [kN]	277.1	291.62	333.64	264.92	296.86
Average value N_{Rm} [kN]	292.83				
Standard deviation s [kN]	26.03				
Coefficient of variation V	0.089				

Table 8

Comparison of measured values of loads N_{ult} and N_{pl}

Specimen	Bz-1	Bz-2	Bz-3	Bz-4	Bz-5
Ratio N_{ult}/N_{pl}	1.01	1.01	1.0	1.02	1.01

Table 9

Results of statistical evaluation for the design buckling resistance N_{Rd}

N_{Rm} [kN]	s [kN]	k	μ_R	N_{Rk} [kN]	γ_M	N_{Rd} [kN]
292.86	26.03	2.33	1.0	232.1	1.0	232.2

6. Analytical solution

6.1. Computational model

The computational model describing the behaviour of the tested built-up columns was developed in the Wolfram Mathematica program [29]. A detailed description of the model is given in the work [21]. The model takes into account nonlinear geometric relationships for the built-up column, linear material characteristics and nonlinear relationships describing

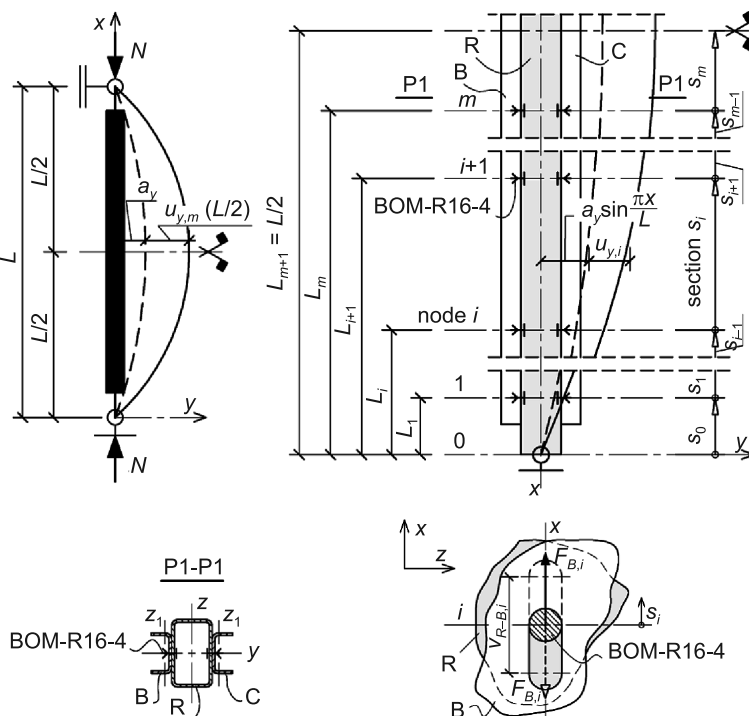


Fig. 22. Scheme of the computational model (description in the text)

the structural behaviour of joints of the branches. The model makes it possible to obtain: the axial force N loading the column; shear forces F_i acting in the joints of branches in nodes $i = 1 - m$ (Fig. 22); a lateral deflection in the xy plane at any point along the column length. Results may be achieved for given amplitudes of initial curvature $-a_y$ and lateral deflection of the column under the load $N - u_{y,m}(L/2)$.

The solution, in the general form, for column buckling about z axis, is governed by the set of equations that are assigned to sections $s_0 - s_m$ (Fig. 22) along half of the column length:

- describing lateral deflection of the column axis (7)–(9) and the angle of the inclination of the tangent to this axis (10)–(11)

$$u_{y,0}(0) = 0, \quad (7)$$

$$u_{y,i-1}(L_i) = u_{y,i}(L_i), \quad (8)$$

$$u_{y,m}(L/2) = u_y, \quad (9)$$

$$u'_{y,i-1}(L_i) = u'_{y,i}(L_i), \quad (10)$$

$$u'_{y,m}(L/2) = 0; \quad (11)$$

- describing bending moments (12–13) and transverse forces (14–16)

$$EI_{\text{RHS},z} u''_{y,0}(0) = 0, \quad (12)$$

$$(2EI_{U,z1} + EI_{\text{RHS},z}) u''_{y,i}(L_i) = -N \left[u_{y,i}(L_i) + a_y \sin \frac{\pi L_i}{L} \right] + w(N_{B,i} + N_{C,i}), \quad (13)$$

$$EI_{\text{RHS},z} u'''_{y,0}(L_1) + Nu'_{y,0}(L_1) = (2EI_{U,z1} + EI_{\text{RHS},z}) u'''_{y,1}(L_1) + Nu'_{y,1}(L_1), \quad (14)$$

$$(2EI_{U,z1} + EI_{\text{RHS},z}) u'''_{y,i-1}(L_i) + Nu'_{y,i-1}(L_i) = (2EI_{U,z1} + EI_{\text{RHS},z}) u'''_{y,i}(L_i) + Nu'_{y,i}(L_i), \quad (15)$$

$$(2EI_{U,z1} + EI_{\text{RHS},z}) u'''_{y,m}(L/2) + Nu'_{y,m}(L/2) = 0; \quad (16)$$

- linking the values of deformations v_i with the values of shear forces $F_{B,i}$ or $F_{C,i}$ occurring in joints of the branches B and R (17) or C and R (18)

$$\sum_i^m \int_{L_i}^{L_{i+1}} \Delta \varepsilon_{R-B,i}(x) dx = v_i(F_{B,i}), \quad (17)$$

$$\sum_i^m \int_{L_i}^{L_{i+1}} \Delta \varepsilon_{R-C,i}(x) dx = v_i(F_{C,i}); \quad (18)$$

where:

$$u_{y,0}(x) = C_{0,3}x + C_{0,4} - \frac{C_{0,1} \cos(k_{\text{RHS}}x) + C_{0,2} \sin(k_{\text{RHS}}x)}{k_{\text{RHS}}^2} + \frac{a_y k_{\text{RHS}}^2 L^2 \sin\left(\frac{\pi x}{L}\right)}{-k_{\text{RHS}}^2 L^2 + \pi^2}, \quad (19)$$

$$u_{y,i}(x) = C_{i,3}x + C_{i,4} - \frac{C_{i,1} \cos(k_{\text{RHS}+U}x) + C_{2,2} \sin(k_{\text{RHS}+U}x)}{k_{\text{RHS}+U}^2} + \frac{a_y k_{\text{RHS}+U}^2 L^2 \sin\left(\frac{\pi x}{L}\right)}{-k_{\text{RHS}+U}^2 L^2 + \pi^2}, \quad (20)$$

$$k_{\text{RHS}}^2 = \frac{N}{EI_{\text{RHS},z}}, \quad (21)$$

$$k_{\text{RHS}+U}^2 = \frac{N}{2EI_{U,z1} + EI_{\text{RHS},z}}, \quad (22)$$

where:

- C_0, C_i – integration constants,
- $EI_{\text{RHS},z}$ – bending stiffness of the main tubular bar in the xy plane (Fig. 22),
- $EI_{U,z1}$ – bending stiffness of the channel branch in the xy plane (Fig. 22),
- $N_{B,i}, N_{C,i}$ – axial forces in the branches B and C, respectively, in section s_i ,
- w – distance between neutral axes of branches R and B or R and C,
- $v_i(F_{B,i}), v_i(F_{C,i})$ – functions defining relationships between the values of deformation and shear force in the i joint of the branches B and R or C and R,
- $\Delta\varepsilon_{R-B,i}, \Delta\varepsilon_{R-C,i}$ – functions describing the state of strains of branches B and R or C and R in the axis of i joint,

the other symbols are in accordance with Fig. 22.

7. Comparison of experimental and analytical results

The calculations were performed in three variants: CW1, CW2 and CW3, depending on the function describing the boundary conditions in the joints of the branches adopted in the analytical solution (Fig. 23):

- obtained from the shear tests: nonlinear C1 according to (6) or linear C2 according to the bi-linear curve shown in Fig. 15,
- C3 which linearly approximates the averaged measured relationships between shear force F_1 and deformation v_1 in the joint of the branches in node 1 (Fig. 22).

The amplitudes of the initial curvature of the built-up column (a_y) were taken in calculations in such a way as to achieve the best possible fit of analytical and experimental curves. As can be seen (Fig. 24), the critical load for the perfectly straight column ($a_y = 0$) calculated in variants CW1 and CW2 was smaller, in many cases, than the value of the measured axial force N (Fig. 24a, b, c, e). The best approximation of the experimental results provide curves CW3 for the amplitudes a_y within the range from 0.48 mm (Fig. 24e) to 2.62 mm (Fig. 24d). The distinct behaviour of the test element Bz-3 (Fig. 24c) can be explained by unintentional partial rotational restraining of the column ends. Comparison of test results – averaged for elements Bz-1, Bz-2, Bz-4 and Bz-5, and analytical results – obtained for the average amplitude $a_y = L/2207 \approx 1.42\text{mm}$ is presented in Fig. 25. On the basis of the course of both curves, it may be concluded that the analytical solution provides satisfactory approximation of the experimental results.

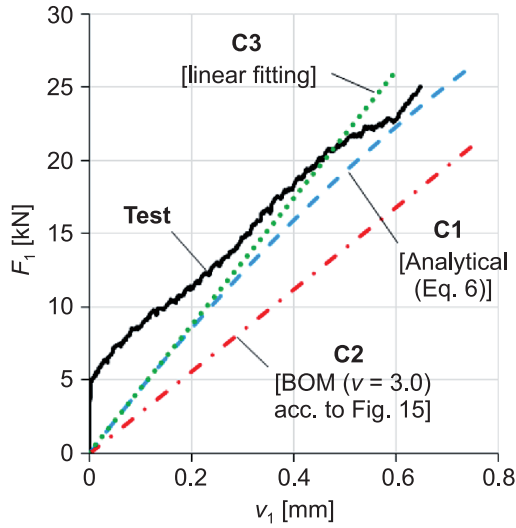


Fig. 23. Relationships $F_1 - v_1$ adopted in the analytical solution

8. Parametric analysis

Using the theoretical model, a parametric analysis was performed adopting linear stiffness function of the joints C3 (Fig. 23) and the averaged magnitude of the amplitude of initial curvature of the built-up column $a_y = L/2207$ in the calculations (Fig. 25).

The structural response of the built-up column was analysed in the case of:

- the change in cross-sectional dimensions of the channel branches at a constant number of connections ($m = 4$, Fig. 22) of the main tubular bar with each of the two channel branches – the continuous curves in Fig. 26,
- an increase in the number of joints of each of the two channel branches U30/60/30×4 with the tubular bar, from eight ($m = 4$) to sixteen ($m = 8$), twenty-four ($m = 12$), thirty-two ($m = 16$) and forty ($m = 20$) – the dashed curves in Fig. 26.

Calculations were carried out up to the moment when the normal stresses in any point of the tube cross-section were equal to the upper yield strength R_{eH} of the RHS material.

Form the performed parametric analysis it may be concluded that (see Fig. 26):

- an increase in the number of joints does not significantly raise the efficiency of strengthening (continuous curves); when doubling the number of joints from eight ($m = 4$) to sixteen ($m = 8$), the carrying capacity of the built-up column increases by approx. 9.5%; further doubling the number of joints (from $m = 8$ to $m = 16$) provides only a 5% increase in the carrying capacity,
- the carrying capacity for the built-up column with forty ($m = 20$) flexible joints of branches with BOM fasteners constitutes nearly 97% of the carrying capacity of the built-up column but with perfectly rigid joints (the dotted curve),

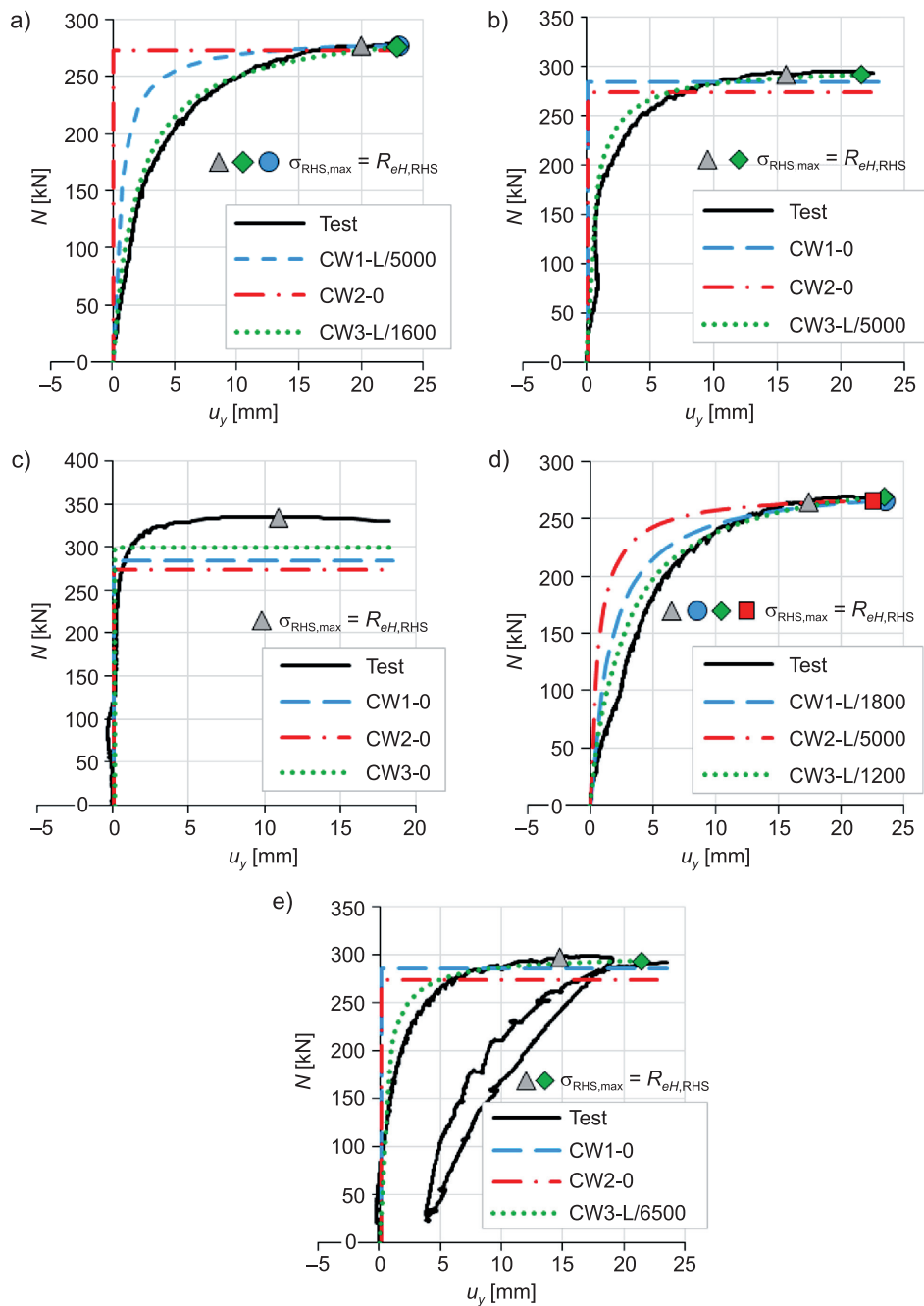


Fig. 24. Comparison of $N - u_y$ relationships measured and obtained in the analytical solution for test elements: a) b) c) d) and e) – Bz-1 to Bz-5, respectively

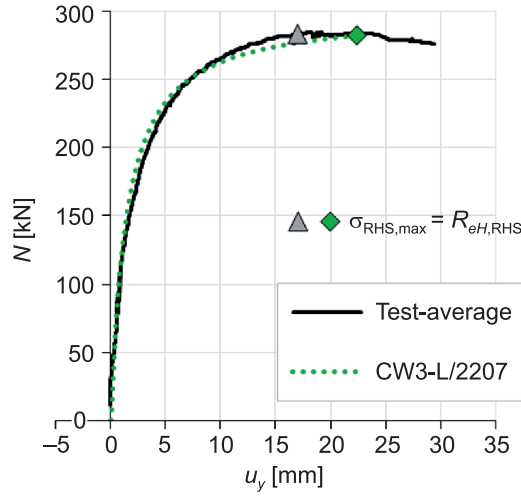


Fig. 25. Relationships $N - u_y$; measured and obtained analytically for the average amplitude α_y

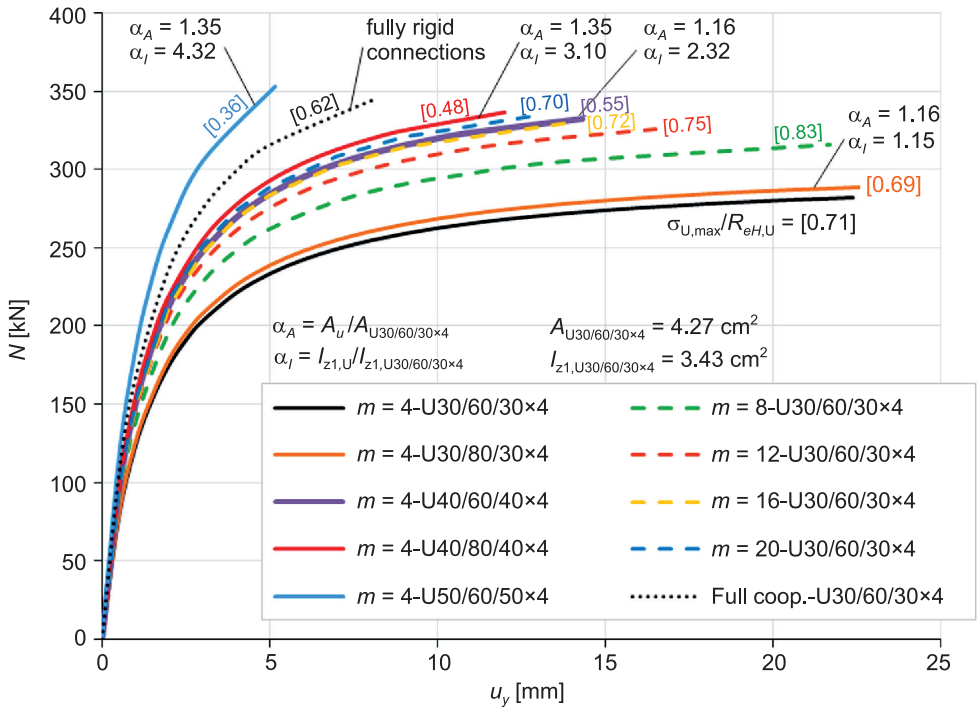


Fig. 26. Relationships $N - u_y$ obtained in the parametric analysis (description in the text)

- the buckling resistance of the column with U40/60/40×4 sections and only eight joints ($m = 4$) of the branches is comparable to the one, calculated for the column with U30/60/30×4 sections and forty joints ($m = 20$),
- the carrying capacity of the column with U50/60/50×4 sections and eight flexible joints ($m = 4$) constitutes approx. 102% of the carrying capacity of the column with U30/60/30×4 sections but with perfectly rigid joints (e.g. welded connections of the branches),
- an increase in both: the secondary moment of area $I_{z1,U}$ (α_I ratio) of the strengthening branches and the number m of the joints is accompanied by the decreasing strenuous of the strengthening U-shape branches ($\sigma_{U,max}/R_{eH,U}$ ratio in the square brackets).

9. Conclusions

A four-stage research programme including experimental and theoretical studies was carried out.

The first stage of the programme covered the shearing tests for single-cut joints with BOM-R16-4 fasteners (six test elements). The tests proved that the tested joints exhibit structural properties that are similar to the properties for the joints with standard 8.8 grade M16 bolts. High values of both shear and bearing resistance as well as a great stiffness and deformation capacity in the bearing constitute advantages over other popular blind fasteners such as screws or rivets.

In the second stage of the research programme, five three-branched columns in compression were tested. Results of the tests demonstrated the efficiency of the performed strengthening of the tubular bar using two U-shape sections connected to the strengthened bar using eight lap joints with BOM-R16-4 fasteners. The design buckling resistance of the tested columns was noticeably higher than that for the tubular bar before strengthening. At the same time, due to the flexibility of the joints of the branches, the design buckling resistance of the tested columns was visibly lower than that calculated for the column with perfectly rigid joints.

Within the third stage of the programme, validity of the proposed theoretical model describing the behaviour of the tested columns was proved. However, attention should be paid to the simplifying assumptions made in the analytical solution which limit the scope of the applications of the model.

Results of parametric studies performed within the fourth stage of the programme showed that striving both to increase the secondary moment of the area of the strengthening branches and to reduce the number of joints of the strengthened bar and the strengthening branches is a cost-effective way to gain efficiency of the strengthening process. Due to the high price of labour, a major part of the strengthening cost has a direct relationship with the fabrication of connections of the branches. Therefore, it is better to save labour at the expense of material – admission to only partial strenuous of strengthening branches.

Within the scope of further research, work on the development of a numerical model based on FEM will be undertaken. This model will not only enable the analyses of built-up columns with various geometrical and strength parameters but also the arbitrary arrangement

of joints of cooperating branches. It will be also possible to take into account the influence of the existing states of load and imperfections in the bar which is to be strengthened on the buckling resistance of the built-up member after strengthening.

Results of the performed research programme proved that BOM blind fasteners may be an efficient and cost-effective alternative to standard bolts in lap connections of strengthened bars with closed rectangular cross-section and strengthening branches with open cross-sections. It may be also stated that due to the relatively small labour consumption, the described strengthening method meets the demands of sustainable development in building industry.

This publication was supported by project 11.11.100.197/AS.

References

- [1] Dawood M., Rizkalla S., *Environmental durability of a CFRP system for strengthening steel structures*, Construction and Building Materials, Vol. 24, 2010, 1682-1689.
- [2] Shaat A., Fam A., *Axial loading tests on short and long structural steel columns retrofitted using carbon fibre reinforced polymers*, Canadian Journal of Civil Engineering, Vol. 33(4), 2006, 458-470.
- [3] Lanier B., Schnerch D., Rizkalla S., *Behavior of steel monopoles strengthened with high-modulus CFRP materials*, Thin-Walled Structures, Vol. 47, 2009, 1037-1047.
- [4] Piekarczyk M., *Zastosowanie technologii klejenia w budowlanych konstrukcjach metalowych*, Wydawnictwo Politechniki Krakowskiej, Kraków 2013.
- [5] Teng J.G., Yu T., Fernando D., *Strengthening of steel structures with fiber-reinforced polymer composites*, Journal of Constructional Steel Research, Vol. 78, 2012, 131-143.
- [6] Żółtowski W., Wierzbicki S., Król P., Witkowski J., *Błędne założenia projektowe przyczyną awarii konstrukcji hali*, XXIII Konferencja Naukowo-Techniczna Awarie Budowlane, Szczecin-Międzyzdroje, 2007, 699-706.
- [7] Di Lorenzo G., Landolfo R., *Shear experimental response of new connection systems for cold-formed structures*, Journal of Constructional Steel Research, Vol. 60, 2004, 561-579.
- [8] Mucha j., Witkowski W., *The experimental analysis of the double joint type change effect on the joint destruction process in uniaxial shearing test*, Thin-Walled Structures, Vol. 66, 2013, 39-49.
- [9] Becque J., Rasmussen K.J.R., *Experimental investigation of the interaction of local and overall buckling of stainless steel I-columns*, Journal of Structural Engineering, Vol. 135(11), 2009, 1340-1348.
- [10] Stone T., La Boube R.A., *Behavior of cold-formed steel built-up sections*, Thin-Walled Structures, Vol. 43, 2005, 1805-1817.
- [11] Zhang J.H., Young B., *Compression tests of cold-formed steel I-shaped open sections with edge and web stiffeners*, Thin-Walled Structures, Vol. 52, 2012, 1-11.
- [12] Bolte W.G., LaBoube R.A., *Behavior of curtain wall stud to track connections*, Thin-Walled Structures, Vol. 42, 2004, 1431-1443.
- [13] LaBoube R.A., Yu W.W., *Recent research and developments in cold-formed steel framing*, Thin-Walled Structures, Vol. 32, 1998, 21-39.
- [14] ALCOA Fastening Systems, *The Huck Product Range – BOM*, (online) homepage: <http://pdf.directindustry.com/pdf/huck-r/the-huck-r-product-range/34809-323383.html> (access: 07.07.2015).

- [15] Wuwer W., *Podatne połączenia na sworznie jednostronne w prętowych konstrukcjach cienkościennych*, Wydawnictwo Politechniki Śląskiej, Gliwice 2006.
- [16] Wuwer W., *The behaviour and design of lap-joints in thin-walled bar constructions*, Advanced Steel Construction an International Journal, Vol. 4(1), 2008, 59-83.
- [17] Wuwer W., *Flexible nodes in calculations of thin-walled structures*, 3rd International Conference on Steel Structures Eurosteel, Coimbra, 2002, 1189-1198.
- [18] Swierczyna S., *Nośność i sztywność jednoczętych połączeń sworzniowych w konstrukcjach z kształtowników giętych*, Doctoral thesis, (online) homepage: http://delibra.bg.polsl.pl/Content/1317/calosc_rozprawa.pdf (access: 07.07.2015).
- [19] Swierczyna S., Wuwer W., *Thin-walled latticed frame with semi-rigid bolted joints*, 12th International Conference on Steel Structures Progress in Steel and Composite Structures, Wrocław, 2011, 256-257.
- [20] Swierczyna S., Wuwer W., *Evaluation of bearing resistance of blind bolt lap joints*, 7th European Conference on Steel and Composite Structures Eurosteel, Naples, 2014, 256-257.
- [21] Słowiński K., *Badanie nośności ściskanych osiowo elementów bliskogałęziowych z podatnymi połączeniami*, Doctoral thesis, Gliwice 2013.
- [22] PN-EN ISO 6892-1 Metale – Próba rozciągania – Część 1: Metoda badania w temperaturze pokojowej.
- [23] ECCS TC7 TWG 7.10 Connections in cold-formed structures – The testing of connections with mechanical fasteners in steel sheeting and sections.
- [24] PN-EN 1990 Eurokod – Podstawy projektowania konstrukcji.
- [25] PN-EN 1993-1-8 Eurokod 3 – Projektowanie konstrukcji stalowych – Część 1–8: Projektowanie węzłów.
- [26] Galambos T.V., *Guide to stability design criteria for metal structures 5th edition*, John Wiley & Sons, New York 1998.
- [27] Krentz J.St., Haller W., *Zur Einstufung von rechteckigen und quadratischen hohlprofilen in DIN 18800*, Der Stahlbau, Vol. 57, 1988, 129-134.
- [28] PN-EN 1993-1-1 Eurokod 3 – Projektowanie konstrukcji stalowych – Część 1–1: Reguły ogólne i reguły dla budynków.
- [29] Grzymkowski R., Kapusta A., Kuboszek T., Słota D., *Mathematica 6*, Wydawnictwo Pracowni Komputerowej Jacka Skalmierskiego, Gliwice 2008.

CONTENTS

Boroń J., Marszałek K.: Distribution of the temperature factor in terms of building envelope protection against mould growth.....	3
Fiertak M., Stryżewska T., Kańka S.: The sustainable construction industry vs. the final phase life cycle assessments of the internal layer of industrial chimneys	17
Gryc A., Radoń J., Nawalany G.: Measurements and calculations of temperature in the ground and in assemblies adjacent to an intermittently heated basement	33
Janus-Michałska M., Jasińska D.: A comfort comparison of a foam seat against a seat with an auxetic spring skeleton	43
Karcińska P., Malara J.: Evaluation of the efficiency of construction workers on different days of the week in terms of fuzzy sets	53
Michałowski T.: Selected issues of aerodynamics of steel chimneys	63
Piekarczyk M., Michałowski T., Kowalczyk D.: Examples of designing steel shell structures according to Eurocodes	75
Politański W.: The loading pattern's influence on the stress increment in prestressing steel and bending moment resistance in multi-span members post-tensioned with unbonded tendons.....	87
Rzeszut K., Szumigala M., Polus Ł.: Selected aspects of the proper application of structural materials in terms of corrosion.....	97
Słowiński K., Wuwer W.: Experimentally and analytically based shaping of a built-up compression bar with deformable joints of the branches	107

TREŚĆ

Boroń J., Marszałek K.: Rozkład wartości czynnika temperaturowego w aspekcie ochrony przegród budowlanych przed ozwojem pleśni	3
Fiertak M., Stryżewska T., Kańka S.: Zrównoważone budownictwo a końcowa faza cyklu życia wnętrza kominów przemysłowych.....	17
Gryc A., Radoń J., Nawalany G.: Pomiary i obliczenia temperatury w gruncie i przegrodach w piwnicy ogrzewanej okresowo.....	33
Janus-Michałska M., Jasińska D.: Porównanie komfortu siedziska fotela piankowego i siedziska o szkieletcie auksetycznym.....	43
Karcińska P., Malara J.: Ocena wydajności pracowników budowlanych w poszczególnych dniach tygodnia roboczego w kategoriach zbiorów rozmytych	53
Michałowski T.: Wybrane zagadnienia aerodynamiki kominów stalowych.....	63
Piekarczyk M., Michałowski T., Kowalczyk D.: Przykłady projektowania stalowych konstrukcji powłokowych według Eurokodów	75
Politański W.: Wpływ schematu obciążeń na przyrost naprężeń w stali sprężającej oraz nośność na zginanie w elementach wieloprzęsłowych sprężonych ciągnami bez przyczepności	87
Rzeszut K., Szumigala M., Polus Ł.: Wybrane aspekty poprawnego stosowania materiałów konstrukcyjnych w warunkach korozji.....	97
Słowiński K., Wuwer W.: Kształtowanie na drodze doświadczalnej i analitycznej sciskanego pręta złożonego z odkształcalnymi połączeniami gałęzi	107